RMZ

MATERIALS and GEOENVIRONMENT

MATERIALI in GEOOKOLJE

RMZ – M&G, **Vol. 61**, No. 4
pp. 211–274 (2014)

Ljubljana, December 2014

RMZ – Materials and Geoenvironment
RMZ – Materiali in geookolje
ISSN 1408-7073

Old title/Star naslov
Mining and Metallurgy Quarterly/Rudarsko-metalurški zbornik
ISSN 0035-9645, 1952–1997

Published by/Izdajatelj
Faculty of Natural Sciences and Engineering, University of Ljubljana/
Naravoslovnotehniška fakulteta, Univerza v Ljubljani

Associated Publisher/Soizdajatelj
Institute for Mining, Geotechnology and Environment, Ljubljana/
Inštitut za rudarstvo, geotehnologijo in okolje
Velenje Coal Mine/Premogovnik Velenje

Editorial Address/Naslov uredništva
RMZ – Materials and Geoenvironment
Aškerčeva cesta 12, p. p. 312
1001 Ljubljana, Slovenija
Tel.: +386 (0)1 470 45 00
Fax.: +386 (0)1 470 45 60
E-mail: rmz-mg@ntf.uni-lj.si

Design and DTP/Oblikovanje, prelom in priprava za tisk
IDEJA za ITGTO

Print/Tisk
Birografika BORI, d. o. o.
Printed in 200 copies./Naklada 200 izvodov.

Published/Izhajanje
4 issues per year/4 številke letno

Partly funded by Ministry of Education, Science and Sport of Republic of Slovenia./Pri financiranju revije sodeluje Ministrstvo za izobraževanje, znanost in šport Republike Slovenije.

Articles published in Journal "RMZ M&G" are indexed in international secondary periodicals and databases:/Članki, objavljeni v periodični publikaciji „RMZ M&G", so indeksirani v mednarodnih sekundarnih virih: Civil Engineering Abstracts, CA SEARCH® – Chemical Abstracts® (1967–present), Materials Business File, Inside Conferences, ANTE: Abstract in New Technologies and Engineering, METADEX®, GeoRef, CSA Aerospace & High Technology Database, Aluminium Industry Abstracts, Computer and Information Systems, Mechanical & Transportation Engineering Abstracts, Corrosion Abstracts, Earthquake Engineering Abstracts, Solid State and Superconductivity Abstracts, Electronics and Communications Abstracts.

Annual subscription for individuals in Slovenia: 16.69 EUR, for institutions: 22.38 EUR. Annual subscription for the rest of the world: 20 EUR, for institutions: 40 EUR/Letna naročnina za posameznike v Sloveniji: 16,69 EUR, za inštitucije: 33,38 EUR. Letna naročnina za tujino: 20 EUR, inštitucije: 40 EUR.

Current account/Tekoči račun
Nova Ljubljanska banka, d. d., Ljubljana: UJP 01100-6030708186

VAT identification number/Davčna številka
24405388

Online Journal/Elektronska revija
www.rmz-mg.com

Table of Contents

Kazalo

Historical Review

More than 90 years have passed since the University Ljubljana in Slovenia was founded in 1919. Technical fields were united in the School of Engineering that included the Geologic and Mining Division, while the Metallurgy Division was established only in 1939. Today, the Departments of Geology, Mining and Geotechnology, Materials and Metallurgy are all part of the Faculty of Natural Sciences and Engineering, University of Ljubljana.

Before World War II, the members of the Mining Section together with the Association of Yugoslav Mining and Metallurgy Engineers began to publish the summaries of their research and studies in their technical periodical Rudarski zbornik (Mining Proceedings). Three volumes of Rudarski zbornik (1937, 1938 and 1939) were published. The War interrupted the publication and it was not until 1952 that the first issue of the new journal Rudarsko-metalurški zbornik – RMZ (Mining and Metallurgy Quarterly) was published by the Division of Mining and Metallurgy, University of Ljubljana. Today, the journal is regularly published quarterly. RMZ – M&G is co-issued and co-financed by the Faculty of Natural Sciences and Engineering Ljubljana, the Institute for Mining, Geotechnology and Environment Ljubljana, and the Velenje Coal Mine. In addition, it is partly funded by the Ministry of Education, Science and Sport of Slovenia.

During the meeting of the Advisory and the Editorial Board on May 22, 1998, Rudarsko-metalurški zbornik was renamed into "RMZ – Materials and Geoenvironment (RMZ – Materiali in Geookolje)" or shortly RMZ – M&G. RMZ – M&G is managed by an advisory and international editorial board and is exchanged with other world-known periodicals. All the papers submitted to the RMZ – M&G undergoes the course of the peer-review process.

RMZ – M&G is the only scientific and professional periodical in Slovenia which has been published in the same form for 60 years. It incorporates the scientific and professional topics on geology, mining, geotechnology, materials and metallurgy. In the year 2013, the Editorial Board decided to modernize the journal's format.

A wide range of topics on geosciences are welcome to be published in the RMZ – Materials and Geoenvironment. Research results in geology, hydrogeology, mining, geotechnology, materials, metallurgy, natural and anthropogenic pollution of environment, biogeochemistry are the proposed fields of work which the journal will handle.

Editor-in-Chief

Zgodovinski pregled

Že več kot 90 let je minilo od ustanovitve Univerze v Ljubljani leta 1919. Tehnične stroke so se združile v tehniški visoki šoli, ki sta jo sestavljala oddelka za geologijo in rudarstvo, medtem ko je bil oddelek za metalurgijo ustanovljen leta 1939. Danes oddelki za geologijo, rudarstvo in geotehnologijo ter materiale in metalurgijo delujejo v sklopu Naravoslovnotehniške fakultete Univerze v Ljubljani.

Pred 2. svetovno vojno so člani rudarske sekcije skupaj z Združenjem jugoslovanskih inženirjev rudarstva in metalurgije začeli izdajanje povzetkov njihovega raziskovalnega dela v Rudarskem zborniku. Izšli so trije letniki zbornika (1937, 1938 in 1939). Vojna je prekinila izdajanje zbornika vse do leta 1952, ko je izšel prvi letnik nove revije Rudarsko-metalurški zbornik – RMZ v izdaji odsekov za rudarstvo in metalurgijo Univerze v Ljubljani. Danes revija izhaja štirikrat letno. RMZ – M&G izdajajo in financirajo Naravoslovnotehniška fakulteta v Ljubljani, Inštitut za rudarstvo, geotehnologijo in okolje ter Premogovnik Velenje. Prav tako izdajo revije financira Ministrstvo za izobraževanje, znanost in šport.

Na seji izdajateljskega sveta in uredniškega odbora je bilo 22. maja 1998 sklenjeno, da se Rudarsko-metalurški zbornik preimenuje v RMZ – Materiali in geookolje (RMZ – Materials and Geoenvironment) ali skrajšano RMZ – M&G. Revijo RMZ – M&G upravljata izdajateljski svet in mednarodni uredniški odbor. Revija je vključena v mednarodno izmenjavo svetovno znanih publikacij. Vsi članki so podvrženi recenzijskemu postopku.

RMZ – M&G je edina strokovno-znanstvena revija v Sloveniji, ki izhaja v nespremenjeni obliki že 60 let. Združuje področja geologije, rudarstva, geotehnologije, materialov in metalurgije. Uredniški odbor je leta 2013 sklenil, da posodobi obliko revije.

Za objavo v reviji RMZ – Materiali in geookolje so dobrodošli tudi prispevki s širokega področja geoznanosti, kot so: geologija, hidrologija, rudarstvo, geotehnologija, materiali, metalurgija, onesnaževanje okolja in biokemija.

Glavni urednik

Original scientific paper

Received: June 20, 2014
Accepted: July 10, 2014

Possibilties of further increasing the hot workability of ledeburitic tool steels

Možnosti nadaljnjega izboljšanja vroče preoblikovalnosti ledeburitnih orodnih jekel

Tatjana Večko Pirtovšek, Iztok Peruš, Goran Kugler, Peter Fajfar, Milan Terčelj*
Faculty of Natural Sciences and Engineering, University of Ljubljana, Aškerčeva cesta 12,1000 Ljubljana, Slovenia
*Corresponding author. E-mail: milan.tercelj@omm.ntf.uni-lj.si

Abstract

Ledeburitic tool steels are characterized by variable and essentially lower hot workability in comparison to other steels. In this contribution importance of selecting of appropriate values for some relevant process parameters in ledeburitic steels production, i.e. casting temperature, cooling rate at solidification and soaking temperature needed for improving of their intrinsic hot deformability, is given. Inappropriate selection of casting temperature and cooling rate results in precipitation of unusual eutectic carbides which decreases hot workability of these steels. With selection of appropriate soaking temperature a temperature range of safe hot working can be extended.

Key words: ledeburitic tool steels, process parameters, carbides, hot workability

Izvleček

Za ledeburitna orodna jekla je značilna variabilna in zelo nizka vroča preoblikovalnost v primerjavi z drugimi jekli. V tem prispevku je prikazana pomembnost pravilne izbire vrednosti nekaterih relevantnih procesnih parametrov pri izdelavi teh orodnih jekel, tj. pravilna izbira vrednosti za temperaturo litja, hitrost ohlajanja med strjevanjem in temperaturo ogrevanja za izboljšanje vroče preoblikovalnosti. Nepravilna izbira temperature litja in hitrosti strjevanja vodi do izločanja za ta jekla neobičajnih evtektičnih karbidov, kar znižuje vročo preoblikovalnost. Z izbiro pravilne temperature ogrevanja lahko precej razširimo temperaturno področje varnega preoblikovanja.

Ključne besede: ledeburitna orodna jekla, procesni parametri, karbidi, vroča preoblikovalnost

Introduction

Surface cracking during hot deformation of ledeburitic tool steels reduces mechanical properties and consequently their profitability. These tool steels have high hardness, wear resistance as well as high tempering resistance on one hand, and high flow stresses and low hot deformability on the other hand. Decreased hot deformability of the tool steels is attributed to type, size, shape, distribution, fraction of eutectic carbides and/or other phases and their melting points, grain and carbides growth at upper limit while precipitation of secondary carbides (fraction) and decreased recrystallization rate at lower limit of temperature working range. Increased hot workability in temperature range of 1 020–1 070 °C is attributed to combination of high recrystallization rate, low fraction of precipitated secondary carbides and relative low grain growth rate in this temperature range[1–5].

Occurrence of cracks on most exposed areas of workpiece are related to areas where similar conditions related to upper and/or lower limit of temperature working range prevail, i.e. areas with accelerated cooling, areas with higher value of accumulated strains where also decreased recrystallization rate with presence of higher tensile stresses simultaneously takes place, furthermore areas of workpiece which are due to combustion conditions in furnace heated on higher temperatures, etc. Thus areas, where combination of previous mentioned conditions prevail, are more exposed to cracking. This additionally suggests that hot deformability of ledeburitic tool steel should be considered as a complex problem. Publications in the literature with regards to hot deformability of tool steels are predominately of a partial nature thus all reasons for unexpected occurrence of cracks are not sufficiently explained in available literature so far. Furthermore modern practice proves that previous processing parameters significantly influence the hot deformability and thus this cannot be considered as a constant value. During heating, soaking and hot deformation various processes take place: decay (decomposition) of carbides, formation of new carbides, growth and dissolution of carbides, etc. Thus depending on variation of process parameters and of chemical composition, that consequently influences the processes related to carbides, shifting of decreased deformability at both limits of temperature working range to higher and/or to lower temperatures can occur[5–11].

In this contribution importance of proper selection of casting temperature, cooling rate and soaking temperature on hot workability of ledeburitic tool steels are presented. In the study M42, W.Nr. 1.2690 and D2 tool steels were included.

Description of applied tool steels and experiments

Applied tool steel

The proposed new approach will be illustrated with particular results obtained in thermo-mechanical processing of ledeburitic tool steels, i.e. M42 (super HSS) and W.Nr. 1.2690. All these steels contain C and carbide-forming elements, i.e. Cr, W, Mo and V (chemical compositions are given in Table 1). The microstructure of these steels consists of a martensitic matrix in which the ledeburitic and secondary carbides are inserted. In Figures 1a typical microstructures of ledeburitic tool steels for as-cast initial state are presented.

An optical microscope (OM, Carl Zeiss AXIO Imager.A1m) and a field-emission gun scanning electron microscope (FE SEM) in combination with an attached EDS (INCA x-SIGHT LN2 with INCA ENERGY 450 software) and EBSD (INCA CRYSTAL 300) analytical tools were used to observe the microstructures and to determine the type of carbides.

Table 1: *Chemical composition of applied tool steels in mass fractions, w/%: M42, W.Nr.1.2690 and D2*

	C	Si	Mn	Cr	Mo	V	W	Co
AISI M42	1.09	0.26	0.25	3.81	9.32	1.09	1.40	8.20
W.Nr. 1.2690	1.17	0.24	0.26	11.3	1.35	1.48	2.24	–
AISI D2	1.54	0.32	0.31	11.82	0.79	0.95	0.10	

Laboratory and industrial experiments for selection of appropriate process parameters

The influences of the selected casting temperature on hot workability, influence of cooling rate on obtained microstructure and selection of appropriate soaking temperature for selected initial microstructures were studied combining laboratory and industrial experiments. The industrial investigation of the hot workability involved studies of the influence of the casting temperature, the cooling rate and the soaking temperature on the initial microstructure as well as occurrence of cracking during the hot forging and hot rolling of ingots and billets. Laboratory hot compression tests for selecting of appropriate soaking temperatures were carried out on Gleeble 1500D thermo-mechanical simulator. Appropriate soaking temperature was determined individually for each of three different as-cast initial states (obtained at three different cooling rates) applying special procedure. The criterion for the assessment was the appearance of cracks on the compressed specimen's surface at appointed strain, strain rate and soaking time and the corresponding microstructure of the deformed cylindrical specimen with initial dimensions Φ = 10 mm × 15 mm. The procedure was repeated from the initial 1 200 °C and at decreasing temperatures until the compressed sample exhibited a crack-free surface. A detailed description of this procedure for determining the appropriate soaking temperature is given in[1]. The hot workability of selected tool steels was verified in industrial conditions using previously laboratory determined appropriate soaking temperature and then compared with a too-high temperature.

Casting at various temperatures and testing of hot workability

Results of influence of casting temperature on hot workability will be given at forging of 1.2690 tool steel. Hot forging of ingots with Φ = 143 mm, that were cast at a too-high and at appropriate temperature, respectively, were carried out and appearance of internal cracks in the central region of the forged and rolled billets were investigated.

Laboratory estimation of appropriate soaking temperature

Importance of selection of appropriate soaking temperature for initial as-cast microstructures obtained at various cooling rates; i.e. at cooling rate of 0.25 K/s and 0.16 K/s, on hot workability will be presented for M42 tool steel. Namely, at ledeburitic tool steels the cooling rate strongly influences the obtained microstructure, selection of appropriate soaking temperature and consequently also the hot workability. By applying the previously described procedure (detailed description is given in[1]) for hot compression test on Gleeble 1500D appropriate soaking temperatures for each initial as-cast microstructure were assessed. After laboratory assessment of appropriate soaking temperature this procedure was checked in industrial conditions, i.e. at hot rolling of ingots and continuously casted billets.

Results

Influence of casting temperature on microstructure and on hot workability

During the ultrasonic testing of the soft-annealed billets Φ = 143 mm from the 1.2690 tool steel, hot-forged from ingots that were cast at too-high temperature, for some billets or parts of billets internal defects were detected in their central region. The temperature of heat at the end of the vacuum treatment was 1 512 °C, which was recognized as being a too-high temperature. Figure 1a shows microstructure of carbide stringer perpendicular to the forging direction in the central region of a hot-forged and soft-annealed billet, which consists of spheroidised carbides, a larger quantity of ledeburitic carbides (which is unusual for this type of steel), microporosity and ferrite. Detail of carbide stringer is shown in Figures 1b, where beside carbides M_7C_3 and $M_{23}C_6$ which are usually present in these types of tool steels, also MC and M_6C carbides were found. All these carbides were confirmed by combined EBSD and EDS analyses. Inspection of microstructure also showed larger eutectic colonies with larger eutectic carbides, especially in the centre of the ingot, and consequently in thicker carbide

stringers in the microstructure after plastic deformation. Such kind of morphology is a consequence of too-high casting temperature that resulted in more intensive segregations of vanadium and tungsten and the precipitation of their carbides. Despite enormous carbide segregations in the ingot core the deformed steel did not crack during the radial hot forging. But during the subsequent hot rolling of the billets in a profile of $\Phi = 61$ mm, where tensile stress states are predominately present, the yield was approximately 15 % lower in comparison to charges that were cast at appropriate temperature. It is worth to mention that the microstructure which was taken from the centre of forged and rolled billet (ingot previously casted at appropriate temperature), consisted of ferrite, spheroidised carbides of type $M_{23}C_6$ and smaller ledeburitic carbides of type M_7C_3 while no MC and M_6C carbides were found.

A detailed investigation of the internal cracks in the central region of the billets with the optical microscope, FE SEM and the combined EDS and EBSD analyses of microstructure revealed that cracks did not follow the stringers consisting of the usual M_7C_3 and $M_{23}C_6$ types of carbides. Namely, cracks occur along the stringers that contain previously mentioned carbides that are unusual for this type of tool steels and are not present in case of appropriate casting temperature; i.e. small vanadium eutectic carbides and small complex eutectic carbides (see Figures 1c–d). The complex carbides are composed of small vanadium carbides of type VC surrounded by M_7C_3 in the central part and of precipitated $M_{23}C_6$ in the outer part. Thus in the regions where the carbide segregations are present (vanadium and complex carbides), the tool steels will crack during hot deformation.

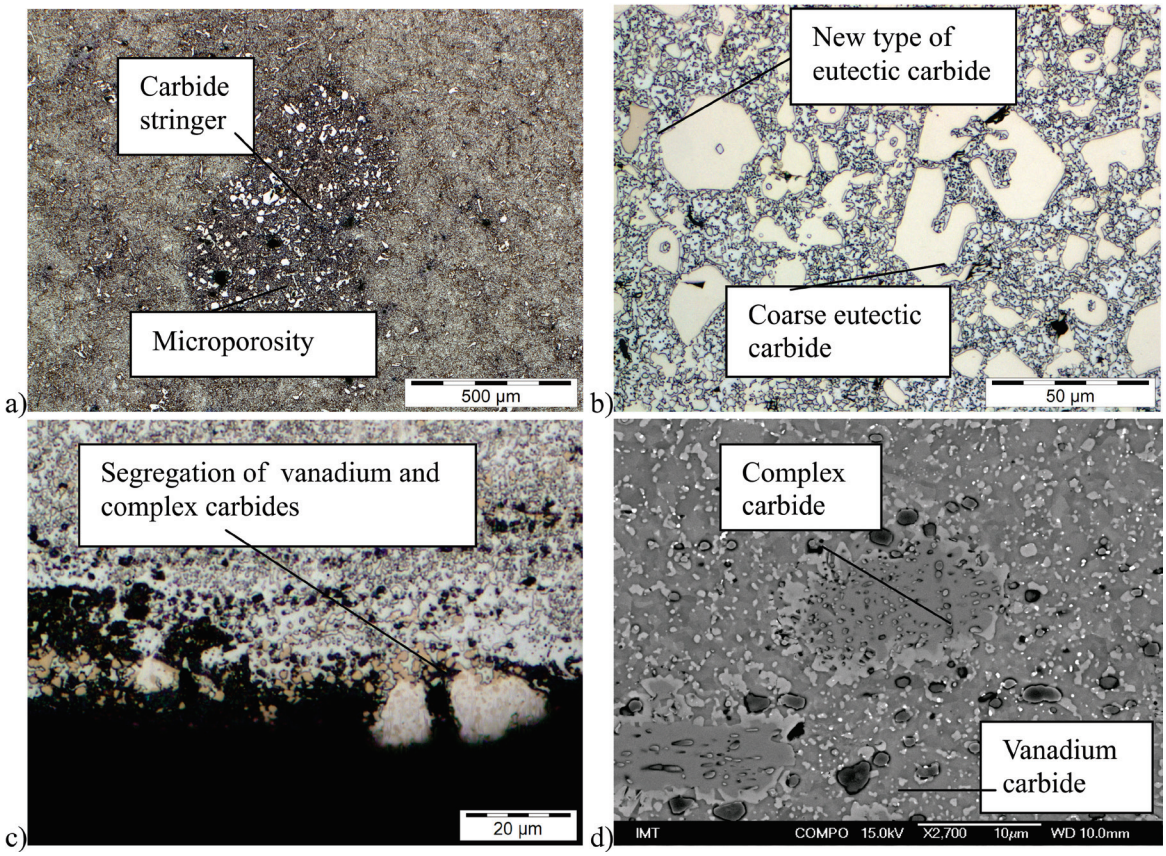

Figure 1: *The microstructure of a soft-annealed forged billet of $\Phi = 143$ mm from W.Nr. 1.2690 tool steel (perpendicular to the deformation direction): enormous carbide stringer in the centre of the billet, OM (a); larger eutectic carbides and a new type of carbide in the base microstructure from spheroidised carbides and ferrite in the carbide stringer, OM (b); appearance of cracking in the central part of the soft-annealed rolled billet steel along unusual segregations of "yellow-coloured" vanadium carbides, OM (c); segregation of vanadium and complex carbides at cracks (d).*

Appropriate soaking temperature and hot workability for various initial as-cast microstructures

Influence of soaking temperature on hot workability for microstructures in casting ingot

In cast ingot a variety of microstructure is usually obtained since each selected spot on ingot cross-section towards ingot centre different cooling rate. Thus for M42 tool steel and cooling rate of 0.25 K/s a microstructure shown in Figure 2a had obtained; the fine lamellar as-cast microstructure with precipitated M_2C type of carbides. On the other hand at cooling rate of 0.16 K/s beside M_2C type of carbides also for this tool steel unusual type of eutectic carbides, i.e. M_6C, precipitates (see Figure 2b). For cooling rate of 0.25 K/s and applying of inappropriate, i.e. too high soaking temperature (1 180 °C), a microstructure with coarse grains and coarse eutectic carbides (Figure 2c) in final rolled piece was obtained. Further, it was found out that in the case of too high soaking temperature at upper limit of temperature working range, due to coarsening of carbides, the hot workability was decreased. Namely, the number of small carbides decreases and the size of big carbides increases although their fraction changed according to phase equilibrium (diagram). On the contrary in the case of an appropriate soaking temperature (1 150 °C) the initial as-cast microstructure can be transformed into a fine grained microstructure with fine and equally (regularly) distributed eutectic carbides (Figure 2d); the number of large carbides is reduced which results in increased hot workability at upper and lower limits of temperature working range. Thus, the coarser carbides and/or carbide clusters, that have been formed during soaking, represent the spots for initiation of micro-cracks during initial stage of hot deformation as well as during final stage of hot deformation; thus by applying of appropriate soaking temperature the process of coars-

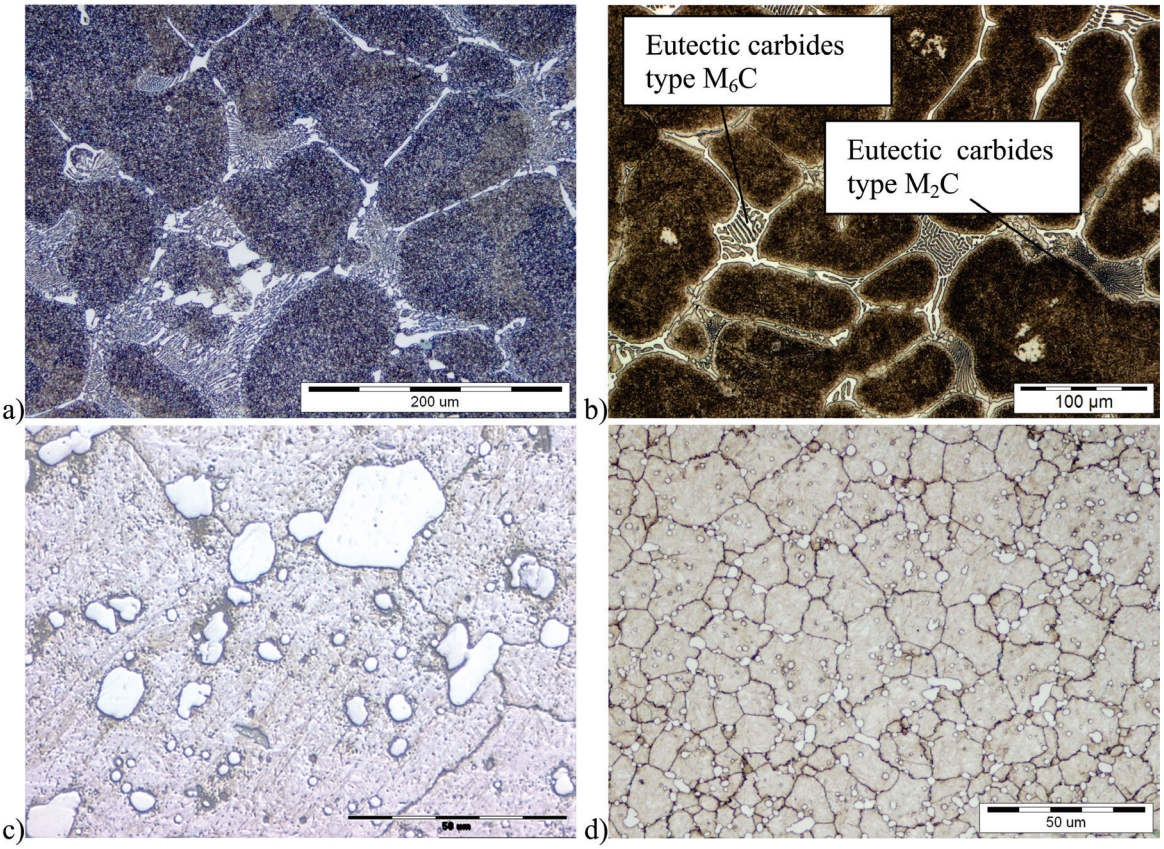

Figure 2: *Microstructure for M42 tool steel obtained at solidification rate of* 0.25 K/s *(a) and at solidification rate of* 0.16 K/s *(b), obtained microstructure after hot rolling applying of inappropriate (too high) soaking temperature of* 1 180 °C *for (c) and microstructure obtained in rolled piece at appropriate soaking temperature* 1 150 °C *(d).*

ening of carbides will be avoided which leads to extended temperature range of safe hot working. Similar results regarding the soaking conditions were obtained also for D2 and W.Nr.1.2690 tool steels.

Furthermore, these results show that the process of dissolution of fine carbides and coagulation as well as growth of coarser carbides during soaking before the hot deformation is irreversible. In the case of applying of too high soaking temperature with subsequent hot rolling the coarser carbides that form during soaking cannot be broken down and consequently coarser eutectic carbides are present in the final microstructure which also influences the mechanical properties of the final product.

Thus applying the soaking at too high temperature leads to decreased deformability at upper as well as at lower limits of temperature working range; this plays important role especially in hot deformation in several heats (reheating – deformation cycles) in industrial conditions.

Too slow cooling rates (microstructure on Figure 2b), as in the case of casting at too-high temperature (for 1.2690 tool steel (Figure 1)) result in occurrence of a new type of eutectic carbides that further leads to decreased hot deformability as it has been already presented in the case of casting at too high temperature. Thus too high casting temperature and too slow cooling rates of ledeburitic tool steels cannot be considered as mutual independent but as mutual dependent influential parameters.

Influence of soaking temperature on hot workability for microstructures in continuously casted billet

Influence of initial microstructure on selection of appropriate soaking temperature (M42 tool steel) will be illustrated on continuously cast billet square of 130 mm. Figure 3a shows as-cast microstructure 25 mm under the surface of the billet. In accordance with the described procedure in section 2 or in[1] temperature of

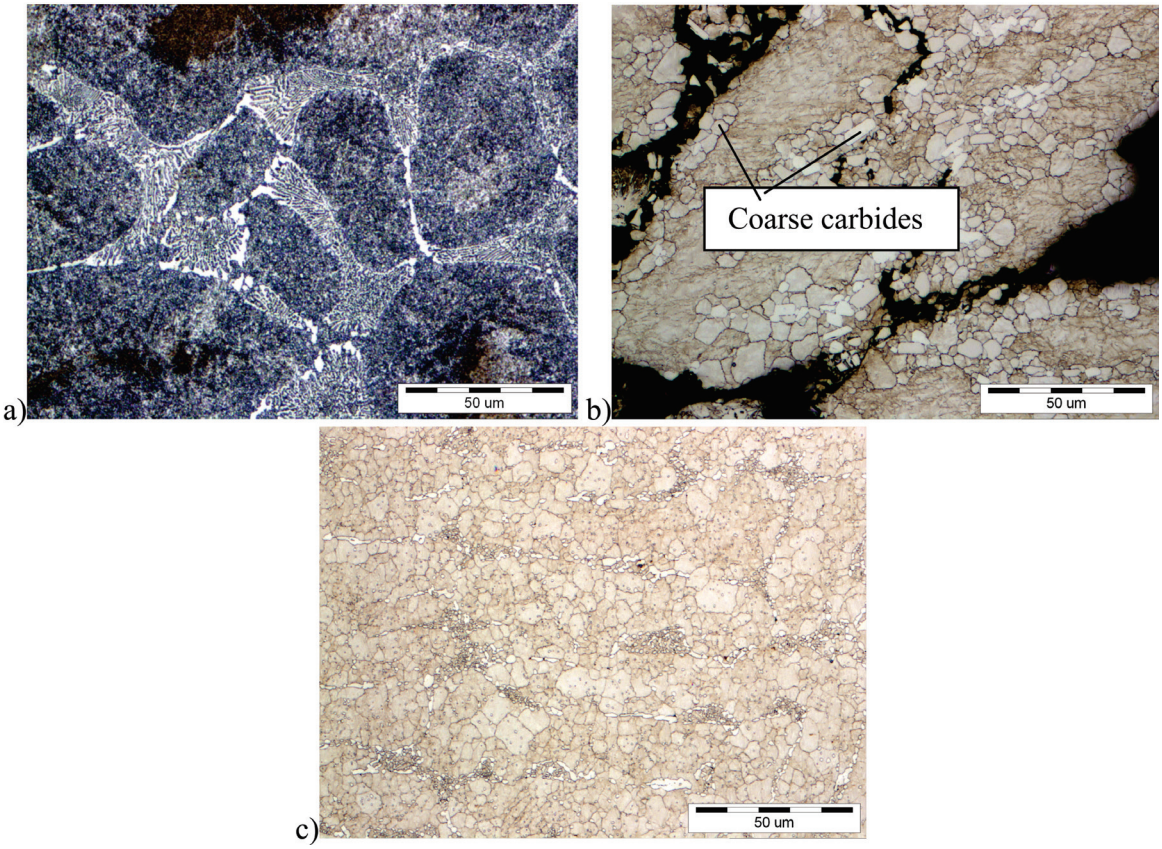

Figure 3: *Influence of soaking temperature on coarsening of carbides and on hot deformability for continuously cast M42 tool steel on upper limit of temperature range: initial as-cast microstructure (a); soaking and deformation temperature* 1 170 °C *(b); soaking and deformation at temperature of* 1 140 °C *(c).*

1 140 °C was determined as appropriate soaking temperature. Figures 3b-c shows the results of the influence of soaking on coarsening of carbides so at appropriate (1 140 °C) as well as at too high (1 170 °C) temperature and their influence on hot deformability. During soaking at 1 170 °C coarse carbides were formed that lowers hot deformability; this results in cracking along previous dendrite grain boundaries, where these carbides are concentrated (Figure 3b). At soaking temperature of 1 140 °C the coagulation and coarsening of carbides was not remarkable and the deformed sample did not crack (Figures 3c). It means that also in the case of soaking at too high temperature and subsequent hot deformation on lower temperature (a.m. 1 140 °C) the material will exhibit lower hot deformability due to presence of oversized carbides in matrix. Applying the soaking temperature of 1 150 °C, which was appropriate for the microstructure obtained at 0.25 K/s, for the continuously cast billet in Figure 3a led to decrease in hot deformability. Thus for each initial as-cast microstructure appropriate soaking temperature should be individually selected.

Conclusions

The results of the study of the influences of casting temperature, cooling rate and soaking temperature on the hot workability of ledeburitic tool steels can be summarised as follows:

— Selecting the correct values for casting and cooling rate as well as for soaking temperatures improves the intrinsic hot workability of the investigated ledeburitic tool steels.
— At a too-high casting temperature small unusual and/or small complex carbides additionally precipitate in the matrix during solidification. Cracking during hot deformation then predominately occurs along these carbides.
— A too-low cooling rate also results in precipitation of additional type of carbides, which are usually not formed during solidification at higher cooling rate. Due to their different properties they deteriorate the hot workability and influence the properties of the final products.
— The soaking temperature influences the dissolution, the spheroidisation, the coagulation and the growth of carbides, and the growth of austenitic grains. Selecting the appropriate soaking temperature extends the temperature range of safe hot working, so at its lower as well as at its upper limits. A too-high soaking temperature for a particular soaking time results in coarser carbides which leads to decrease of the hot workability at both limits of the temperature working range.

References

[1] Večko Pirtovšek, T., Kugler, G., Godec, M., Terčelj, M. (2011): Microstructural characterization during the hot deformation of 1.17C-11.3Cr-1.48V-2.24W-1.35Mo ledeburitic tool steel. *Materials Characterization*, 62(2), pp. 189–197.
[2] McQueen, H. J., Imbert, C. A. C. (2000): *Influence of carbides on the hot working of steel. Deformation, Processing and Properties of Structural Materials.* Edited by E. M. Tallef, C. K. Syn, and D. R. Lesuer, The Minerals, Metals & Materials Society, pp. 79–92.
[3] Liu, J., Chang, H., Wu, R., Hsu, T. Y., Ruan, X. (2000): Investigation on hot deformation behaviour of AISI T1 high-speed steel. *Materials Characterization*, 45, pp. 175–186.
[4] Imbert, C. A. C., McQueen, H. J. (2001): Hot ductility of tool steels. *Canadian Metallurgical Quarterly*, 40, pp. 235–244.
[5] Ghomashchi, M. R., Sellars, C. M. (1993): Microstructural Changes in As-cast M2 Grade High Speed Steel during Hot Forging. *Metallurgical Transactions A*, 24A, pp. 2171–2180.
[6] Brandis H., Haberling, E., Weigard, H. H. (1980): *Metallurgical Aspects of Carbides in High Speed steels. Processing and Properties of High Speed Tool Steels.* M. G. H. Wells and L. W. Lherbier, Ed., TMS_AIME, pp. 1–18.
[7] Fischmeister, H. F., Riedl, R., Karagöz, S. (1989): Solidification of High-Speed Tool Steels. *Metallurgical Transactions A*, 20A, pp. 2133–2148.
[8] Boccalini, M., Goldenstein, H. (2001): Solidification of high speed steels. *International Materials Review*, 46(2), pp. 92–115.
[9] Luan, Y., Song, N., Bai, Y., Kang, X., Li, D. (2010): Effect of solidification rate on the morphology

and distribution of eutectic carbides in centrifugal casting high-speed steel rolls. *Journal of Materials Processing Technology*, 210, pp. 536–541.

[10] Ding, P., Shi., G., Zhou, S. (1993): As-Cast Carbides in High-Speed Steels. *Metallurgical Transactions A*, 24A, pp. 1265–1272.

[11] Di, H., Zhang, X., Wang, G., Liu X. (2005): Spheroidizing kinetics of eutectic carbide in the twin roll-casting of M2 high speed steel. *Journal of Materials Processing Technology*, 166, pp. 359–363.

Original scientific paper

Received: Januar 7, 2014
Accepted: November 17, 2014

Compositional characteristics and petrogenetic features of metasediments of Ijero-Ekiti area, Southwestern Nigeria

Značilnosti sestave in petrogeneze metasedimentov z območja Ijero-Ekiti v jugozahodni Nigeriji

Oluwatoyin O. Akinola[1,*], Olugbenga A. Okunlola[2]
[1]Ekiti State University, Department of Geology, Ado-Ekiti, Nigeria
[2]University of Ibadan, Department of Geology, Ibadan, Nigeria
*Corresponding author. E- mail: oluwatoyinakinola@ yahoo.com

Abstract

Metasediments and subordinate mafic-ultramafic units within ancient migmatite-gneiss complex intruded by granite and pegmatite characterize the basement terrain of Ijero-Ekiti. Compositional characteristics and petrogenetic features of the metasediments (quartzite, biotite schist and amphibole schist) were investigated and reported. Mineralogical determinations from optical studies show that Ijero-Ekiti quartzite is composed of quartz and microcline, while the schistose units contain varying proportions of quartz, muscovite, biotite, and hornblende with subordinate opaque minerals.

Analytical data on major elements composition using Inductively Coupled Plasma Mass Spectrometry (ICP-MS) method revealed the siliceous (SiO_2 content ranging from 65.96–70.40 %) nature of the rocks. Trace element geochemistry using X-ray fluorescence (XRF) techniques show abundance of Ba, Zr, Sr, Rb and Ni in the quartzite, while the schistose rocks show enrichment in Ni and Rb. Ternary plots of MgO-CaO-Al_2O_3 and variation plot of Na_2O/Al_2O_3 versus K_2O/Al_2O_3 suggests sedimentary protolith for the investigated rocks. SiO_2 versus CaO and Na_2O versus K_2O plots show all samples in the field of greywacke. K_2O versus SiO_2 plot and ternary plot of (Na_2O + K_2O)-Fe_2O_3-MgO indicate calc-alkaline affinity for all samples. Provenance indicators such as Ba, and the concentration of immobile trace elements like Th in the quartzite unit suggests derivation of this sedimentary protolith from weathering of granitic rocks. Chemical Index of Alteration (CIA) for the schistose units shows moderate weathering intensity while index of compositional variability (ICV) reveals average compositional maturity for the sediments.

Key words: metasediments, protolith, Ijero-Ekiti, provenance, calc-alkaline

Izvleček

Metasedimenti in podrejeno mafično-ultramafične kamnine v starem migmatitno-gnajsnem kompleksu, intrudiranem z granitom in pegmatitom, so značilni za kristalinično podlago v Ijero-Ekiti. Poročamo o raziskavah značilnosti sestave in petrogeneze metasedimentov (kvarcita, biotitovega skrilavca in amphibolovega skrilavca). Mikroskopsko določene mineraloške značilnosti pričajo o tem, da sestoji ijero-ekitski kvarcit iz kremena in mikroklina, medtem ko vsebujejo skrilave kamnine različne deleže kremena, muskovita, biotita in rogovače s podrejenim deležem neprozornih mineralov. Analizni podatki o sestavi glavnih kemičnih prvin, določenih z induktivno vezano plazemsko masno spektrometrijo (ICP-MS), nakazujejo silikatno oz. silicijsko naravo kamnin (vsebnost SiO_2 se giblje med 65,96 % in 70,40 %). Geokemična sestava slednih prvin, določena z rentgensko fluorescenco (XRF), razkriva vsebnosti Ba, Zr, Sr, Rb in Ni v kvarcitu in obogatitev z Ni in Rb v skrilavih kamninah. Ternarni diagrami MgO-CaO-Al_2O_3 in variacijski diagrami Na_2O/Al_2O_3 s K_2O/Al_2O_3 nakazujejo sedimentno poreklo protolita raziskovanih kamnin. Na diagramih SiO_2 s CaO in Na_2O s K_2O se uvrščajo vsi vzorci v polje muljastega peščenjaka. Diagram K_2O z SiO_2 in ternarni diagram (Na_2O+K_2O)-Fe_2O_3-MgO pričajo o kalk-alkalni afiniteti vseh preiskanih vzorcev. Kazalniki porekla, kot je Ba, in vsebnosti nemobilnih slednih prvin kot Th v kvarcitni enoti nakazujejo, da izvira ta sedimentni protolit iz preperevanja granitnih kamnin. Indeks kemijskega preperevanja (CIA) skrilavih kamnin priča o zmerni stopnji preperevanja, medtem ko nakazuje indeks spremenljivosti sestave (ICV) povprečno sestavno zrelost izvornih sedimentov.

Ključne besede: metasedimenti, protolit, območje Ijero-Ekiti, izvor, kalk-alkalne kamnine

Introduction

The basement complex of Nigeria comprises Neoproterozoic-Early Paleozoic rocks and rocks of Pan-African age. These basement rocks, are loosely classified into three main lithological units. These are the ancient migmatite-gneiss complex, the schist belts and the Pan African granites[1] (Figure 1). The migmatite-gneiss suites are mainly sedimentary series with associated minor igneous rocks which have been variably altered by metamorphic, migmatic and granitic processes[2–4]. Schist belts more prominently occur in the western part of the country as an integral part of the basement rocks. They form essentially N-S trending belts of low to medium grade supracrustal rocks with minor metavolcanic assemblages of mafic to ultramafic rocks (Figure 1). The schist belts are composed largely of metamorphosed pelitic and psammitic assemblages. These bodies were believed to occur along west of 8° Meridian[2, 5, 6]. However, some poorly developed schist belts exist beyond these limits[7–10]. Schist belts exhibit distinct petrological and structural features. Some of these belts in the southwest include the Iseyin-Oyan, Igarra, Egbe-Isanlu and Ife-Ilesha schist belts[11–14]. The others are Lokoja-Jakura, Toto-Gadabuike belts[13, 15, 16] while the Obudu schist belt is the recently highlighted belt in southeastern Nigeria[10]. This study, presents geochemical and petrogenetic features of the metasediments around Ijero-Ekiti. The results are bringing better understanding to the evolution of schistose assemblages.

Lithological Association and Petrography

The study area is located 42 km northwest of Ado-Ekiti, the Ekiti State capital. The area lies between latitudes 7°46′N to 7°53′N and longitudes 5°00′E to 5°07′E. The metasediments of Ijero-Ekiti area are quartzite, biotite schist and amphibole schist. The schistose rocks underlie the central region where they are associated with units of migmatite gneiss complex. The latter comprises migmatite gneiss, biotite gneiss and calc gneiss, with subordinate epidiorite, granite and pegmatite (Figure 2). Quartzite occurs in isolated lenses around Ijero-Ekiti town and as thick-bedded, steeply inclined and extensive ridge around Oke-Oro (Figure 3). Biotite schist in the study area shows a north-south foliation trend and are poorly exposed. They are geomorphologically characterized by extensive lowlands particularly when they

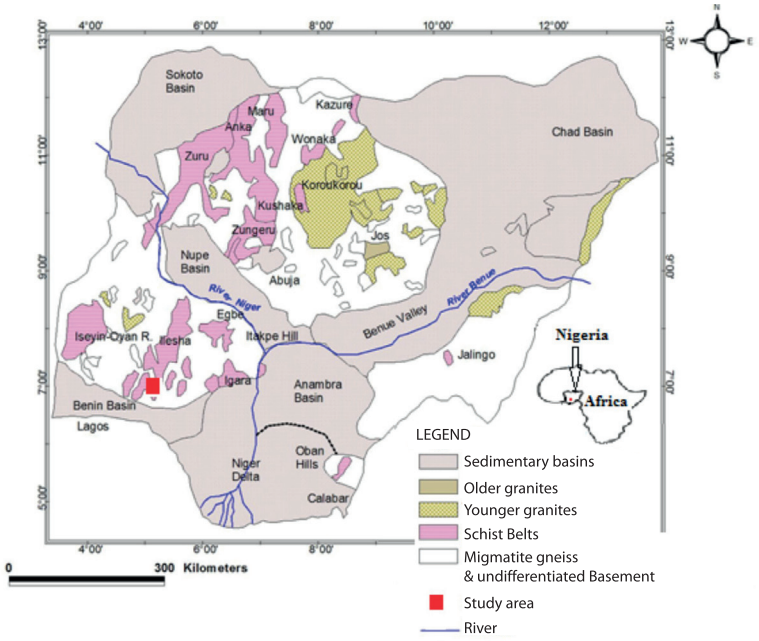

Figure 1: *Geological map of Nigeria showing location of the study area within the undifferentiated basement complex of the country.*

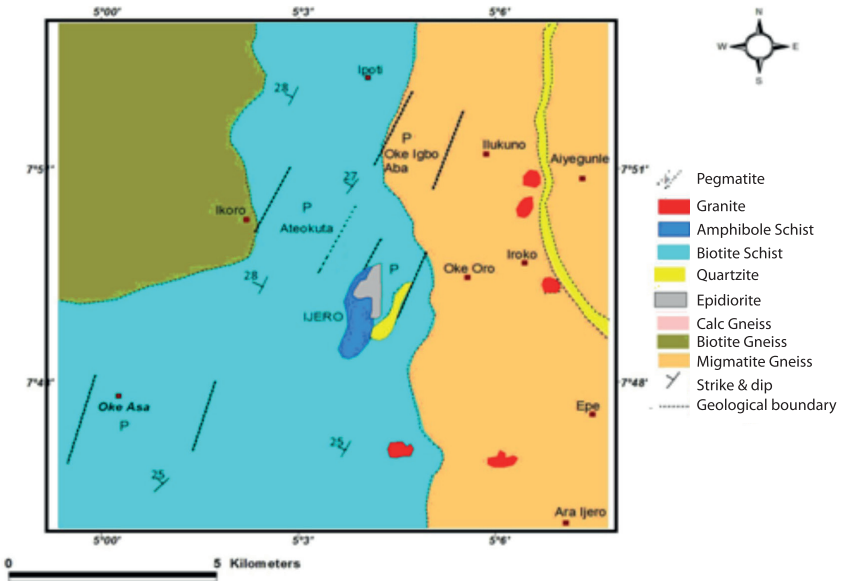

Figure 2: *Geological map of Ijero-Ekiti*[17].

Figure 3: *Exposure of the massive, thickly bedded, and steeply inclined Quartzite in the study area.*

occur in contact with quartz ridge or gneisses. This is a direct result of high susceptibility to weathering due to pronounced fissility. Therefore some outcrops occur as highly denuded masses along the major river channels. The occurrence of amphibole schist is restricted to the centre of the study area. Direct contacts between metasediments and associated rocks are poorly exposed. Pegmatite bodies form intrusions in older schistose rocks. Migmatite gneisses in the eastern part of the study area are found as denuded and highly foliated outcrops. They are invaded by scattered discontinuous but extensive north-south trending quartzite lenses. The northwestern part of the area is covered by fine-grained biotite gneisses. Calc-gneisses are restricted to the area around Ijero-Ekiti town. They are equigranular exhibiting weak foliation and are composed of quartz, muscovite and rare microcline crystals. Characteristic feature of calc-gneisses is their grayish to greenish colour and the lack of quartz vein intrusions.

Materials and methods

The study involves systematic geological mapping, samples were collected using standard geological techniques and thin sections study of each rock unit was undertaken. Forty-five samples (fifteen each for the three metasediments) were collected. Caution was taken to ensure that all the samples used are fresh, not weathered and uncontaminated. Subsequently, the samples were crushed, pulverized and sieved using sieve size 0.075 mm for geochemical investigations. 0.2 g sample aliquot was weighed into a graphite crucible and mixed with 1.5 g of $LiBO_2/LIBO_4O_7$. The sample charged was heated in a muffle furnace for 30 min at 980 °C. The cooled beads was dissolved in 100 m/L of 5 % HNO_3 (ACS grade Nitric acid) in de-mineralized water. An aliquot of the solution was poured into a propylene test tube. Calibration standard and verification standard were included in the sample sequence. Sample solution was aspirated into an ICP Mass Spectrometer (Perkin-Elmer Elan 9000) for the determination of major oxide at the Activation Laboratories in Ontario Canada.

Results and discussion

Petrography

For the biotite schist, biotite, muscovite and quartz are evidently visible minerals (Figure 4) but the amphibole schist shows preponderance of hornblende while quartz, biotite and accessory opaque minerals are the minor components (Figure 5). In thin section, quartz in biotite schist occurs as tiny and sub-angular grains with weak birefringence and low relief. In the amphibole Biotite occurs abundantly as the major schist, quartz grains occur as small, colourless and sometimes cloudy xenomorphic crystals. groundmass minerals and its characteristic green and brown colours, medium relief, weak birefringence colours and a low extinction angle ranging between 5° and 12° are its peculiarities. Modal analysis of the metasedimentary rocks are given in Table 1.

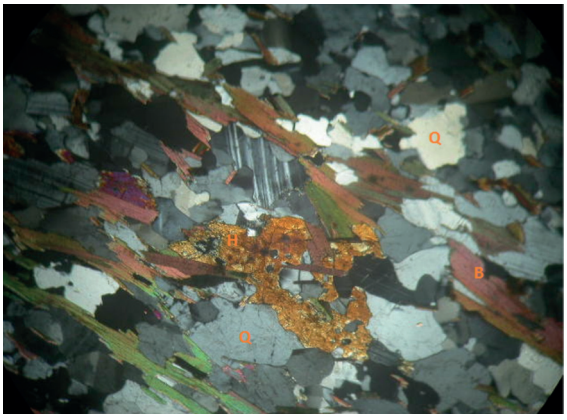

Figure 4: *Photomicrograph of Ijero-Ekiti biotite schist in transmitted light showing biotite (B), quartz (Q) and hornblende (H).*

Figure 5: *Photomicrograph of amphibole schist in transmitted light showing fine-grained sub-angular crystals of quartz (Q), stretched Hornblende(H) and aligned Biotite (B).*

Geochemical features

Analytical result (Table 2) indicates that average SiO_2 value in quartzite is 70.01 %. This value however, is slightly lower than the Okemesi quartz schist[18], quartz schist of Ibadan area[19]. Also, many other quartzite samples in the Nigerian metasedimentary belts[1, 20, 21]. These values make them chemically similar to quartz sandstones[22] and comparable to Jebba quartzite and micaseous quartzite of central Nigeria[23]. Conversely, the average SiO_2 value in the biotite schist (67.01 %) and amphibole schist (67.91 %) is within the limits for average schistose rocks of Nigeria[24, 25]. They are also similar to Jakura quartz mica schist[1]. Average Al_2O_3 content is lowest in quartzite (10.72 %) while amphibole schist (15.29 %) has higher average value than biotite schist (12.35 %) does. Conversely, Fe_2O_3 values in biotite schist ranges between 6.73 % and 7.79 % with an average of 7.26 % while in amphibole schist the

Table 1: *Modal composition of metasediments of Ijero-Ekiti*

Minerals	Quartzite			Mean	Biotite Schist			Mean	Amphibole Schist			Mean
Quartz	58	56	55	56	32	35	34	34	29	25	31	28
Hornblende	2	7	4	4	4	6	4	5	35	34	38	36
Biotite	8	5	6	10	43	37	46	42	9	11	8	9
Muscovite	26	23	26	25	12	15	13	13	9	4	4	6
Feldspar	4	3	4	4	3	3	3	3	10	18	10	13
Opaque	4	6	4	1	5	4	–	3	8	8	7	8
Total	100	100	100	100	100	100	100	100	100	100	100	100

values that range between 5.56 % and 6.03 % with an average of 5.88 %. Quartzite records iron oxide content ranging between 7.50 % and 9.12 % with a mean value of 8.14 %. Mean MnO content is generally lower than 1.5 % in all the metasediments. The values of SiO_2, Al_2O_3, Fe_2O_3 and MnO are however within the range for most metasediments[26]. MgO, CaO and Na_2O have average values that are generally less than 3.00 % with biotite schist (2.33 %) recording the highest mean MgO content. However, amphibole schist (2.04 %) has the highest mean CaO content and Na_2O (1.67 %) values as against 1.15 % and 1.56 % respectively for biotite schist and 1.49 % and 1.60 % for quartzite. Average Na_2O content of Ijero biotite schist is comparable to the phyllitic schist around Lokoja-Jakura area[1]. The average TiO_2 content is generally low in all the samples, however amphibole schist (0.05 %) records a slightly higher value as against quartzite (0.03 %) and biotite schist (0.03 %) from Okemesi area[18], but the values are lower than quartz schist and biotite muscovite schists of the same area. These values are comparable to the Ibadan quartz schist[19]. Mean K_2O content of biotite schist (4.03 %) is higher than quartzite (2.55 %) with amphibole schist (1.66 %) recording the least

Table 2: *Chemical composition of metasediments of Ijero-Ekiti*

Oxides (%)	Quartzite (*N* = 15 samples)		Biotite Schist (*N* = 15 samples)		Amphibole Schist (*N* = 15 samples)	
	Range	Mean	Range	Mean	Range	Mean
SiO_2	69.20–70.40	70.01	65.96–67.46	67.01	66.97–68.11	67.91
Al_2O_3	9.98–12.44	10.72	11.07–13.05	12.36	14.60–16.04	15.29
Fe_2O_3	7.50–9.12	8.54	6.73–7.79	7.26	5.56–6.03	5.88
MnO	1.14–1.56	1.35	0.10–0.27	0.18	0.11–0.24	0.17
MgO	0.82–1.20	1.08	1.74–3.61	2.33	1.09–1.43	1.25
CaO	1.38–1.63	1.49	1.13–1.20	1.15	1.94–2.16	2.04
Na_2O	1.62–1.93	1.60	1.53–1.80	1.56	1.34–2.00	1.67
K_2O	2.00–2.75	2.55	1.80–4.08	4.03	1.54–1.80	1.66
TiO_2	0.03	0.03	0.03–0.050	0.03	0.03–0.07	0.05
P_2O_5	0.31–0.51	0.39	0.84–1.02	0.92	0.01–0.033	0.01
LOI	1.30–2.90	2.23	2.80–3.90	3.10	3.51–4.70	4.01

Table 3: *Trace element composition of metasediments of Ijero-Ekiti*

Trace elements (µg/g)	Quartzite		Biotite Schist		Amphibole Schist	
	Range	Mean	Range	Mean	Range	Mean
Ba	15.0–76.0	52	85–211	123	94–162	121.2
Sr	19–55	34	43–94	59	59–281	183.7
Ni	4–32	18	115–192	134.7	164–223	196.3
Cu	5–21	11.5	15–53	29.5	42–70	53.7
Rb	17–31	24.5	35–157	101.2	75–128	99.8
Zr	169–242	199.2	50–143	88.3	39–102	70
U	15.4–28.2	19.5	15.8–29.3	21.4	7–23	11
Th	2.0–23	11.7	7.4–26	18.2	15–43	23
La	2–9	5	5–12	7	14–28	19
La/Th		0.43		0.39		0.83
Th/U		0.6		0.38		2.1
CIA (%)	**63–69**	**66**	**65–73**	**69**	**73–75**	**74**
ICV	**1.17–1.70**	**1.43**	**1.11–1.48**	**1.25**	**0.78-0.86**	**0.82**

mean value. The values are still within the limits for metasedimntary rocks[27] and comparable to that of Scottish metapelites[20], Igarra quartz mica schist[28], Okemesi quartz schist[18], the Burum marble[16]. These values are however higher than those for Ibadan quartz schist[19]. The metasediments (Table 3) shows a pronounced enrichment in Ba, Sr, Ni and Rb in biotite schist and amphibole schist than in the quartzite. Zr content of all the rocks is appreciably high but Cu values are comparatively low in all the rocks.

Provenance of the protolith and Tectonic Setting

Generally, when compared to similar rocks, the average SiO_2, Na_2O and K_2O values of Ijero metasediments are low. This may suggest addition of argillaceous materials, hence fluctuating energy levels in the environment. The indiscernible trend in the K_2O versus SiO_2 diagram (Figure 6) may imply that K-metasomatism or metamorphic differentiation within each rock group was minimal. The petrogenetic character of the rocks as established on the Na_2O/Al_2O_3 versus K_2O/Al_2O_3 plot (Figure 7)[29] shows the entire samples plotting in the sedimentary/metasedimentary field, implying that the rocks are largely of sedimentary origin, hence a common origin for the protolith of the rock units. In the MgO-CaO-Al_2O_3 diagram (Figure 8;[30], the samples plot outside the magmatic field also supporting the sedimentary antecedent of the rocks. These features makes the Ijero-Ekiti metasediments similar to those of Ilesha[13], Birnin-Gwari schist[31] and Jebba schists[23, 32]. The provenance of sedimentary rocks inferred from the framework constituents of the rocks[23, 33–35]. From a low Ba, Rb and Sr content of quartzite (Table 3) as against biotite and amphibole schist, and in particular, the high Zr content in all the samples may reflect the presence of detrital zircon in the rocks[13]. There is also a strong possibility of a sedimentary source of greywacke composition, although the contribution of a felsic source is certain[23, 32, 36]. This is further supported by the plot of the samples within the field of Franscisian greywacke on the SiO_2 versus CaO diagram of[27] (Figure 9).

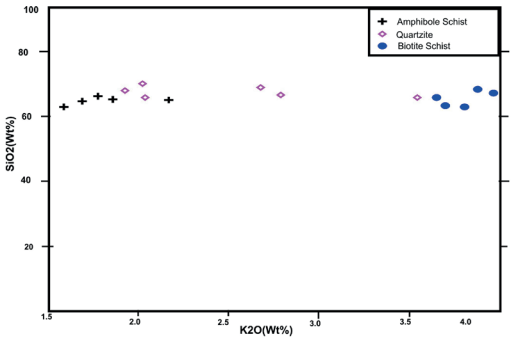

Figure 6: *SiO_2 versus K_2O plot of Ijero metasediments (After[37]).*

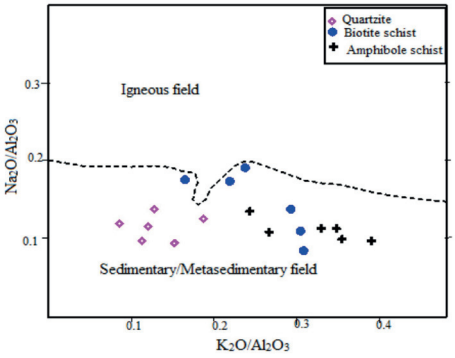

Figure 7: *Na_2O/Al_2O_3 versus K_2O/Al_2O_3 plot of Ijero metasediment (After[29]).*

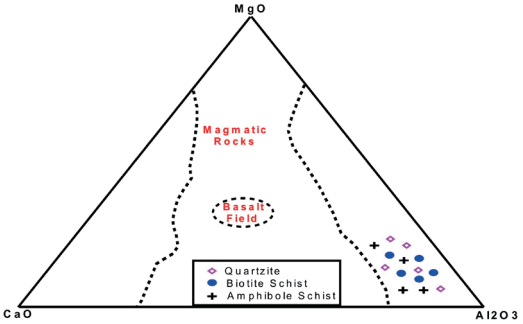

Figure 8: *MgO-CaO-Al_2O_3 plot of Ijero metasediments (After[27]).*

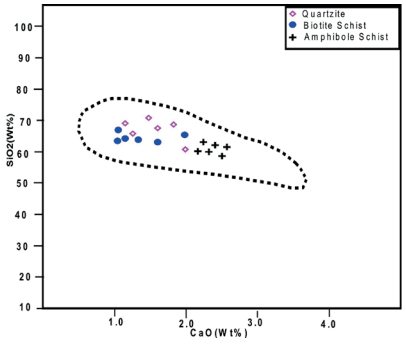

Figure 9: *SiO_2 versus CaO plot of Ijero metasediments (After[38]).*

These features makes the Ijero-Ekiti metasediments similar to those of Ilesha[13], Birnin-Gwari schist[31] and Jebba schists[23, 32]. The provenance of sedimentary rocks inferred from the framework constituents of the rocks[23, 33–35]. From a low Ba, Rb and Sr content of quartzite (Table 3) as against biotite and amphibole schist, and in particular, the high Zr content in all the samples may reflect the presence of detrital zircon in the rocks[13]. There is also a strong possibility of a sedimentary source of greywacke composition, although the contribution of a felsic source is certain[23, 32, 36]. This is further supported by the plot of the samples within the field of Franscisian greywacke on the SiO_2 versus CaO diagram of[27] (Figure 9). The plot of Na_2O versus K_2O (Figure 10) further indicates the metasediments plotting within the greywacke field. The plot of lg (Fe_2O_3/K_2O) versus lg (SiO_2/Al_2O_3) diagram[39] (Figure 11), shows the quartzite and most of the amphibole schist plotting in the Fe-sand field, while the biotite schist plot in the greywacke field. This agrees with the relatively high Ba and Rb content (Table 2) indicating contribution of felsic components since high Ba indicates K-feldspar-rich source rocks,[20, 40]. For all the metasediments, the total alkali versus silica plot of[38] (Figure 12) reveals samples plotting in the dacite field indicating a protolith of dacitic composition. The ($Na_2O + K_2O$) – Fe_2O_3 – MgO ternary plot (Figure 13) after[41] further discriminates the samples as having a calc-alkaline affinity. A further confirmation by the K_2O versus SiO_2 plot (Figure 14) after[38] shows that the schistose rocks of Ijero-Ekiti area have a petrogenetic character that is similar to those in Okemesi area[18]. However, this characteristic differentiates them from many schistose rocks of tholeiitic with Archean metabasalt affinity in the basement complex of Nigeria[1, 13, 20, 21, 24].[42] have indicated the importance of such immobile trace elements as Th and La in provenance study of pelitic metasediments because they often reflect those of source rocks. The Th content of Ijero-Ekiti metasediments (2.0–23.0 µg/g) is comparable to those derived from granitic composition and is similar to those of Okemesi schistose rocks[18]. The low La/Th and Th/U especially those for the biotite and amphibole schists are

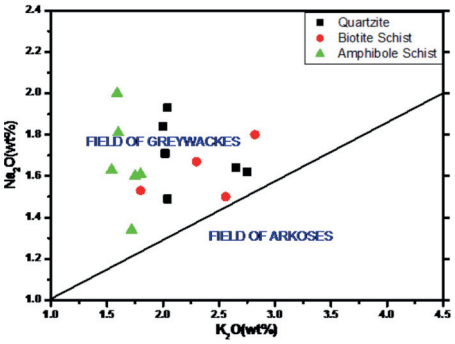

Figure 10: *Na_2O versus K_2O plot of Ijero metasediments (After[39]) metasediments.*

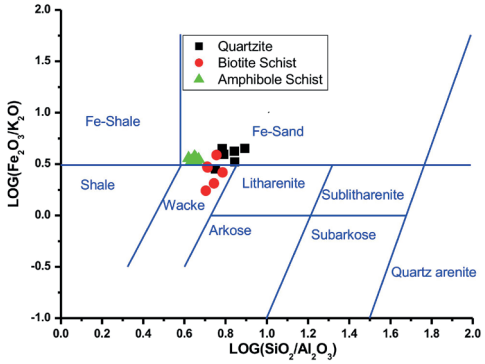

Figure 11: *Log (Fe_2O_3/K_2O) versus. Log (SiO_2/Al_2O_3) of Ijero.*

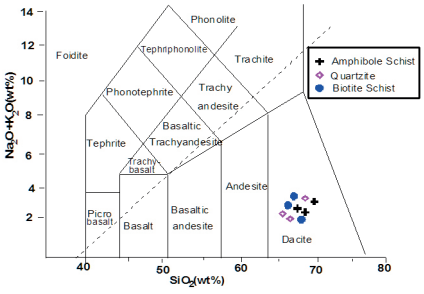

Figure 12: *Na_2O+K_2O versus SiO_2 (Total alkali versus Silica) plot of Ijero metasediments (After[38]).*

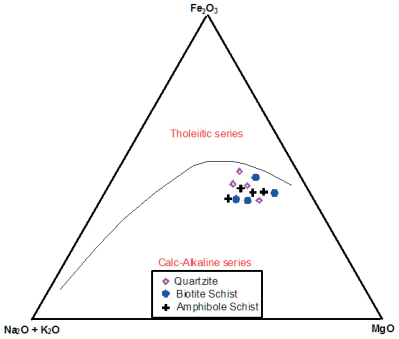

Figure 13: *(Na_2O+K_2O)-Fe_2O_3-MgO plot for metasediments of Ijero-Ekiti (After[41]).*

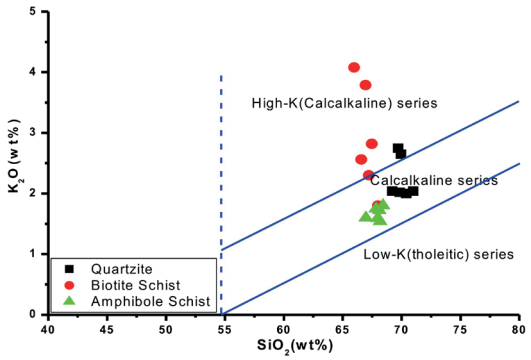

Figure 14. *K_2O vs SiO_2 Ternary plot for the metasediments of Ijero-Ekiti (After[38]).*

comparable to those of post Archean recycled upper crust sources[30, 42].

The results of the Chemical Index of Alteration (CIA)[43, 44] defined as

$CIA = [Al_2O_3 / (Al_2O_3 + CaO + Na_2O + K_2O)] \times 100$

(Table 3) reveal average values for the quartzite (66 %), biotite schist (69 %) and amphibole schist (74 %); these values indicate relatively intense chemical weathering of the source rocks. The Index of Compositional Variability (ICV)[45] defined as

$ICV = (Fe_2O_3 + K_2O + Na_2O + CaO + MgO + TiO_2) / Al_2O_3$

(*w*/%) which measures the abundance of alumina relative to other constituents of the rock except SiO_2 show that the quartzite, biotite schist and amphibole schist have average ICV value of 1.43, 1.25, and 0.82 respectively (Table 3). Compositionally immature pelitic rocks have high ICV, whereas mature pelitic rocks with little non-silicates possess low values (< 0.6)[1]. The calculated ICV value for the quartzite (1.43) shows the immature nature of the sedimentary protolith prior to meramorphism. Mature to moderately mature metasediments are characteristics of relatively stable cratonic environments[26]. This may mark sediment recycling or moderate to very intense chemical weathering of first cycle material[46].

Conclusions

Systematic geological mapping, petrographic study and geochemical evaluation of the schistose rocks around Ijero-Ekiti show that the metasediments are continental post-Archean supracrustal assemblages. The sedimentary protolith prior to metamorphism have had greywacke affinity, and are derived from granitic source rocks rich in felsic components the quartzite was derived from moderate to fairly intense weathering of these rocks. The schistose rocks were probably deposited in a miogiosynclinal basin that was characterized by subsidence with rapid rates of sedimentation.

References

[1] Elueze, A. A., Okunlola, O. A (2003): Geochemical features, petrogenetic affinity of Precambrian amphibolites of Burum area, central Nigeria. *Journal of Mining and Geology,* 39(2), 1–9

[2] Oyawoye, M. O. (1972): *The Basement complex of Nigeria in: Dessauvagie*. T. F. J. and Whiteman, A. J. (eds) African Geology, University of Ibadan, pp. 66–102.

[3] Rahaman, M. A. (1988): Recent advances in the study of the basement complex of Nigeria. Precambrian Geol. of Nigeria, (Eds. Oluyide et al), *Geol. Surv. Nigeria,* pp. 11–41.

[4] Okunlola, O. A. (2005): Metallogeny of Ta-Nb mineralization of the Precambrian pegmatites of Nigeria. *Mineral wealth,* 137.

[5] Oyawoye, M. O. (1964): The Geology of the Nigerian basement complex Nigeria. *Journal of Mining Geology and Metallurgical Soc.,* 1, pp. 97–102.

[6] McCurry, P. (1976): *The Geology of the Precambrian to lower Paleozoic rocks of Northern Nigeria - a review.* In C. A. Kogbe (ed.). Geology of Nigeria; Elizabethan Publ., Lagos, pp. 15–39.

[7] Ajibade, A. C. (1976): *Provisional Classification and Correlation of the schist belt of Northwestern Nigeria.* Geology of Nigeria; Kogbe, C. A (ed.), Elizabethan Pub. Co., Lagos, pp. 85–90

[8] Emeronye, B. F. (1988): *Appraisal of manganese mineralization around Ikpeshi, Bendel State, Nigeria.* Abstract of seminar GSN 5p.

[9] Eneh, K. E., Mbonu, W. C., Ajibade, A. C. (1989): The Nigerian metasedimentary belts. Facts, fallacies and New Frontiers. In: Oluyide, P.O. (ed.) Precambrian geology of Nigeria. *Geol. Survey of Nigeria,* 201 p.

[10] Ekwueme, B. N., Shing, R. (1987): *Occurrence, Geochemistry and Geochronology of Mafic-Ultramafic rock in the Obudu Plateau, southeastern Nigeria*. In Srivasta. R. K. and Chadta, R. (eds) Magmatism in relation to diverse tectonic settings. pp. 42–57.

[11] Rahaman, M. A. (1976): *Review of the Basement geology of Southwestern Nigeria.* In Geology of Nigeria (C. A. Kogbe. Ed), Elizabethan pub. Co., Lagos, pp. 41–58.

[12] Odeyemi, I. B. (1977): *The basement rocks of Bendel state of Nigeria.* Unpublished Ph. D. Thesis, University of Ibadan.

[13] Elueze, A. A. (1981): Rift system for proterozoic schist belt in Nigeria. *Tectonophysics,* 209, pp. 167–169.

[14] Annor, A. E., Olobaniyi, S. B., Mucke, A., (1996): A note on the Geology of Isanlu area, in the Egbe-Isanlu schist belt, S. W. Nigeria. *Min. Geol.,* 32(1), pp. 47–52.

[15] Muotoh, E. O. G., Oluyide, P. O., Okoro, A. U., Mogbo, O. E. (1988): *The Muro Hills banded iron formation G. S. N.* Annotated technical reports, 1358, pp. 15–25.

[16] Okunlola, O. A. (2001): *Geological and Compositional Investigation of Precambrian Marble bodies and associated rocks in the Burum and Jakura areas, Nigeria.* Ph. D. Thesis, University of Ibadan, Nigeria, 193 p.

[17] Okunlola, O. A, Akinola, O. O. (2010): Petrochemical Characteristics of the Precambrian rare metal pegmatite of Oke-Asa area, southwestern Nigeria: implication for Ta-Nb mineralization. *RMZ-Materials and Geoenvironment,* 57(4), pp. 525–538.

[18] Okunlola, O. A. , Okoroafor, R. E (2009): Geochemical and petrogenetic features of schistose rocks of the Okemesi fold belt, southwestern Nigeria. *RMZ-Materials and Geoenvironment,* 56(2), pp. 148–162.

[19] Okunlola, O. A., Adeigbe, O. C., Oluwatoke, O. O. (2009): Compositional and Petrogenetic features of schistose rocks of Ibadan area, southwestern Nigeria. *Earth Science Research Journal,* 13(2), pp. 29–43.

[20] Okonkwo, C. T. (1992): Structural geology of basement rocks of Jebba area, Nigeria. *Journal of mining and Geology,* 28(2), pp. 203–209.

[21] Okunlola, O. A., Akintola, A. I., Egbeyemi, R. O. (2006): Compositional features and petrogenetic affinity of Precambrian amphibolitic schists of Sepeteri area , southwestern Nigeria. *Journal of Geological sciences,* 4(2), pp. 199–207.

[22] Blatt, H., Middleton, C., Murray, R. (1972): *Origin of sedimentary rocks.* Prentence-Hall Inc. Englewood Cliffs, New Jersey, 643 p.

[23] Okonkwo, C. T. (2006): Chemical Evidence for the Sedimentary Origin of Igarra Supracrustal Rocks S. W. Nigeria. *Journal of Mining and Geology,* 22, pp. 97–104.

[24] Ajayi, T. R (1980): On the origin and Geochemistry of amphibolites of Ife-Ilesha area, southwestern Nigeria. *Jour. of Min. and Geol.,* 17, 170–195.

[25] Elueze, A. A. (1985): Petrochemical and petrogenetic characteristics of Precambrian amphibolites of the Alawa district, Northwest Nigeria. *Chemical Geology,* 48, 29–41.

[26] Weaver, C. E. (1989): *Clays, muds and shales.* Elsevier, Amsterdam, 820 p.

[27] Brown, E. H., Babcock, R. S., Clark, M. D. (1979): Geology of Precambrian rocks of Grand Canyon in Petrology and structure of Vishu Complex. *Prec. Res.,* 8, pp. 219–241.

[28] Okeke, P. O, Meju, M. A. (1985): Chemical evidence for the metasedimentary origin of Igarra Supracrustal rocks S. W. Nigeria. *Journal of Mining and Geol.,* 22(1 and 2), pp. 97–104.

[29] Garrels, R. M, Mackenzie, F. F. (1971): *Evolution of sedimentary rocks.* W. M. Norton and Co., New York, 394 p.

[30] Leyleroup, A., Duppy, C., Andrianmbolona, R. (1977): Chemical composition and consequence of Evolution of French Massive Central Precambrian crust. *Mineral Petrol,* 62, pp. 283–300.

[31] Ajibade, A. C (1980): *Geotectonic evolution of the Zungeru region Nigeria.* Unpub. Ph. D. Thesis, University Col. Wales, 303 p.

[32] Okonkwo, C. T., Winchester, J. A. (1996): Geochemistry and geotectonic Setting of Precambrian Amphibolites and Granitic gneisses in the Jebba Area, Southwestern Nigeria. *Journal of Mining and Geol.,* 32(1), pp. 11–18.

[33] Pettijohn, T. J. (1975): Sedimentary rocks. Harper and Brothers, New York, 718 p.

[34] Potter, P. E. (1978): Petrology and chemistry of modern big river sands. *J. Geol.,* 86, pp. 423–449.

[35] Dickinson, W. R., Vallani, R. (1980): Plate settings and provenance of sands in Modern ocean basins. *Geology,* 8, pp. 82–86.

[36] Van De Kamp, P. C., Leake, B. E. (1986): Petrography and Geochemistry of Feldsparthic and Mafic Sediments. *Trans. Roy. Soc. Edin. Earth Sci.,* pp. 411–499.

[37] Okunlola, O. A (2003): Petrochemical and Petrogenetic Characteristics of metasedimentary rocks of Lokoja-Jakura Schist belt, Central Nigeria. *Journal of Mining and Geology,* 39(1), pp. 21–28.

[38] Le Maitre, R. W., Batman, P., Dudek, A. M., Keller, J., Lameyre, Le Bas, M. J., Sabine, P.A., Schmid, R., Sorensen, H., Streekensen, A., Wolley, A. R ,Zenettin, B. (1989): *Classification of Igneous rocks and glossary of terms.* Recommendations of the international Union of Geological Sciences, Sub-commission on the systematic of Igneous Rocks (Oxford, U K, Blackwell Scientific Publications).

[39] Winkler, H. G. F. (1967): *Petrogenesis of metamorphic rocks.* Rev. second Edition. Springer Verlag, Berlin, 237 p.

[40] Okonkwo, C. T., Winchester, J. A. (1998): Petrochemistry and Petrogenesis of migmatitic gneisses and metagreywackes in Jebba area, southwestern Nigeria. *Journal of Mining and Geology,* 36(1), pp. 1–8.

[41] Kuno, H. (1968): *Differentiation of Basaltic magma.* In Hess, H. H. and Poldervaart (eds), Basalt: The Poldevaart Treatise on rocks of basaltic composition, Vol. 2, Interscience, New York, pp. 623–688.

[42] Taylor, S. R., Mclannan, S. M. (1985): *The continental crust: Its composition and Evolution.* Oxford, 311 p.

[43] Nesbitt, H. W., Young, G. M. (1982): Early Proterozoic Climates and Plate Motions inferred from Major element chemistry of Lutites. *Nature,* 199, pp. 715–717.

[44] Okunlola, O. A., Jimba, S. (2006): Compositional trends in relation to Tantalum-Niobium mineralization in Precambrian pegmatites of Aramoko-Ara-Ijero area, Southwestern Nigeria. *Journal of Mining and Geology,* 42 (2), pp. 113–126.

[45] Cox, R., Lowe, D. R. (1995): Controls on sediment composition on a regional scale. Conceptual view; *Journal of Sed. Research*, 65, pp.1–12.

[46] Bershad, I. (1966): *The effect of a variation in precipitation on the nature of clay mineral formation in soils from acid and basic igneous rocks.* Proceedings, International, Clay conference, pp. 167–173.

Original scientific paper

Received: February 7, 2014
Accepted: November 19, 2014

Distribution of radioactive elements of some rocks in South-western Nigeria

Porazdelitev radioaktivnih prvin v nekaterih kamninah jugozahodne Nigerije

M. A. Oladunjoye[1,*], A. Akinmosin[2], U. K. Ekugum[1]
[1]University of Ibadan, Department of Geology, Ibadan, Nigeria
[2]University of Lagos, Department of Earth Sciences, Akoka, Lagos, Nigeria
*Corresponding author. E-mail: ma.oladunjoye@yahoo.com

Abstract

Rock samples obtained from two locations in parts of south-western Nigeria were studied to establish the distribution of U, Th and K, present in them. Field data were collected using a gamma ray scintillometer while laboratory studies on the samples included spectrometric analysis, NaI(Tl) spectrometry and geochemical analysis (ICP-MS method). Gamma ray scintillometric reading showed that the outcrops present in the study areas gave consistently higher readings than the overburden materials. The analysis of spectrometric data indicated the presence of other radio-nuclides which are different from the three principal radio-nuclides, ^{238}U, ^{232}Th, and ^{40}K. Results of the geochemical data revealed the presence of radioactive elements like Pb, Ce, La, Ti and Fe^{2+}. This study showed that besides the presence of U, Th and K, other elements like Pb, Ce, La and Ti also contributed to the bulk radioactivity measured in rock samples at the study areas. Zircon, xenotime and possibly thorite are the main radioactive minerals present in the studied rocks.

Key words: Radioactive elements, Radio-nuclides, Radioactive minerals

Izvleček

Vzorce kamnin z dveh lokacij na območju jugozahodne Nigerije smo preiskali, da bi v njih določili vsebnosti U, Th in K. Na terenu smo opravili merjenje z gama scintilometrom, v laboratoriju pa dodatno s spektrometrično analizo z NaI(Tl)-spektrometrijo in geokemično analizo po metodi ICP-MS. Gama scintilometrija je pokazala na izdankih kamnine raziskovanega območja dosledno višje vsebnosti kakor v preperini. Analiza spektrometričnih podatkov nakazuje tudi navzočnost dodatnih radioaktivnih nuklidov, drugačnih od glavnih: ^{238}U, ^{232}Th in ^{40}K. Z geokemično analizo so bile ugotovljene kemične prvine Pb, Ce, La, Ti in Fe^{2+}. Iz raziskave izhaja, da prispevajo k celotni radioaktivnosti kamnin, merjeni na raziskovanem ozemlju, razen U, Th in K, tudi prvine, kot so Pb, Ce, La in Ti. Poglavitni radioaktivni minerali v preučevanih kamninah so cirkon, ksenotim in najbrž torit.

Ključne besede: radioaktivne prvine, radioaktivni nuklidi, radioaktivni minerali

Introduction

Gamma-ray spectrometry survey is an important source of information for soil, regolith, rock and geophysical studies. It is essentially a radioelement geophysical technique and its data is a vital sub-component of the geophysical data required for environmental and geological mapping, soil surveying, and mineral exploration and regolith studies. Measurements of gamma radiation at the surface of rock provide information on the abundances of radioactive elements in the rock. Many naturally occurring elements have radioisotopes, but only K, U and Th decay series have radioisotopes that produce gamma-rays of sufficient energy and intensity to be measured by gamma-ray spectrometry[1] because they are relatively abundant in the natural environment. K is a major element in igneous rocks but only one of its isotopes, ^{40}K is naturally radioactive. Although Th is less ubiquitous than U, it is well distributed throughout a considerable pressure-temperature range, chiefly as monazite and thorite, with monazite persisting as the main radioactive mineral of placer deposits[2].

Primary accessory minerals mainly responsible for the bulk of the radioactivity of granitic and intermediate rocks are zircon, sphene, apatite, allanite, xenotime and monazite. Others rarely present but in some cases strongly radioactive, are uranothorite, thorianite, euxenite, thorite, pyrochlore, chevkinite, fluorite, bastnaesite and even davidite[3]. Other possible co ntributors to radioactivity are haematite, pyrite, columbite, ilmenite and rutile and in alkalic rocks are zirconium and cerium silicates. Although uraninite has been reported as an accessory mineral of intrusive igneous rocks, it has not been demonstrated to be of primary origin.

The intensities of nuclear radiation in any particular environment are in general related to the abundances of natural radioactive elements in rocks and soils of that locality[4]. Gamma ray spectrometric methods have been widely used in measurements of radioactive minerals in soils and basement rocks[5]. In many rocks, high radioactivity values are associated with clusters of mafic minerals; e.g. biotite in granites or riebeckite in alkalic granites, largely because radioactive accessory minerals are commonly associated with mafic components.

Charbonneau[6] and Robb and Meyer[7] showed that high radioactive values are associated with clusters of mafic minerals e.g biotite in granites or riebeckite in alkali granites, largely because radioactive minerals such as zircon, apatite, allanite and sphene with the high calcium granites and an assemblage consisting of »monazite-like« phases, and xenotime are commonly associated with mafic components. Oshin[8] showed that the various rock types constituting the Precambrian rocks (granite-gneisses, porphyritic granites and meta-sediments) of south-western Nigeria are characterized by different U and Th contents and that the granite-gneisses and the coarse porphyritic granites corresponding to the older granite series are characterized by high Th and U contents respectively, while the meta-sediments are the most depleted in these radioactive elements. He also suggested an igneous origin for the gneisses (migmatite gneiss and granite gneiss) based on their contents of radioactive elements. Jibiri et al[9] studied the radioactivity levels of granitic rock in Jos (North central), porphyritic granite in Abeokuta (Southwest), augen gneiss in Ibadan (Southwest), shale and coal in Enugu (Southeast) Nigeria which are situated within high natural background radioactive areas and the result were compared with in-situ gamma-ray measurements made at the localities where samples were collected. It was concluded that ^{232}Th was the major contributor of gamma absorbed doses that are received by the population in all different environments in the study areas.

The detection of radioactive mineral deposits since the mid – 1940s by geologists and untrained prospectors yielded the discovery of an important number of new deposits. Many were stumble upon by untrained prospectors using Geiger counters and whose knowledge of uranium geology was insufficient to prejudice them against these »unfavourable« areas and who operated on the basis of »uranium is where you find it«. Modern prospecting methods still follow a similar pattern but with a more systematic approach using equipments with a higher degree of sensitivity like the gamma-ray scintillometer and air-borne gamma-ray spectrometer.

Radioactive raw materials are of great importance because they can be used as supplement to the energy obtained from fossil fuel hence in the last few decades surveying for these minerals have been in practice[10–12]. In Nigeria, the increasing demand of energy and the instability of petroleum supplies make atomic energy an alternative to the energy problems. Although criticisms might arise related to its safe use, the utilization in the area of electricity generation as a supplement to hydro-electricity supply is a possibility. This study therefore aims at determining the distribution of radio-elements such as uranium, thorium and potassium in the different rock types available within the study areas; and to determine the concentration of the major, minor and trace elements present within the samples in order to constrain the possible complimentary role of other radioactive elements to the total radioactivity of the samples analysed. An attempt to establishing the relationship between radioactivity levels and elemental concentrations of the various radioactive elements present within the samples and identifying the different minerals which possibly host these radio-elements will be examined.

Site description and geological setting

The study area falls within sheet 59 of the geological map of south-western Nigeria and comprise an area of approximately 11 655 km^2 (4 500 mi^2). Location 1 is opposite Lagelu industrial estate in Ibadan, Oyo State about 700 m from the Ogunpa channelization and is within latitudes 7° 19.964 N–7° 20.01 N and longitudes 3° 52.741 E–3° 53.224 E. Location 2 is at Odeda, in Ogun State within latitudes 7°14.288 N–7° 15.662 N and longitudes 3°32.076 E–3° 45.116 E (Figures 1 and 2). As a result of the latitudinal location, Ibadan and Odeda have the characteristic of West African monsoon climate, marked by distinct seasonal shift in the wind pattern. Between March and October, the area is under the influence of the mist maritime southwest monsoon winds which blow inland from the Atlantic Ocean. The dry season occurs from November to February

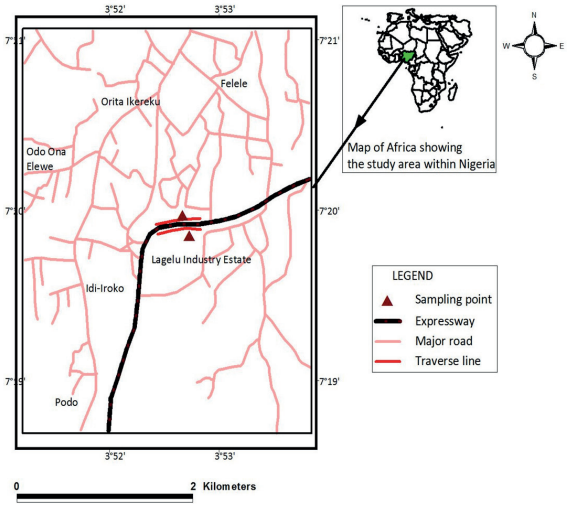

Figure 1: *Location map of Lagelu showing road networks, traverse lines and sampling points.*

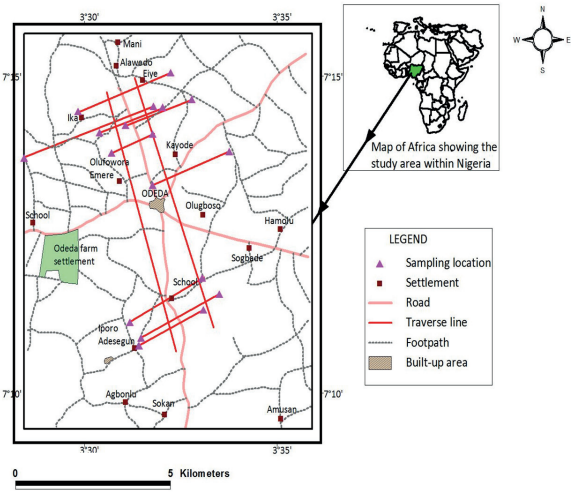

Figure 2: *Location map of Odeda showing road networks, traverse lines and sampling points.*

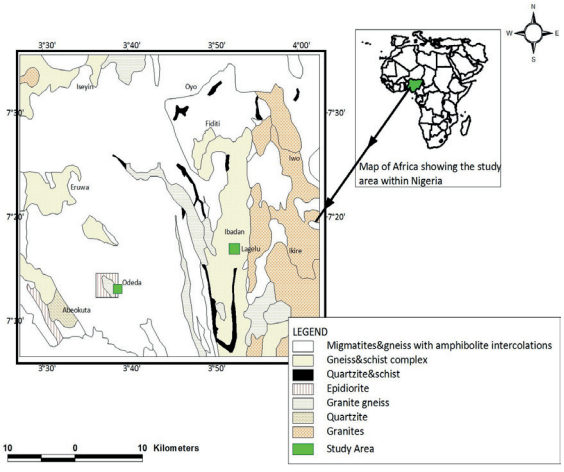

Figure 3: *Geological map of the study area.*

when the dry dust laden wind blows from the Sahara Desert. The mean annual rainfall for the areas is 1 229.39 mm. The mean maximum annual temperature of 28.8 °C occurs in February while the mean minimum temperature of 24.5 °C occurs in August[13].

Geologically, the study area falls within the Precambrian basement complex of Nigeria which occupies about half of the total area of the country. It has been intruded by the Younger Granites of Jurassic age. Cretaceous to recent sediments occupy the other half of the area (Figure 3).

The basement complex of Nigeria has been described as consisting mainly of a variety of gneisses, schists, amphibolites and quartzites most of which have been migmatised[14]. Other major rock types include deformed and undeformed granitic and dioritic intrusives[15–17].

The rock types found in the basement complex rocks of Ibadan can be grouped into major and minor rock types. The major rock types are quartzites of the meta-sedimentary series and a migmatitic complex comprising banded gneisses, augen gneisses and migmatites. The minor rock types include pegmatites, quartz veins, aplites, diorites, amphibolites and xenoliths. Pegmatite is a major intrusion in the banded gneiss, cross-cutting the rock in an East-West direction. The pegmatites are typically coarse grained with quartz and sodic feldspars as dominant minerals. Tourmaline (black variety) is present in small amounts. Most of the outcrops are well exposed as a result of the constructed road (expressway). Many of the rocks have been covered by a veneer of overburden materials. Field investigations have shown that rock types in Odeda area comprise migmatites, coarse grained porphyritic granites, granodiorites, quartz and fine grained porphyritic granites[18].

Methods of study

The radiometric mapping in the profiling mode was carried out using a Gamma Ray Scintillometer (GRS) model GR101A. At Lagelu, two sets of profiles were run parallel to one another and perpendicular to the strike of outcrop (Figure 1). At Odeda, two sets of profiles were run parallel to one another in the north-south direction while eleven smaller profiles were run perpendicular to these two sets of profiles in the east-west direction (Figure 2). All measurements were taken using the full-scale range of 0.3 k and an audio-signal of 50 % of the GRS. The calibration equation $Y = 19\ 514\ X$ gives the count rate Y in count per second in terms of the dose rate X in μSv h^{-1}. The equipment measures the in-situ gamma ray emitted from natural radioactive sources such as ^{40}K, ^{238}U, ^{232}Th and their daughter products such as ^{87}Rb as well as anthropogenic radio nuclides such as ^{137}Cs, ^{90}Sr produced mostly from atomic bomb testing and nuclear explosions or accidents. The radiometric mapping was done to isolate outcrops of high emission counts to make rock sampling easier.

Gamma ray spectrometry analyses of eleven samples were carried out using Canberra 7.6 cm × 7.6 cm NaI(Tl) (Model No 802-series) detector coupled to Canberra serial 10 plus Multichannel Analyzer (MCA) through a pre-amplifier base. The gamma ray transition line of 1 460 MeV was used for the measurement of ^{40}K, 1 760 MeV of ^{214}Bi and 2 615 MeV of ^{208}Ti were respectively used for the measurements of ^{238}U and ^{232}Th.

For geochemical and mineralogical analyses, eleven samples were taken based on the number of rock outcrop encountered when using the gamma ray scintillometer in order to give a better representation of the rocks in the mapped area. Major element oxides and trace element geochemistry was carried out using inductively coupled plasma (ICP) analytical procedures. The ICP method was chosen because of its proven sensitivity, precision and accuracy for many elements and its ability to determine the concentration of a large number of elements simultaneously, thereby reducing the cost and time of analysis. Slides of the different rock samples obtained were made to ascertain the type of heavy minerals plus accessory minerals present and also to identify the possible minerals that might host the radio-nuclides (U, Th, K) as well as other radioactive elements such as Pb and Ce.

Results and discussion

Graphical representations of two profile lines corresponding to the measurement of radioactivity level versus distance are shown in Figures 4 and 5. Generally at both locations (Odeda and Lagelu) maximum peaks were recorded at or near the outcrops. Minimum peaks were recorded across the basement complex rocks area covered by thin or thick overburden materials which are thought to be weathered products of the parent rock. The contributions of radioactivity by the different primary radionuclides ^{238}U, ^{232}Th and ^{40}K are presented in Table 1. This shows the different inputs of these elements in the total gamma ray measured. The largest contribution in terms of concentration is from ^{40}K followed by ^{232}Th and then ^{238}U. The largest contributor in any given locality in terms of total absorbed dose is ^{232}Th. The high radioactivity concentration of radionuclide displayed by ^{40}K in all the samples does not imply high contribution of dose or dose exposure rather it is a function of the energy and number of gamma rays emitted by the radionuclide[19]. The variations in radiation level of the radionuclides may be attributable to the local geology of the area under consideration[20].

For the plots of ^{40}K, ^{238}U, and ^{232}Th against in-situ gamma ray readings, a weak negative correlation was obtained for ^{40}K versus gamma ray readings (–0.605) with correlation being significant at 0.049 levels (2-tailed) i.e. normal distributions curve. Weak positive and negative correlations (0.587 and –0592) were established for ^{232}Th versus gamma ray readings and ^{238}U versus ^{40}K with correlation being almost significant at (0.058 and 0.055 levels) respectively for a two – tailed distribution. For the other radionuclide (^{238}U) no correlation was established with in-situ gamma ray readings and other radio-nuclides of ^{232}Th and ^{40}K (Table 2). Table 3 shows the average concentration of some elements in rocks from the study areas

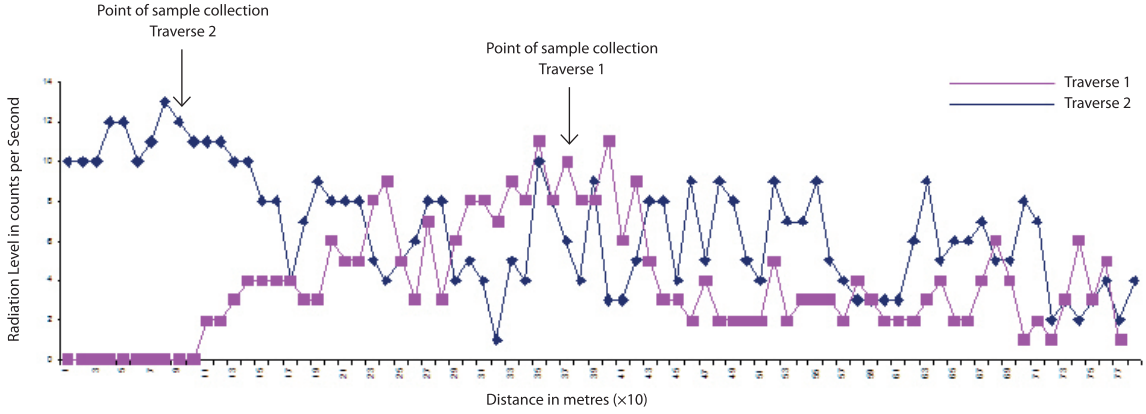

Figure 4: *Plot of radioactive count against distance at Lagelu.*

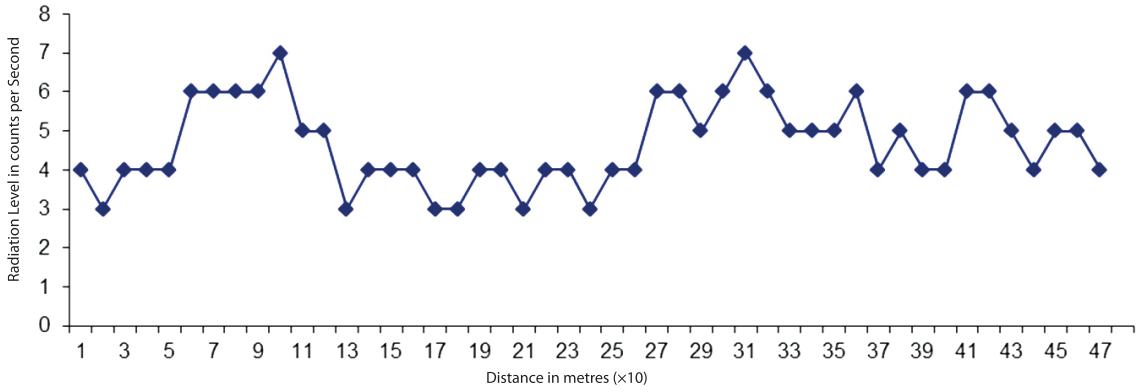

Figure 5: *Plot of radioactive count against distance at Odeda area.*

Table 1: *Concentrations w of ^{238}U, ^{232}Th and ^{40}K of rocks within the study area in (× 10^{-6}). (Conversion factor was introduced to change the values from* Bq kg^{-1}/(× 10^{-6})

Location	Sample name	Count	w (^{40}K)/%	w(^{238}U)/(× 10^{-6})	w (^{232}Th)/(× 10^{-6})
ODEDA	L_1T_1	13	4.947 2	2.400 7	66.23
	L_2T_2	18	4.127 9	3.875 2	94.54
	L_3T_3	20	3.658 6	1.735 9	77.59
	L_4T_4	10	5.051 5	4.043 2	62.67
	L_5T_5	15	4.965 4	3.104 0	29.34
	L_6T_6	8	4.283 2	2.117 3	38.38
	L_7T_7	12	4.486 2	1.848 8	86.83
	L_8T_8	13	3.821 3	4.015 0	79.23
	L_9T_9	11	4.604 9	1.909	56.84
OPP. LAGELU IND. ESTATE	$L_{10}T_{10}$	11	4.706 6	4.080 2	6.65
	$L_{11}T_{11}$	8	8.100 8	4.500 8	14.07

Table 2: *Correlations between gamma ray readings: ^{40}K, ^{238}U, ^{232}Th*

		γ-ray reading	^{40}K	^{238}U	^{232}Th
γ-ray reading	Pearson Correlation (r)	1.00	–0.605	–0.203	0.587
	Significant (2 –tailed)	–	0.049	0.550	0.058
^{40}K	Pearson Correlation (r)	0.605	1.000	0.466	–0.592
	Significant (2 – tailed)	0.049	–	0.149	0.055
^{238}U	Pearson Correlation (r)	–0.203	0.466	1.000	–0.342
	Significant (2 – tailed)	0.550	0.149	–	0.304
^{232}Th	Pearson Correlation (r)	0.587	–0.592	–0.342	1.000
	Significant (2 – tailed)	0.058	0.055	0.304	–

* Correlation is significant at the 0.05 level 2-tailed i.e. at 95 % confidence interval

Table 3: *Concentration of major (w/%), minor (w/%) and trace w/(× 10^{-6}) elements in rock samples within the study area*

Location	Sample name	SiO_2 %	Al_2O_3 %	CaO %	MgO %	FeO %	Na_2O %	K_2O %	T_iO_2 %	P_2O_5 %	U × 10^{-6}	Th × 10^{-6}	K %	Pb × 10^{-6}	Zr × 10^{-6}	Ce × 10^{-6}	La × 10^{-6}	Nb × 10^{-6}
ODEDA	L_1T_1	14.22	68.16	1.79	1.70	5.5.3	2.48	4.84	0.66	0.46	4.6	102.3	4.02	31.5	94.4	311	127.5	20.5
	L_2T_2	13.99	64.79	2.02	2.95	5.72	2.17	4.89	1.48	0.66	4.5	118	4.06	32.4	57.6	445	186.1	18
	L_3T_3	14.15	63.00	2.21	3.09	6.06	2.49	5.33	1.67	0.70	4.6	127.2	4.42	33.3	73.9	487	208.6	20.5
	L_4T_4	13.71	61.89	2.56	2.63	7.80	2.23	5.06	0.84	0.28	2.00	98.4	4.2	28.2	71.3	449	204.9	30
	L_5T_5	15.51	61.48	2.60	2.84	6.12	2.74	5.12	1.35	0.86	4.00	63.2	4.25	35.9	72.2	302	130.7	23.1
	L_6T_6	13.71	67.55	1.62	1.56	5.00	3.02	5.25	0.84	0.30	1.8	82.6	4.36	30.3	100.1	324	147.0	26.6
	L_7T_7	14.51	61.17	2.53	3.54	6.83	2.64	4.71	1.86	0.84	4.1	142.5	3.91	33.7	89.8	561	21.8	23.1
	L_8T_8	13.98	62.48	2.73	2.91	6.71	2.35	4.72	1.87	0.91	3.7	109.1	3.92	29.6	9.8	433	185.9	22.6
	L_9T_9	13.71	61.89	2.56	2.63	7.80	2.23	5.06	1.39	0.28	2.00	98.4	4.20	28.2	71.3	449	204.9	30.0
OPP. LAGELU IND. ESTATE	$L_{10}T_{10}$	14.11	73.88	0.64	0.17	0.6	4.78	4.80	0.03	0.02	8.0	4.0	3.98	137.7	31.7	36.0	19.7	5.1
	$L_{11}T_{11}$	15.60	73.13	0.32	0.07	0.3	3.83	6.58	0.017	0.04	1.5	10.1	5.46	115	9.0	9.0	4.5	0.6

*Samples from Odeda are porphyritic granite
*Samples from opposite Lagelu Industrial Estate are pegmatite

compared to the average crustal and granite concentrations. A plot of $Na_2O + K_2O$ against SiO_2 (Figure 6) showed the granites from Odeda as subalkaline rocks and the Lagelu pegmatites as alkali feldspar granites[21]. A plot of PbO against alumina indicated that all the samples are strongly metaluminous to weakly peraluminous, with the pegmatites plotting higher up due to higher PbO content and mineralogy of the samples (Figure 7).

In order to establish a link between in-situ gamma ray readings and geochemically derived K, U and Th, a plot of these elements was made against the gamma ray readings obtained and matched with those of radiogenic ^{40}K,^{238}U, ^{232}Th. A better correlation was obtained for ^{232}Th and Th vs. gamma ray readings when compared to the matches obtained for uranium and potassium. This indicates that thorium is the main contributor to the gamma ray radiation/emission detected by the scintillometer (Figures 8a, b and c). Since it is clear that the principal radionuclide responsible for the bulk of the radiation is thorium, plots of the concentration of other potentially radioactive elements were plotted against thorium concentration to establish a link between their levels of activity.

- For the plot of Th versus PbO, values $r^2 = 0.77$, $p < 0.001$ were obtained indicating a very high degree of correlation (Figure 9).
- Plot of U versus thorium did not show any correlation ($r^2 = 0.17$, $p < 0.70$, Figure 10).
- Plot of Zr versus thorium did not show any correlation implying that Zircon though radioactive does not contribute significantly to thorium's activity ($r^2 = 0.20$, $p < 0.16$, Figure 11).
- Plot of TiO_2 versus Th showed a very strong positive correlation with r value of 0.927 i.e. $r^2 = 0.86$, $p < 0.001$ thus indicating that TiO_2 contributes significantly to thorium's activity (Figure 12). Both U and Th possess ionic radii and charges which prevent them from fitting comfortably into the lattices of any of the common major rock forming minerals of granite, but they fit into certain accessory minerals such as Zircon, sphene, allanite, rutile and apatite. In zircon for example, U and Th in the (+4) states can substitute for (+4) Zirconium.

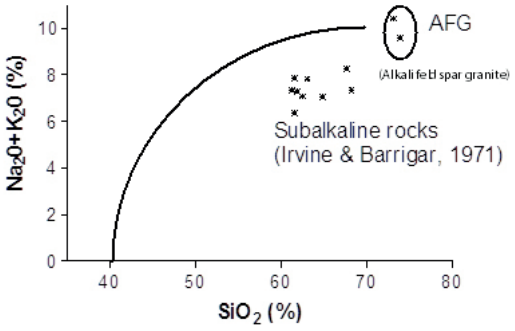

Figure 6: *Plot of $Na_2O + K_2O$ vs. SiO_2.*

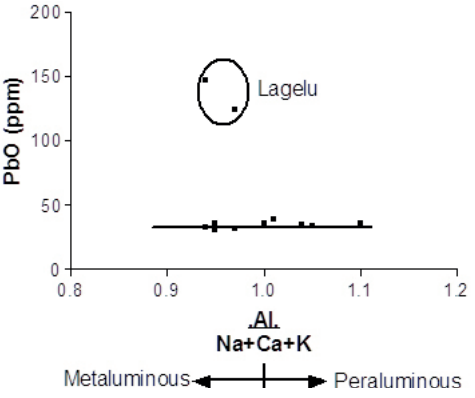

Figure 7: *Plot of PbO vs. Al / Na + Ca + K.*

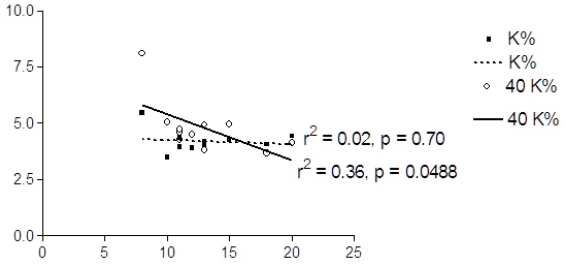

Figure 8a: *Regression plot of geochemical/spectrometric observations of K and ^{40}K against scintillometric readings (counts per second) in samples.*

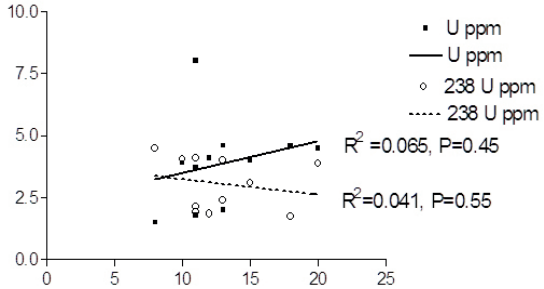

Figure 8b: *Regression plot of geochemical/spectrometric observations of U and ^{238}U against scintillometric readings (counts per second) in samples.*

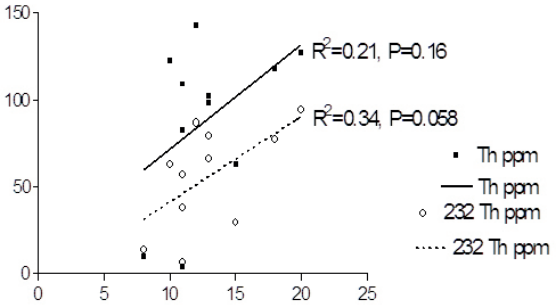

Figure 8c: *Regression plot of geochemical/spectrometric observations of Th and ^{238}Th against scintillometric readings (counts per second) in samples.*

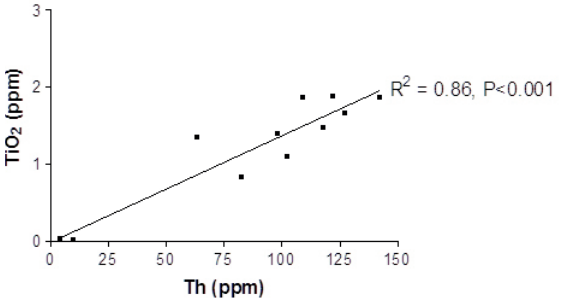

Figure 12: *Plot of TiO_2 vs. Th.*

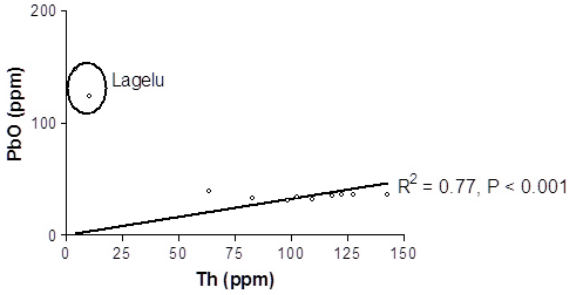

Figure 9: *Plot of PbO vs. Th.*

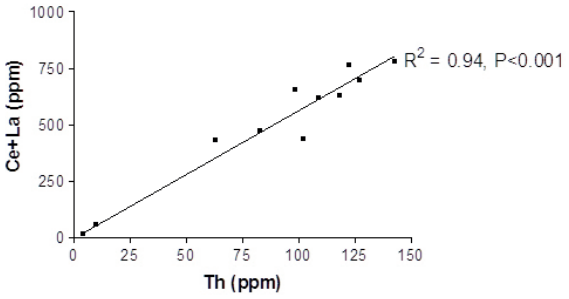

Figure 13: *Plot of Ce + La vs. Th.*

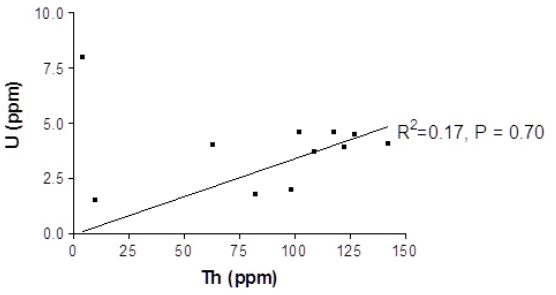

Figure 10: *Plot of U vs. Th.*

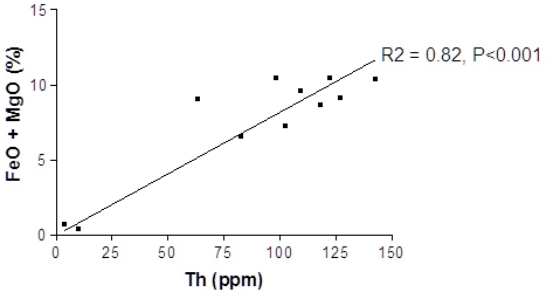

Figure 14: *Plot of Fe0 + Mg0 vs. Th.*

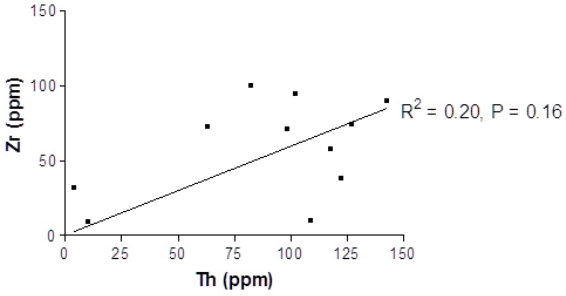

Figure 11: *Plot of Zr vs. Th.*

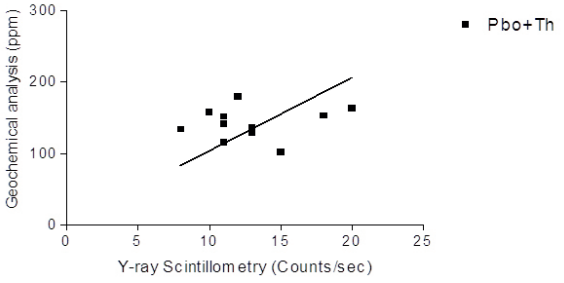

Figure 15: *Plot of PbO +Th vs. Gamma ray scintillometric reading.*

— A very strong positive correlation was established for the plot of Ce + La versus Th with r value of 0.97 and p value < 0.001. This implies that Ce + La contribute significantly to thorium activity. Ce and La are rare earth metals which are naturally radioactive and are found in monazite (Figure 13).
— A strong positive correlation was established for the plot of w(FeO)/% + w(MgO)/% versus Th with r value of 0.905 and p value < 0.001 thus indicating that thorium concentration has a direct relationship with Mg0 and Fe0 (Figure 14). This implies that thorium concentration in rock will increase with increased Mg0 and Fe0 content of such rocks. This could be through cations substitution with elements like titanite, rutile, zircon due to similar ionic size.
— Plot of PbO + Th versus gamma ray counts showed a strong correlation with a r = 0.76 and p < 0.0001 value. The strong positive correlation is due to high concentration of Pb in the rocks where the radioactive measurement was carried out. The Pb content of the pegmatite in the area is responsible for the radioactive level detected in it. (Figure 15).

The study of rock slides in thin sections under the petrograhic microscope revealed the following petrographic features;
— For the different samples observed, zircon is the main radioactive mineral present in all the thin-sections. Another radioactive mineral such as xentomite though in small amounts is also present (Figure 16).
— Titanium rich phases such as rutile and ilmenite could be present which may be responsible for the high Ti content.
— For the pegmatites, the high Pb concentration is attributed to the presence of a lead mineral.
— The high radioactivity observed in some samples can be attributed to the high zircon content as well as the cluster of mafic minerals e.g. biotite largely because radioactive accessory minerals are commonly associated with mafic constituents.
— The major constituents of the rocks sampled are quartz, feldspar and minor amounts orthopyroxene and hornblende.

Figure 16: *Slide showing the accessory minerals (zircon and xentomite) under plane polarized light (mag. 2-times).*

Conclusions and recommendations

This study has been able to infer that rocks of outcrops within the basement complex of south-western Nigeria exhibit high levels of radioactivity compared with the overlying materials except where radioactive materials have been added to the soil through other means. Spectrometric studies of some of the rock samples analysed revealed that the three primary radio-nuclides ^{238}U ^{232}Th and ^{40}K are not the only source of radioactive emissions. Plots of Ce + La + Th + Pb vs. gamma ray scintillometric reading as well as TiO_2 vs. Th gave nearly perfect correlations, thus implying that these elements are the main radioactive phases in the rock samples analysed. Only for the Lagelu pegmatites the bulk radioactivity is attributed to its high lead concentration. Presence of zircon, xenotime, monazite, ilmenite, rutile and galena were observed in the thin sections and corroborated the geochemical evidences. Based on this study, it can be concluded that the distribution of primary radio-elements in areas where nuclear energy generation purposes are intended, particularly U and Th are concentrated in late stage magmatic fractions and in accessory minerals.
It is recommended that further studies such as isotope geochemical analyses as well as multistep spectrometric analyses should be carried out to determine the actual concentration of the radiogenic nuclide to be able to distinguish between stable and unstable phases, determine the concentration of the daughter products and also to determine the presence of other radioactive elements present in the rock samples.

References

[1] IAEA (2003): *Guidelines for radioelement mapping using gamma ray spectrometry data.* (IAEA-TEC-DOC-1363) Vienna, International Atomic Energy Agency.

[2] Sanni, A. O., Schweikert, J. D. (1985): Radioactivity of by-products of tin mining in Nigeria. *Nig. J. Sci.,* 20, 115–120.

[3] Heinrich, E. W. M. (1958): *Mineralogy and Geology of Radioactive Raw Materials.* McGraw-Hill Book Company, New York, p. 654.

[4] Wilford, J. R., Bierwirth, P. N., Craig, M. A. (1997): Application of airborne gamma-ray spectrometry in soil/regolith mapping and applied geomorphology. *Austr. Geol. Geophy.,* 17, pp. 201–216.

[5] Mohanty, A. K., Sengupta, D., Das, S. K., Van, K. V. (2004): Natural radioactivity and radiation exposure in the high background area at Chhaptrapur beach placer deposit of Orissa, India. *Journal of Environmental radioactivity,* 75, 15–33.

[6] Charbonneau, B. (1991): Geophysical Signature, Geochemical Evolution and Radioactive Mineralogy of the ort Smith Radioactive Belt, Northwest Territories. Theophrastus Publishing and Proprietory, Canada. pp. 21–48.

[7] Robb, L. J., Meyer, M. (1991): *Uranium-Bearing Accessory Minerals in Contrasting High-Ca and Low-Ca Granites from the Archean Baberton Mountain Land.* Theophrastus Publishing and Proprietory Co., S. A. Anthens, Greece, pp. 3–20.

[8] Oshin, I. O. (1984): Distribution of uranium and thorium in the basement complex rocks of South-western Nigeria. *Nig. J. Min. Geol.,* 21, pp. 27–33.

[9] Jibiri, N. N., Farai, I. P., Ogunlana, A. M. (1999): Radioactivity levels of some Nigeria rock samples. *Nig. J. Phys.,* 2, pp. 22–25.

[10] Keller, G. V. (1981): *Exploration methods.* Applied Science Publication, UK.

[11] Ehinola, O. A., Joshua, E. O., Opeloye, S. A., Ademola, J. A. (2005): Radiogenic heat production in the cretaceous sediments of Yola arm of Nigeria Benue Trough: Implications for thermal history and hydrocarbon generation. *J. Applied Sci.,* 5, pp. 696–701.

[12] Alabi, O. O., Akinluyi, F. O., Ojo, M. O., Adebo, B. A. (2007): Radiogenic heat production of rock from three rivers in Osun State of Nigeria. *J. Applied Sci.,* 7, pp. 1661–1663.

[13] Filani, M. O., Akintola, F. O., Ikporukpo, C. O. (1994): *Ibadan region, Ibadan.* Rex Charles Publications, pp. 179–190.

[14] Burke, K. C., Freeth, S. J., Grant, N. K. (1976): The structure and sequence of geological events in the basement complex of the Ibadan area, Western Nigeria. *Precambrian Res.,* 3, 537–545.

[15] Oyawoye, M. O. (1972): *The basement complex of Nigeria.* In: Dessauvagie, T. F. J. and Whiteman, A. J. (Editors) African Geology, Ibadan, 1970, Geology Dept. University Ibadan, Nigeria, pp. 67–99.

[16] Rahaman, M. A. (1976): *A review of the Basement Geology of Southwestern Nigeria.* In: Kogbe, C. A. (Editor) Geology of Nigeria, Pub. Elizabethan Publishing Co., Lagos. pp. 41–58.

[17] Rahaman, M. A. (1989): *Review of the Basement Geology of Southwestern Nigeria.* RockView Nig. Ltd., Nigeria, pp. 39–56.

[18] Jones, H. A., Hockey, R. D. (1964): *The geology of part of south-western Nigeria.* Explanation of 1:250,000 sheets Nos. 59 and 68, GSN, Bull. No. 31, Pub. by Authority of the Federal Government of Nigeria, pp. 1–48.

[19] Jibiri, N. N. (1998*): Application of in-situ and gamma ray spectrometry in base studies of gamma ray exposure levels in Nigeria.* Ph. D. Thesis, University of Ibadan, Ibadan, Nigeria.

[20] Gbadebo, A. M. (2011): Natural radio-nuclides distribution in the granitic rocks and soils of abandoned quarry sites, Abeokuta, south-western Nigeria. *Asian Jour. Applied Sci.,* 4, pp. 176–185.

[21] Irvine, T. N., Baragar, W. R. A. (1971): A guide to the chemical classification of the common volcanic rocks. *Canadian Journal of Earth Sciences*, 8, pp. 523–548.

Review paper

Received: June 24, 2014
Accepted: October 10, 2014

MODFLOW USG – the next step in mathematical modelling of underground water

MODFLOW USG – naslednji korak v matematičnem modeliranju podzemne vode

Dragan Kaludjerović[1], Goran Vižintin[2,*]

[1]Advanced Environmental Technology, Milutina Milankovica 120 D, 11070 Novi Beograd, Serbia

[2]University of Ljubljana, Faculty of Natural Sciences and Engineering, Aškerčeva cesta 12, 1000 Ljubljana, Slovenia

*Corresponding author. E-mail: goran.vizintin@ntf.uni-lj.si

Abstract

Since the first software that has been documented in detail and widely accessible to all engineers in the world, the PLASM[1], and until recently the mainstream in mathematical modelling of underground water have been clearly the finite difference and finite elements methods. In 1988 the MODFLOW software package appeared and due to a soft estimation nowadays some 10 000 engineers are using this software package. Besides the fact that other methods have only been used in scientific circles and that no other software gained such popularity as MODFLOW did, all of those have been based on the method of finite difference or finite elements. In the early 2013 the USGS (United States Geological Survey) website published the world premiere of MODFLOW USG. The abbreviation USG is for unstructured grid what represents a new approach in mathematical modelling of underground water. The reaction of GUI (graphical user interface) software developers was rapid and the new version of Groundwater Vistas (ver. 6) implemented this software package. In this paper, the basic characteristics of MODFLOW USG software package that tends to set new standards in groundwater modelling are presented.

Key words: MODFLOW USG, Groundwater Vistas, control volumes, finite differences, PEST, groundwater flow modelling

Izvleček

Od prvih dokumentiranih programskih začetkov matematičnega modeliranja podzemne vode, dostopnih širšim množicam inženirjev (program PLASM), pa vse do današnjih dni so glavna orodja za matematično modeliranje toka podzemne vode metode končnih diferenc in elementov. Leta 1988 se je pojavil program Modflow, ki ga po prosti oceni avtorjev uporablja več kot 10 000 inženirjev. Ne obstaja program, ki bi bil osnovan na metodi končnih elementov ali razlik in ki bi bil bolj popularen od programa ModFlow, razen izjem, ki se uporabljajo v izključno znanstvene namene. V začetku leta 2013 je USGS na svojem domačem internetnem naslovu objavil MODFLOW USG. Kratica USG pomeni nestrukturiran grid in je popolnoma nov način modeliranja toka podzemne vode. Odziv razvijalcev grafičnih vmesnikov je bil hiter, in tudi nova verzija Groundwater Vistas (ver. 6) ga vključuje. V tem članku predstavljamo nekatere nove zmožnosti USG v praksi, ki postajajo nov standard na področju modeliranja.

Ključne besede: MODFLOW USG, Groundwater Vistas, kontrolni volumni, končne diference, PEST, modeliranje toka podzemne vode

Introduction

Prior to MODFLOW USG software package description a short review of some historically important, preceding software packages is given.

The first software that has been documented in detail and widely accessible is the PLASM[1]. This software package was designed for 2D simulations using the numerical method of finite differences. Numerous authors progressively implemented various additional options and in 1981 the option »Random Walk« for contamination transport simulation was added. This software package constitutes the beginning of wider use of numerical methods in hydrogeology of that time.

Considering contamination transport the first successful simulations are related to USGS MOC[2] software package. It is meant for 2D simulations of contamination transport by the method of characteristics and is well documented as well.

Next step represents the launch of MODFLOW software package in 1988 by USGS. This software package has been adopted rapidly throughout the world for many reasons and being well documented may be the quite important one. In the middle of nineties the first GUI (graphical user interface) packages appeared such as Groundwater Vistas, Visual MODFLOW and Model CAD working under Windows operating system and making a precondition for comfort application of 3D numerical modelling. As an open to all (free of charge) software package the MODFLOW obtained many improvements and upgrades, many new physical processes have been implemented as various contamination transport simulations (MT-3DMS, RT3D, PHT3D) too. The current state of the software package is available on USGS website. The most significant fact is that the basic concept represented by continuous layers, orthogonal grid and classical formulation of underground water flow[3], hasn't been changed since 1968.

In the early 2013 the official version of MODFLOW USG software package appeared on USGS website. The abbreviation USG is for unstructured grid what represents a new approach in mathematical modelling of underground water. The reaction of GUI (graphical user interface) software developers was rapid and the new version of Groundwater Vistas (ver. 6) implemented this software package. In the next section the basic characteristics of the MODFLOW USG software package are given.

MODFLOW USG software package fundamentals

As already said the official version of MODFLOW USG software package appeared on the USGS website in March 2013. The leading author is Dr. Sorab Pandey and co-authors are Chris Langevin, USGS, Reston, Rich Niswonger, USGS, Carson City, Joe Hughes, USGS, Tamp and Motomu Ibaraki, Ohio State University. The main advantage of the MODFLOW USG software package is the flexibility in numerical grid design. Looking at finite differences method condensing the numerical grid in the zone of interest shows the influence onto the whole model and very often at the very edge some very irregular shapes of fields and cells occur resulting in inaccurate results and extended time of model calculation. When comparing with MODFLOW USG this problem can not appear as the grid condensation is limited to the desired part of the model.

As shown on Figure 1 the layers in MODFLOW USG do not need to be continuous but it is possible to simulate faults and discontinued layers thus considerably improving the conceptual model of the treated aquifer.

Numerical method implemented in MODFLOW USG software package bases on the finite volume method called CVFD (control volume finite difference) that enables the flexibility of grid elements geometry, field dimensions and elements that can easily be modified and customized. (Figures 2 and 3).

It is also important to mention that the cells have to be of prismatic shape, having vertical sides and flat top and bottom and also have to be convex. (Figure 3).

Speaking of discretization in the profile, some various options are possible (Figure 4): Figure 4a shows that it is still possible to mark the layers in the profile both pre- and post- result processing. Figure 4b shows the possibility of

discontinued layers and Figure 4c shows the possibility to define several layers in one layer at only specific part of the model.
There are a few conditions on which the precision of the method is dependant. The most important condition is to have a right angle between the line connecting two nodes of the cell and the line at the contact of two cells (Figure 5). In the Groundwater Vistas software package the option Ghost Node Correction (GNC) is implemented enabling to define fictive nodes that meet this condition (Figure 6).

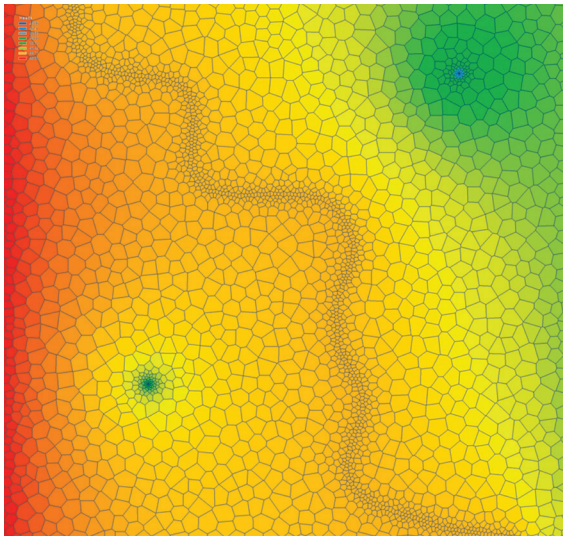

Figure 1: *Possible variants of discretization in MODFLOW USG software package[4].*

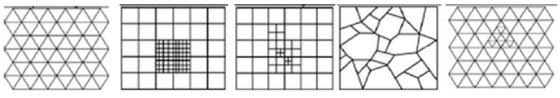

Figure 2: *Numeric grid in software package MODFLOW USG[4].*

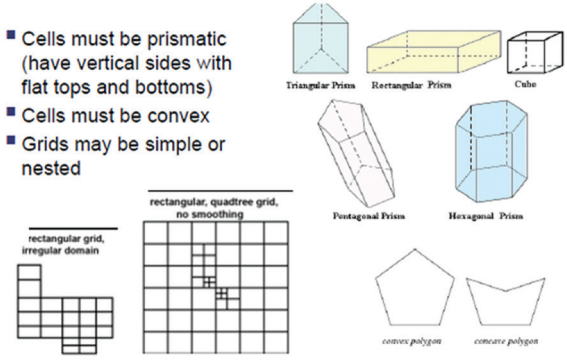

Figure 3: *Elements' shapes in CVFD method[4].*

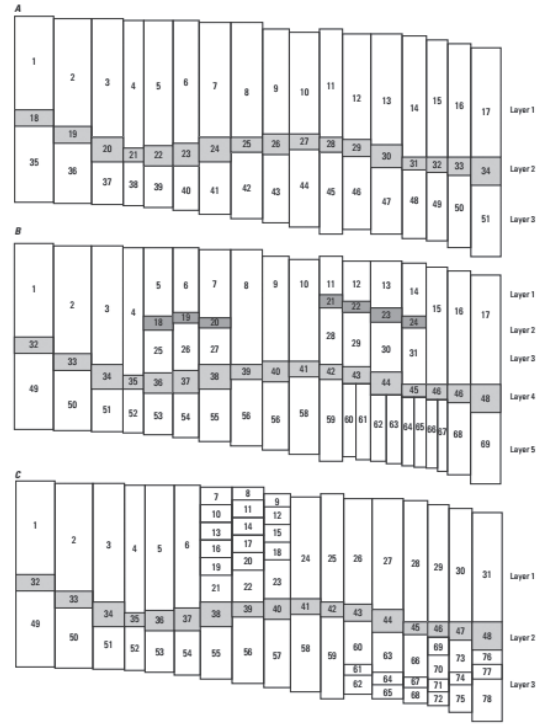

Figure 4: *Layers in MODFLOW USG[4].*

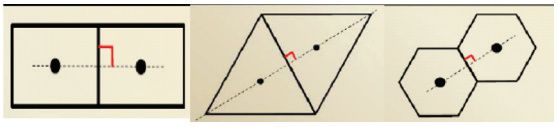

Figure 5: *Condition for precision of CVFD method[5].*

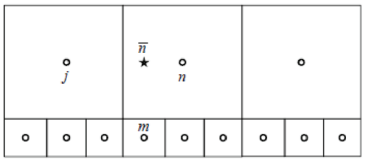

$$Q_{nm} = C_{nm}(h_m - h_n) \quad \text{standard finite volume formulation}$$

$$Q_{nm} = C_{nm}(h_m - h_{\overline{n}}) \quad \text{ghost-node formulation}$$

$$h_{\overline{n}} = \overline{\alpha} h_n + (1-\overline{\alpha}) h_j \quad \text{head at ghost node}$$

$$Q_{nm} = C_{nm}(h_m - \overline{\alpha} h_n - (1-\overline{\alpha}) h_j) \quad \text{optional formulation in MODFLOW-USG}$$

Figure 6: *Ghost Node correction in Groundwater Vistas software package, ver.6[5].*

Some of basic MODFLOW USG software package characteristics were described above. It is important to note that this package is most effective in case of big hydraulic gradients (rivers, wells) and/or complex geology in the model (Figure 1).
There are a few conditions on which the precision of the method is dependant. The most

important condition is to have a right angle between the line connecting two nodes of the cell and the line at the contact of two cells (Figure 5). In the Groundwater Vistas software package the option Ghost Node Correction (GNC) is implemented enabling to define fictive nodes that meet this condition (Figure 6).
Some of basic MODFLOW USG software package characteristics were described above. It is important to note that this package is most effective in case of big hydraulic gradients (rivers, wells) and/or complex geology in the model (Figure 1).

Figure 7: *Satellite image of »Grmić« water source and wider surroundings.*

A practical example of MODFLOW USG software package usage implemented in GUI Groundwater Vistas - regional model of water source »Grmić« in Bijeljina

Basic data on the water source

Water supply system of the Bijeljina town and the surroundings gets (Figure 7) the potable water from the water source »Grmić« located in the alluvium on the left bank of Drina river, very close to the town zone. »Grmić« water source is being exploited since 1961, when ten wells were made together with the pumping station of 105 l/s capacity and 80 l/s of backup. Later the capacity rose up to 335 l/s due to addition of new wells. Between 1991 and 1995 a rapid increase of inhabitants occur because of war operations. In 1995 the initial number of inhabitants doubled to reach round 80 000. Underground water exploitation of the water source in 1995 (470 l/s + 50 l/s backup) resulted in underground water regime change and in increased risk for contamination by the potential pollutants located nearby and upstream (cesspits, cemetery, illegal dumps, hospital waste, etc.)
Due to preventive reasons the first five wells (western part, closer to town) were excluded from the water supply system Bijeljina in the beginning of 1995. Exclusion resulted in loss of round 130 l/s of the total capacity but the latest data from 2006 show that the capacity is still round 520 l/s.

3D Geological model of Semberija aquifer

In the general hydrogeological profile of Semberija three unities can be observed:

- *surface roof horizon,* low permeability, composed of clays or sandy clays, 5–7 m thick in the southern, southeastern and northern part of Semberija, but 0.5–2.5 m thick in the central part.
- *Aquifer,* very good permeability, consists of two layers:
  - gravel, alluvial origin, 10–15 m thick in the southern and southwestern part of Semberija, but 30–35 m thick in the northern, northeastern and eastern part.
  - gravel – sandy sedimentary compleks of Qaternary age, possibly of lacustrine origin. In the western and southern part of the region the thickness ranges from 10–40 m, but in the northern and eastern part 60–90 m.
- Floor strata made of clayey – sandy sediments of Pliocene age

Following a detailed analysis of all the available studies and projects the geological model has been finished for the regional Semberija aquifer, shown on Figures 8 and 9. This is a computer generated and not a drawn model.

The 3D hydrodynamic model of Semberija aquifer

The 3D geological model served as a base of a 3D hydrodynamic model. To make the model complete it is required to do the discretization, to set the boundary conditions, to input the water balance values and measured water table values and to calibrate the model.

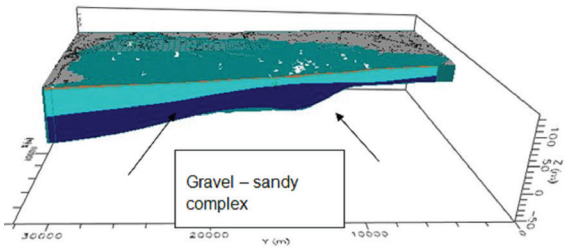

Figure 8: *Semberija aquifer - computer generated geological profile North – South.*

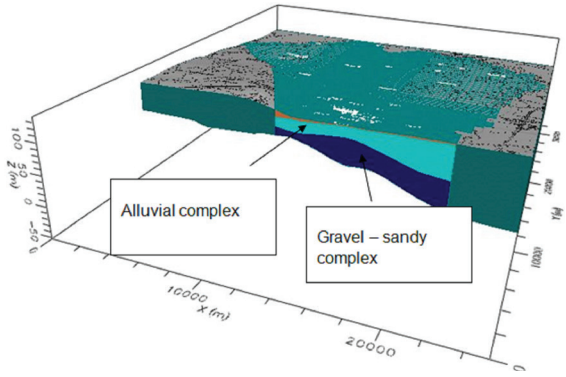

Figure 9: *Semberija aquifer - computer generated geological profile East – West.*

Aquifer discretization is shown on Figure 10. The model area measures round 32 km × 25 km. Discretization has been done using various field size for the edge 550 m × 550 m and for the water source zone round 250 m × 250 m. Vertical division is described in the previous section so the model is composed of three unities.

Borders of the regional underground water flow model in Semberija are the following:

— Drina river in the East; border to constant potential and the given gradient.
— Sava river in the North; border to constant potential and the given gradient.
— gravel – sandy layer extent border in the southwest (contact with Pliocene) as a »no flow« or the impermeable border.

For calibration of the model the state with most piezometer measurements (38 over the whole model in the first half of November 1985) has been adopted (Figure 11). Based on measurements over many months this period has been chosen for stationary flow and dry season, just to ensure that vertical balance insignificantly affects the underground water flow. Through this the calibrating parameters are more reliable as there are less of them. After calibration the underground water table values of the Semberija aquifer resulted from the model. There are no precise data for the total capacity of the water source for 1985 but the estimated value is round 270 l/s. As the goal of this 3D model the representative characteristics for the permeability coefficient zones are set so these can serve for underground water flow prognosis for the present conditions for which there are not nearly as much measurements of water table in piezometers as for the earlier periods. Figure 12 shows the distribution of permeability coefficient in the model for the second layer, the Alluvial gravels[6].

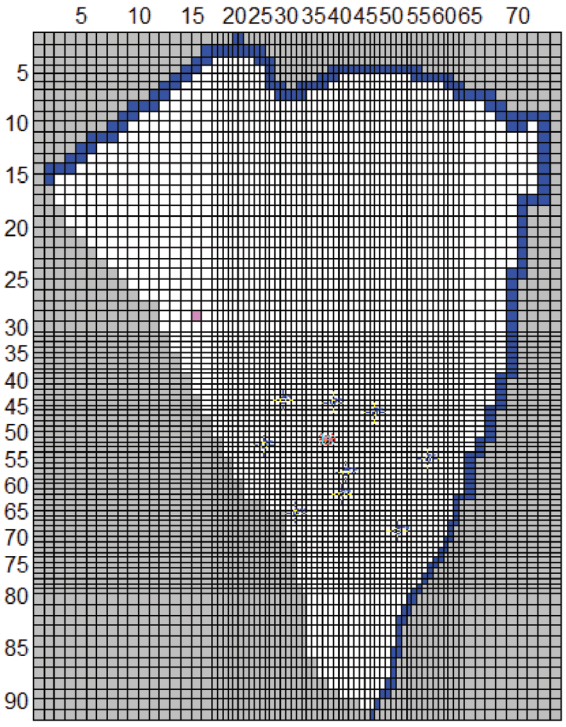

Figure 10: *Discretization of the mathematical model of Semberija aquifer.*

MODFLOW USG control simulation

Prior to MODFLOW USG simulation description it is necessary to mention that there are two versions of the MODFLOW USG software package. First version is supported by USGS and can be found on their website. The other version is called advanced (or BETA version) and comes

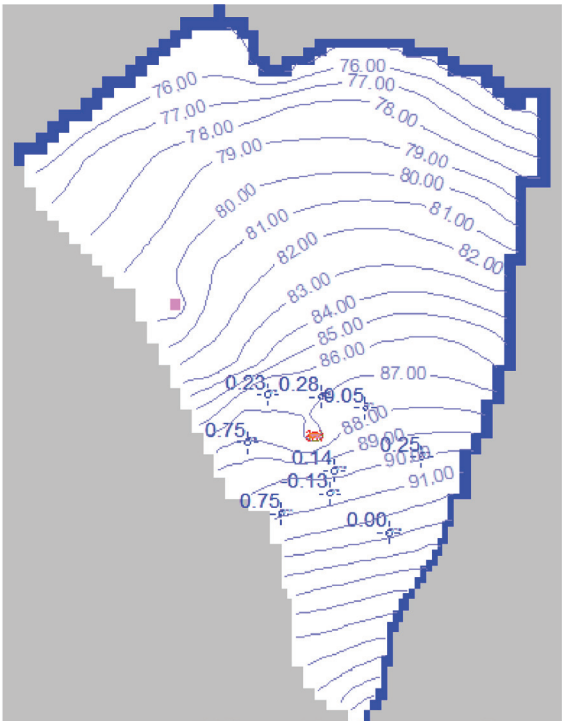

Figure 11: *Contour lines of the water table level in November 1985.*

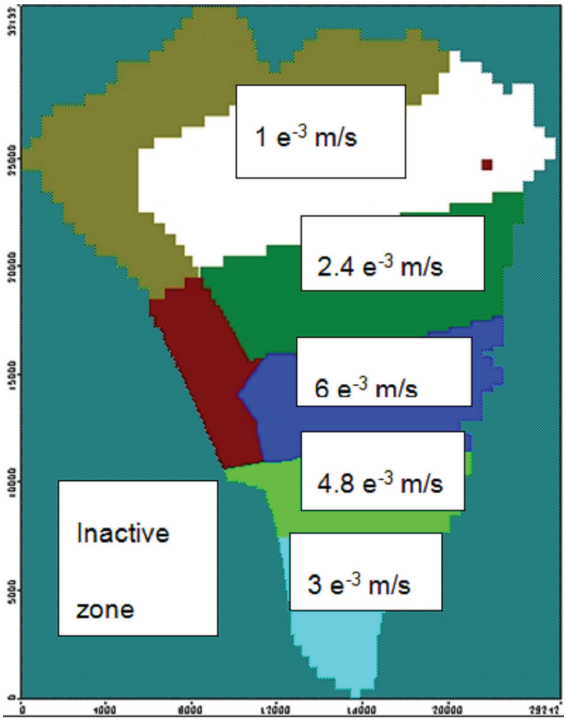

Figure 12: *Permeability coefficient distribution for the second layer – Alluvial gravels.*

in the Groundwater Vistas software package where some advanced options are included such as simulation of unsaturated flow conditions (Richards equation).

Authors of the USG software advise to start modelling from the basic grid that is not very condensed (or is only a little more condensed) and to ensure the correct execution of the model[5]. After that the MODFLOW USG discretization is to be added in the zone of interest. Exactly the advised procedure has been adopted in this case so teh simulation from the previous section served as a base for the new MODFLOW USG model – discretization of this new model is shown on Figure 13. Each field in the zone of the well at water source is condensed with 3 × 3 fields but only in the zone of interest. All the rest including boundary conditions remained the same. As it can be seen there are no big differences in general water flow except the resolution is significantly better in the zone of the well and the results are more detailed. In this case the time of model execution did not appear critical (a few seconds) but certainly some significant savings of the simulation time can be obtained.

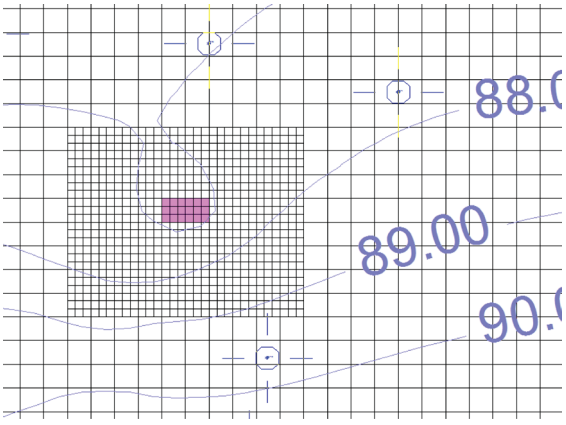

Figure 13: *Nested MODFLOW USG grid added to the classical MODFLOW grid.*

Discussion

MODFLOW USG is still in the development phase, since, as already mentioned in the paper first release was published in March 2013. The planned further improvements are in variable active domain where the fields can switch the

status from active to inactive. This is very important for open pit dewatering simulations. Next improvement is implementation of Richard's equation and the dual porosity flow option. Speaking of pollution spread, the option is already active and has been tested by the authors of this paper during ongoing research.
Using the MODFLOW USG software, the most important feature is the possibility for discretization exactly in the specific part of the model where necessary and without any redundant supplements. In such way the simulation is significantly faster, enabling at the same time much more efficient use of the inverse methods such as PEST. Some case studies in USGS show the calculation to be more than 20 times faster. Calculation speed is very important with the new method called Pilot Point and Null Space Monte Carlo implemented in PEST as the usage depends on model execution time. Application of these two software packages the MODFLOW USG and PEST, significantly contributes to the model quality and to the research topic on model indeterminacy quantification.

Conclusion

Considering underground water modeling the MODFLOW USG represents an important step forward. In spite of the fact not being the only one nor the first one of the kind, implementation of the new CVFD method into MODFLOW is of great importance for wide professional and scientific public. Modeling will improve in quality and increase in use. The MODFLOW USG software package is in the phase of continuous updating as for instance the software version MODPATH that should be finished in a few months. In case of contamination transport simulation the MODFLOW USG is not compatible to MT3DMS but has got its own transport in the advanced version based on the TVD numerical method. In this field a broad application of MODFLOW USG software is anticipated especially bearing in mind the numeric dispersions and bogus oscillations due to big fields in the grid. It is important to mention that the PEST software is compliant with MODFLOW USG software package so all the benefits from using PEST are valid for MODFLOW USG too.

References

[1] Prickett, T. A., Lonnquist, C. G. (1971): *Selected Digital Computer Techniques for Groundwater Resources Evaluation*. Illinois State Water Survey Bulletin 55, 62 p.

[2] Konikow, L. F., Bredehoeft, J. D. (1978): *Computer model of two-dimensional solute transport and dispersion in ground water: U.S. Geological Survey Techniques of Water-Resources Investigations*, book 7, chap. C2, 90 p.

[3] Anderson, M. P., Woessner, W. W. (1992): *Applied Groundwater Modeling: Simulation of Flow and Advective Transport*: New York. NY, Academic Press, 361 p.

[4] Panday, S., Langevin, C. D., Niswonger, R. G., Ibaraki, M., Hughes, J. D. (2013): *MODFLOW–USG version 1: An unstructured grid version of MODFLOW for simulating groundwater flow and tightly coupled processes using a control volume finite-difference formulation: U.S. Geological Survey Techniques and Methods*, book 6, chap. A45, 66 p.

[5] Environmental Simulation (2013): *Groundwater Vistas* 6, USA.

[6] Kaluđerović, D. (2012): *Prilog kalibraciji I oceni parametara matematičkih modela podzemnih voda – poređenje manuelne, automatske i 'pilot point' metode sa regularizacijom, Vodoprivreda*, 258–260, pp. 233–240.

Professional paper

Received: August 4, 2014
Accepted: November 11, 2014

The effect of welding flux and welding wire on the microstructure and characteristics of the welded joint

Vpliv varilnega praška in varilne žice na mikrostrukturo ter lastnosti zvarnega spoja

Marica Prijanovič Tonkovič[1,*], Matjaž Humar[2], Gregor Bizjak[2]

[1]ŠC Novo mesto, Višja strokovna strojna šola, Šegova 112, 8000 Novo mesto, Slovenia

[2]Letrika, d. d., Polje 15, 5290 Šempeter pri Gorici, Slovenia

*Corresponding author. E-mail: marica.prijanovic-tonkovic@guest.arnes.si

Abstract

The tendency in the production process is to make products of good quality with minimal cost. The same applies for the products - yokes that are welded with submerged arc welding. Because we were dealing with yokes that were not of good quality, we analysed the process of the existing production method. We checked the dimensions of the products and measured their hardness. There was waste due to irregular shape of the welding piece after calibration. We searched for causes of this fault in connection with the weld hardness. We made four different specimens for our research, which differed in the chemical composition of the welding flux, type of the welding wire and preheating of the base material. At the end of welding we used specimens to carry out measurements of concentricity of the products after the process of calibration, made metallographic examination, measured tensile strength and hardness of the weld. The hardness was measured in the weld, base material and heat affected zone. The results of our research showed that hardness of the weld was lowest in specimen 3, which was welded with basic welding flux and preheated welding piece. Measurements of the concentricity of the product showed that it is the best in specimen 3 and the worst in specimen 1, which was welded by the existing filler materials.

Key words: submerged arc welding, concentricity, hardness

Izvleček

V proizvodnji je težnja izdelati kakovosten izdelek hitro in z minimalnimi stroški. To velja tudi za izdelke okrove, ki smo jih varili po postopku varjenja pod praškom. Zaradi preveč nekakovostnih okrovov smo analizirali potek dosedanje izdelave. Izdelke smo pregledali dimenzijsko in izmerili trdoto. Izmet se je pojavil zaradi nepravilne oblike varjenca po kalibraciji. Vzroke za napako smo iskali v povezavi s trdoto zvara. Za preiskavo smo izdelali štiri različne preizkušance, ki so se razlikovali v kemični sestavi varilnega praška, vrsti varilne žice in predgrevanju osnovnega materiala. Po končanem varjenju smo pri preizkušancih opravili meritev koncentričnosti izdelka po procesu kalibracije, naredili smo metalografsko analizo, izmerili natezno trdnost in trdoto zvara. Trdoto smo merili v varu, osnovnem materialu in toplotno vplivani coni. Rezultati preiskave so pokazali, da je trdota vara najmanjša pri preizkušancu 3, varjenem z bazičnim varilnim praškom in predgrevanim varjencem. Meritve koncentričnosti izdelka pa so pokazale, da je ta najboljša pri preizkušancu 3, najslabša pa pri preizkušancu 1, varjenem s sedanjimi dodajnimi materiali.

Ključne besede: varjenje pod praškom, koncentričnost, trdota

Introduction

The production process constantly strives for the best possible quality of products. This, however, depends on various factors, such as machines, man, working methods and material[1]. In searching for faults we use different techniques such as Ishikawa diagram or Deming circle, which help us to find possible causes of problems that can be systematically eliminated. Our problem was increased waste in the process of submerged arc welding or SAW.

SAW is a type of electric arc welding[2], where in the place of welding, welding wire, base material and welding flux melt. During the welding process the arc is invisible, because it is covered with welding flux that is introduced to welding area from a flux hopper. During the welding process part of the welding flux does not melt while the other part does. This melted flux protects the arc and the melted weld metal from the atmospheric influences, attracts impurities and oxides, stabilizes the arc and metallurgically work the melt of the weld.

This process of welding is suitable for unalloyed steels and low-alloyed steels. Based on the base material we choose the right combination of the welding flux and the welding wire. Elements and their concentration which affect the weld quality are silicon, manganese, carbon, phosphorus and sulphur.

Fluxes for SAW are a mixture of various components in the powder form[3–7] that differ among each other by their grain size, chemical composition and way of production. The most widely used formula to calculate the basicity of the flux is the Bonisszewski formula. The basicity of the welding flux[8] can also be determined with equation 1.

$$B = \frac{CaO + MgO + BaO + CaF_2 + Na_2O + K_2O + \frac{1}{2} \times (MnO + FeO)}{SiO_2 + \frac{1}{2} \times (Al_2O_3 + Ti_2O + ZrO_2)} \quad (1)$$

In our research we welded the yoke by the SAW procedure. After the welding process the yokes were calibrated. At that point there was eccentricity between the inner and the outer diameter. This occurrence of difference in the thickness of a yoke wall is important, as it affects magnetic characteristics during the operation. Thus we set a goal to determine what influences the difference in wall thickness of a yoke after calibration in the process of submerged arc welding.

Experimental work

Due to the fact that there was eccentricity present on the workpieces, we analyzed bad products. We presumed that the cause of differences in wall thickness of the yoke after the calibration was caused by filler materials which are currently in use. We made four types of specimens. These were yokes from the series production. Figure 1 a) shows the final product which had a cylindrical form. The wall thickness of base material for the production of yoke was 5.5 mm and the width was 86 mm. After bending them, semi products were welded by the SAW procedure.

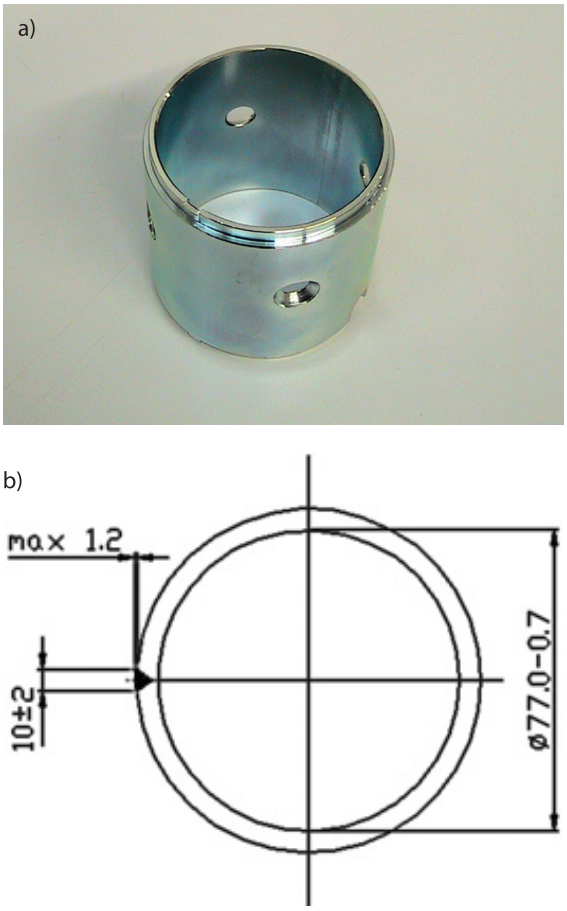

Figure 1: *a) Finished yoke, b) drawing of the welding spot .*

Welding was performed by the welding machine manufactured by OVEN. The welding wire and welding flux were introduced from the upper part of the welding machine. For the purpose of this research, the rectifier ESAB LAF 635 DC with maximum voltage of 44 V at direct current of 630 A was used.

During the welding process we made sure that the depth of penetration did not exceed 2/3 of the thickness of the base material. The weld width was between 8 mm and 12 mm, height of the weld face was not allowed to be higher than 1.2 mm (Figure 1 b). After the welding process the products cooled slowly on the stationary air.

Weldability is an important factor in welding. It was determined with the help of carbon equivalent (equation 2). In our case carbon equivalent for base material was 0.17. This type of steel is known to have good weldability without the need of preheating.

$$C^{eqIIW} = C + \frac{Mn}{6} + \frac{Cr + Mo + V}{5} + \frac{Ni + Cu}{15} \quad (2)$$

Results and discussion

The yoke did not have the required regular form. We expect differences in wall thickness of the welded yoke (as much as 0.5 mm and more) and irregular concentricity after calibration because of differences in the weld hardness and height of the weld face, since harder welds have lower plasticity than the base material. Base material for the production of yokes was steel sheet in strips 86 mm in width and 5.5 mm in thickness. Chemical composition of base material is in table 1.

Table 1: *Chemical composition of base material*

Type of workpiece	Chemical composition in mass fractions, (w/%)				
	C	Mn	S	P	Al
Steel	0.10	0.45	0.035	0.035	0.025

We prepared four specimens for the test and they differed in type of welding wire, welding flux and preheating temperature (table 2). For specimen 1 we used the welding wire with 0.1 % of carbon, 0.15 % of silicium and 1 % of manganese and aluminate rutile welding flux which is used for automatic welding of regular construction steels. Flux basicity by Boniszewski was 0.5, which means that the flux had more acid than basic components.

The welding wire for specimens 2 and 3 contained 0.09 % of carbon, 0.06 % of silicium and 0.5 % of manganese. The specimens differed in their state, since the workpiece of specimen 2 was not preheated while the workpiece of specimen 3 was. They were both welded with the basic welding flux of basicity 1.1 by the Boniszewski rating.

Table 2: *Chemical composition of welding wire, type of welding flux and state of workpiece*

Specimen type	Chemical composition of welding wire (w/%)			Type of flux	State of workpiece
	C	Mn	Si		
Specimen 1	0.10	1	0.15	Flux 1	Not preheated
Specimen 2	0.09	0.5	0.06	Flux 2	Not preheated
Specimen 3	0.09	0.5	0.06	Flux 2	Preheated
Specimen 4	0.09	0.5	0.1	Flux 3	Not preheated

Welding wire and type of welding flux of specimen 4 are presented in table 2. The welding wire used for welding specimen 4 contained 0.09 % of carbon, 0.1 % of silicium and 0.5 % of manganese, while the welding flux was basic. Its basicity was 1.6 by the Boniszewski rating. Table 3 shows chemical composition of welding fluxes and table 4 presents chemical composition of all weld metal according to their manufacturer's specifications.

For testing there were the same starting welding parameters used for all three tested combinations of filler materials (welding voltage 26.25 V; welding current 284 A). In welding workpieces 2 and 3 the penetration was too deep at same welding parameters, which led us to raise the welding voltage to 28 V and reduce the welding current to 260 A. At this welding voltage and welding current we reached the depth of penetration that was in tolerance by the technological drawing, i.e. up to 2/3 of the base material thickness. At the end of the welding process and the calibration we measured the concentricity of the yokes (Figure 2). The Figure 2 shows the measurements of devia-

Table 3: *Chemical composition of welding flux*

Type of welding flux	Chemical composition (w/%)										
	SiO_2 + TiO_2	Al_2O_3 + MnO	CaO + MgO	SiO_2	MnO	MgO	CaF_2	Na_2O	Al_2O_3	CaO	TiO_2
Flux 1	30	55	/	/	/	/	5	/	/	/	/
Flux 2	/	/	/	19	11	17	12	2	32	2	2
Flux 3	20	35	25	/	/	/	0.3	/	/	/	/

Table 4: *Chemical composition of all weld metal according to the manufacturer's specifications*[9–11]

Typical all weld metal properties	Chemical composition (w/%)		
	C	Mn	Si
Weld 1	0. 06	1.35	0.6
Weld 2	0.05	1	0.2
Weld 3	0.07	1	0.2

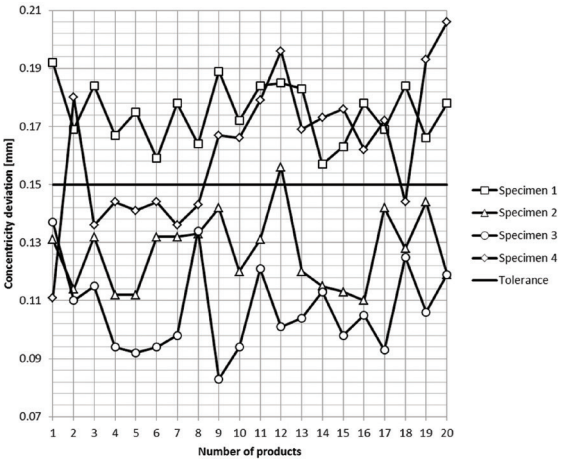

Figure 2: *Deviations in measurements of concentricity on products with different specimens.*

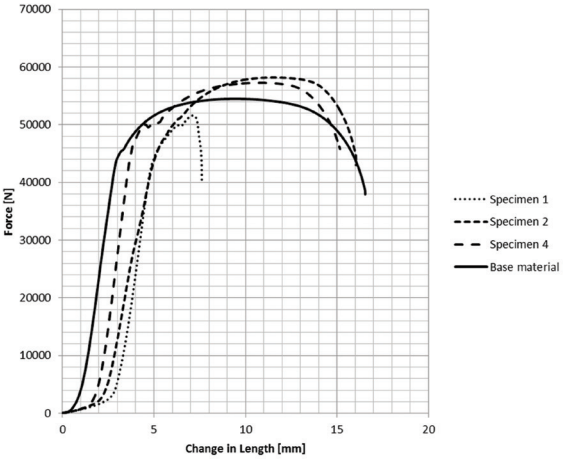

Figure 3: *Diagram force – change in length of specimens 1, 2, 4 and base material.*

tions of concentricity in using different welding flux and welding wire. The lowest deviation in concentricity occurred in using welding flux and welding wire for the welding specimen number 2, which is additionally caused by preheating.

We also measured tensile strength of base material and the welded joint. Figure 3 shows the results of measurements. With the tensile test we determined that the characteristics of the welded joint are completely comparable with the characteristics of the workpiece base material.

To determine the hardness of the welding joint we made metallographic samples from the workpieces (Figure 4). To prepare the samples we used a saw for cutting metals and in the middle of the welding joint we cut samples across the whole weld including the heat affected zone and base material, 30 mm in length and 5 mm in width.

Figure 4: *Polished and etched sample ready to be measured for hardness.*

We carried out the measurements of hardness on the computer operated measuring device Struers Duramin–A300 by Vickers HV5. The measurements of hardness were done diagonally from the weld face, across heat affected zone and to the base material. The points of measurements were set up the same in all cases, where the 1st point of measurement was on the weld face, points of measurements 7 and 8 were on the base mate-

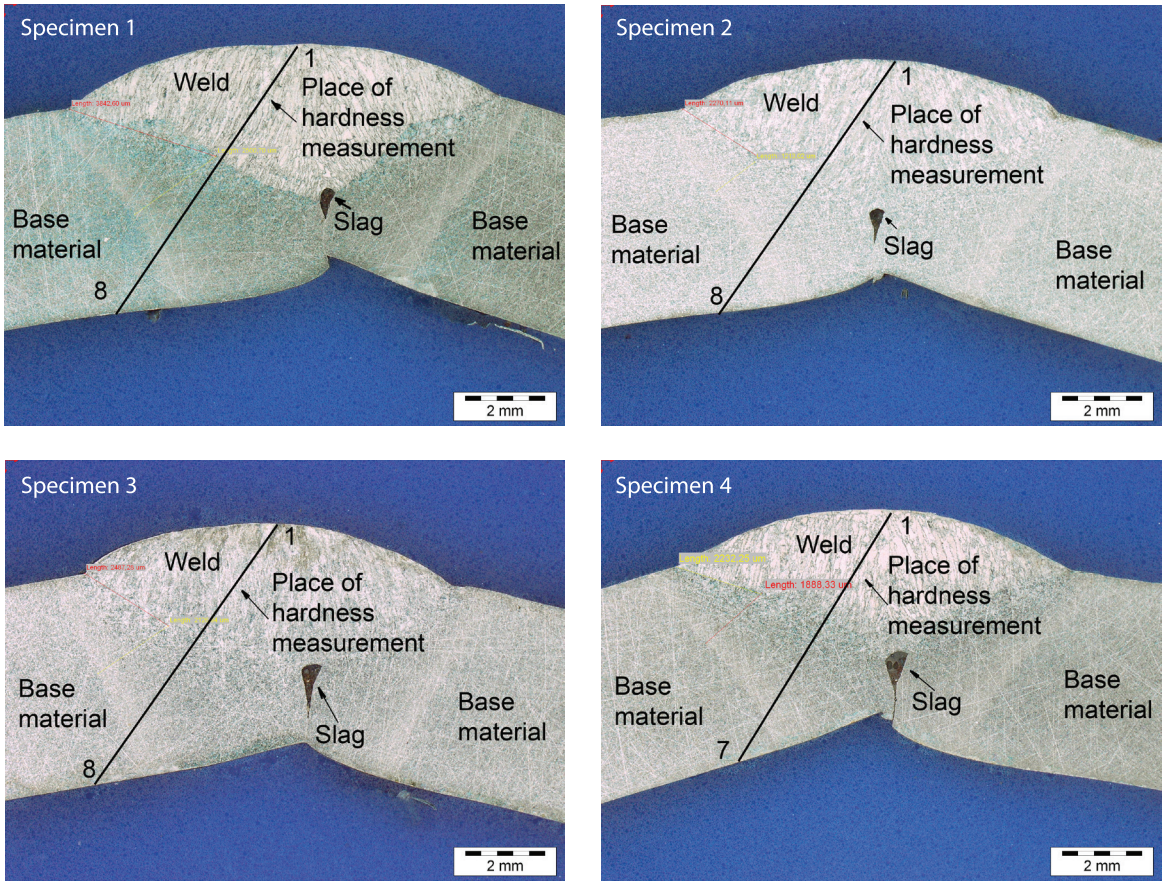

Figure 5: *Course of hardness measurements.*

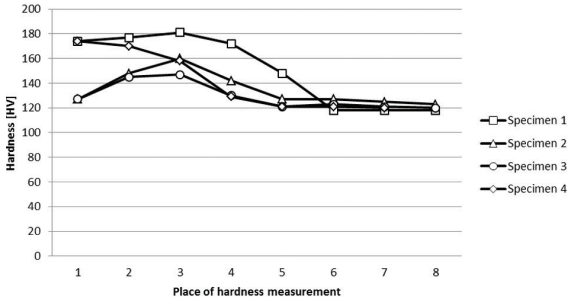

Figure 6: *Course of hardness on the welded specimens.*

rial, which can be seen in Figure 5. All results of these measurements are graphically shown in Figure 6. Under the root of the weld, there is a large dark inclusion of the welding slag. The lowest hardness was measured in specimen 3.

Figure 7 shows the microstructure of the welds, which consists of ferrite and bainite. In welds of specimens 2 and 3 there is more ferrite while in weld of specimen 1 and 4 the amount of bainite is higher.

Conclusions

Weld quality depends on various factors, one of them being the welding method. We analysed bad products due to the occurrence of eccentricity on the welded pieces. We found that irregular concentricity after calibration has to do with differences in hardness among different welds welded with different filler materials and heights of weld face. Differences in hardness are due to different chemical composition and microstructure of the welds. That is why we made specimens on which we measured the weld hardness and product dimensions.

Currently, the flux used in the production process is a rutile flux (marked flux 1) for SAW. The usage of this flux is advisable since it is not as sensitive to atmospheric moisture as the basic welding flux is.

In this research we studied the effect of the welding flux and welding wire on the mechanical characteristics of the weld as well as the dimensional characteristics of the product.

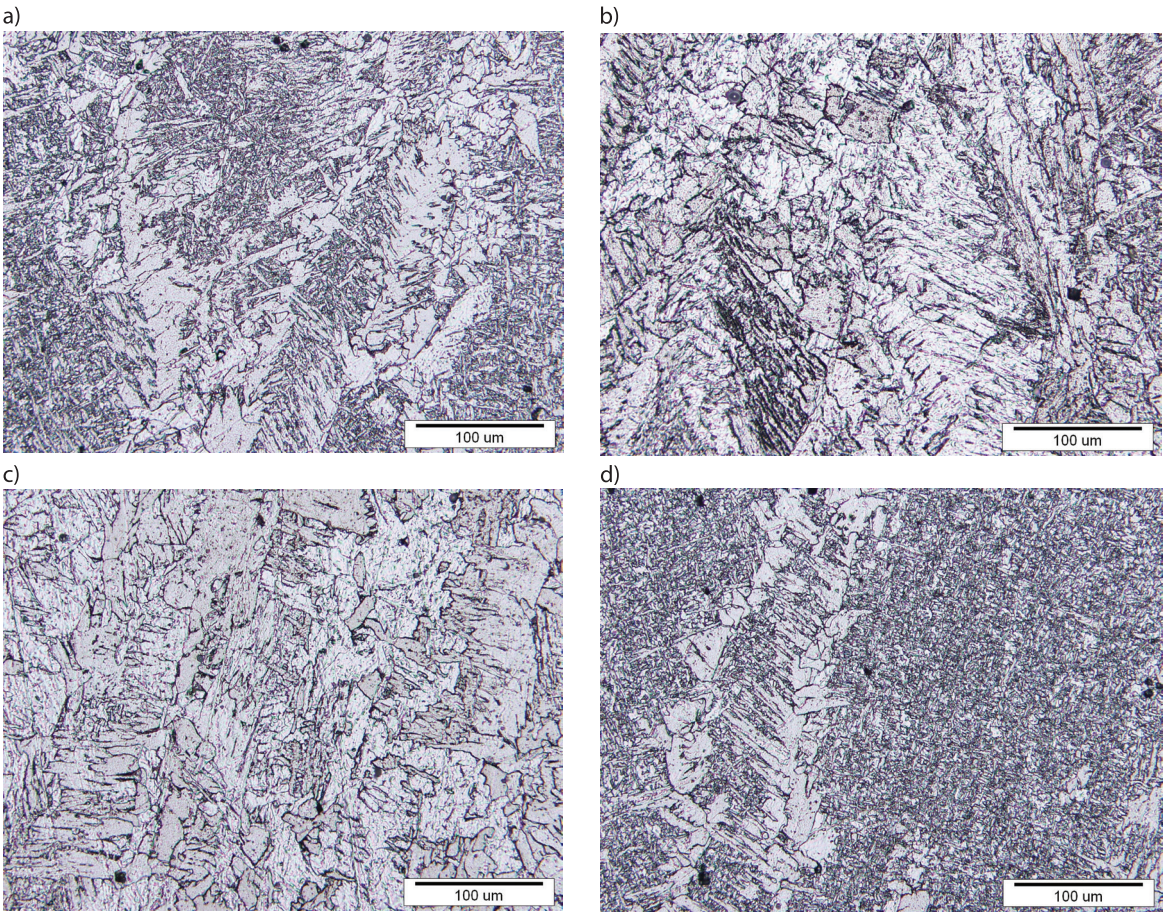

Figure 7: *Microstructure of the welds in specimens: a) 1, b) 2, c) 3, d) 4.*

Based on the measurements it is evident that the usage of combination of welding flux 2 and welding wire with 0.09 % of carbon, 0.06 % of silicium and 0.5 % of manganese is the most suitable for the production process. The weld hardness is additionally reduced in case the workpiece is preheated, which is evident in observing hardness of specimen 3. This specimen has the best concentricity.

The results of these measurements show that the dimensional deviations are much improved and with them also stability of the production process.

References

[1] Vrčko, M. [et al.] (2004): *Poslovno sporazumevanje in vodenje*. Novo mesto [i. e.] Ljubljana: Biro Praxis.

[2] *Improving productivity with submerged arc welding* [online]. A publication of the Fabricators & Manufacturers Association, 2014, [cited 25/7/2014]. Available on: < http://www.thefabricator.com/article/arcwelding/improving-productivity-with-submerged-arc-welding >.

[3] SIST EN 760 (1996): *Dodajni materiali za varjenje. Varilni praški za varjenje pod praškom*. Razvrstitev: prevzet standard EN 760:1996.

[4] Tušek, J. (2006): *Tehnike spajanja; praktične in računske vaje*. Ljubljana: Fakulteta za strojništvo.

[5] Kejžar, R., Kejžar, B. (1994): Dodajni materiali na osnovi izbranih sintetičnih repromaterialov z dodatkom alkalijskih oksidov. *Kovine zlitine tehnologije*, 28(3).

[6] Paniagua-Mecado, A. M., Lopez-Hirata, V. M. (2011): *Chemical and physical propertis of flux for SAW low-carbon steels*. Instituto Politechnico National Mexico, [cited 25/7/2014]. Available on: <www.intechnopen.com>.

[7] Singh, J., Singh, K, Garg, J. (2011): Reuse of Slag as Flux in Submerged arc Welding arc Welding & its Effect on Chemical Composition, Bead Geometry & Microstructure of the Weld Metal. *International Journal of Surface Engineering & Materials Technology*, 1(1).

[8] Polajnar, I. (2013/2014): Varjenje pod praškom I. del: *Varilni procesi in oprema*. Inštitut za varilstvo, Specializacija IWE/IWT, Ljubljana.

[9] *Katalog izdelkov Elektrode Jesenice* [online], 2014, [cited 1/ 7/ 2014]. Available on: <http://www.elektrode.si/html/slo/katalog/index_katalog.html>.

[10] *Products & Offers* [online], 2014, [cited 8/5/2014]. Available on: <http://www.lincolnelectric.com/en-us/Pages/default.aspx>.

[11] *Safety date sheet* [online], 2014, [cited 8/5/2014]. Available on: <http://www.esabna.com/msds/7960.pdf>.

Professional paper

Received: February 27, 2014
Accepted: September 25, 2014

Integrated geophysical and geotechnical investigations of a proposed dam site, Southwestern Nigeria

Kombinirane geofizikalne in geotehniške raziskave predlagane lokacije za pregrado v jugozahodni Nigeriji

Michael Adeyinka Oladunjoye[1], Isaac Oluwatosin Babatunde[1,*], Adebisi O. Oshoko[2]
[1]University of Ibadan, Department of Geology, Ibadan, Nigeria
[2]Integrated Geosciences Services, Ibadan, Nigeria
*Corresponding author. E-mail: isaac.oluwatosin10@gmail.com

Abstract

Earth and rock-fill dams are designed to operate under steady state but geological defects may lead to failure of the dam, especially in unconsolidated or fractured terrains. Integrated geophysical and geotechnical investigations were undertaken to assess the vulnerability of a proposed dam site, South-western Nigeria. The study area is underlain by undifferentiated schist.

The field investigations involved use of Very Low Frequency (VLF) electromagnetic and Vertical Electrical Sounding (VES) using the Schlumberger array to generate curves and 2D-imaging lines. Geotechnical investigation entailed establishing points for Standard Penetrometer Test (SPT).

The VLF-EM result revealed localized regions of anomalous conductivity/resistivity. The VES result delineated topsoil, weathered basement and fractured/fresh bedrock. The geotechnical results revealed low stability for the proposed dam axis.

The uneven nature of the basement topography is a potential threat to the stability of engineering structures. As a result, the site was considered unsuitable for concrete dam but suitable for earth dam. If the dam will however be constructed, proactive measures, such as deep excavation and grouting must be taken against the structural and geological defects.

Key words: Geophysical and geotechnical, Damsite, Clayey overburden, Poorly drained, Proactive measures.

Izvleček

Zemljinske in nasute kamninske pregrade so projektirane za obratovanje v normalnih okoliščinah, toda neugodne geološke lastnosti, zlasti nekonsolidiranost in razpokanost kamnine, utegnejo privesti do okvar. S kombiniranimi geofizikalnimi in geotehniškimi raziskavami smo ocenili ranljivost neke predlagane lokacije pregrade v jugozahodni Nigeriji. Podlago raziskovanega območja tvorijo nerazčlenjene skrilave kamnine. Uporabljene terenske metode so obsegale zelo nizkofrekvenčno (VLF) elektromagnetno in vertikalno električno sondiranje (VES) po Schlumbergerjevem razporedu z izdelavo krivulj in 2D-linij. V okviru geotehniških raziskav so opravili v izbrani mreži standarni penetrometrični preizkus (SPT).

Glede na rezultate preiskav VLF-EM smo omejili območja anomalne prevodnosti/upornosti. Z VES smo ločili v podlagi tla, preperelo kamnino in razpokano svežo kamnino. Geotehniški preizkusi so nakazali pomanjkljivo stabilnost v osi predlagane pregrade. Neravna oblikovanost podlage je potencialna nevarnost za stabilnost predlaganih objektov. Kot rezultat raziskave smo ocenili, da lokacija ni ugodna za betonsko pregrado, vsekakor pa je primerna za zemljinsko pregrado. Če se bodo odločili za gradnjo, bo treba predhodno izvesti primerne ukrepe, kot so globoki vkopi in injekcijske zavese, da zavarujejo objekte pred strukturnimi in geološkimi nevarnostmi.

Ključne besede: geofizikalne in geotehniške preiskave, lokacija za pregrado, glinasta tla, slabo odvodnjavanje, predhodni ukrepi

Introduction

Dams are among the largest and most important projects in civil engineering[1]. They are major engineering structures that are designed and constructed with long life expectancy[2, 3]. Due to the fact that dam constructions serve tremendous purpose to the human community, the design and construction of a dam is expected to create a stable structure that will last for a very long period of time. Out of the various natural factors that directly influence the design of dams, none is more important than the geological, not only do they control the character of the foundation but they also govern the materials available for construction[4]. For geologic, hydrologic and topographic reasons, there are limited numbers of ideal sites for dams' placement[5]. It is therefore very important to intensely scrutinize any proposed dam site. There are many problems which give a broad variety of special tasks to the geophysicist, beginning with prospecting for geological near-surface structures and ending in the determination of the properties of soils and rocks by geophysical methods. Concealed fractures are structures which pose great difficulties in public works and their non-localization may lead to failure of otherwise well planned projects. The prospects of surface water development through the construction of a water dam in crystalline basement complex area are considerably enhanced by carefully planned and well executed preliminary geophysical investigations[6–10]. Pre-construction site study is a prerequisite for the construction of dams and other hydraulic structures in order to avoid locating such structures on undesirable subsurface features such as buried stream channels, near-surface fractures, joints, fissures etc.[2]. The unpredictability of the near-surface ground often complicates site investigations and budgetary constraints may limit the number of boreholes. Geophysics can provide powerful tools to complement other forms of site investigation. Geophysical studies carried out prior to the intrusive investigation in form of borings and trial pits may locate anomalous areas associated with significant subsurface features. The identification of anomalies allows borings and trial pits to be appropriately targeted. The appropriate location of borings on the basis of prior geophysical surveys may result in borehole data being more representative of site conditions. Essentially, geophysics may enhance the value of borehole data. On a complex site, geophysics may be utilized to determine the geology between boreholes, since interpolation between borehole logs may be ambiguous. Comparison of geophysical survey results with directly obtained geological information permits the extrapolation of geophysical results into areas where little or no borehole information is available[3, 11]. On large sites in particular, the design of the spatial location of direct sampling points may be contentious and important underground targets may be missed completely. However, in order to reduce the duration and cost of investigation, geophysical techniques are often employed and small number of boreholes are then drilled to yield subsurface information that could serve as control on the geophysical interpretation[6, 12–15]. Hence, an integrated geophysical (electrical resistivity and electromagnetic surveys) and geotechnical (borehole drilling/coring) investigations were carried out at the proposed Obafemi Awolowo University Teaching Hospital complex mini earth dam intended at supplying potable water to the College of Medicine community in OAU Ile-Ife Southwestern Nigeria. This study was aimed at evaluating the geo-structural setting of the concealed bedrock along the proposed dam axis and the flanks of the proposed dam site. Dam transmits and exerts tremendous forces on the foundation, including the thrust of the impounded water which can be of the order of millions of tons, in addition to weight of the biggest man-made structures. The stresses generated from these two main factors, water pressure and deadweight are further aggravated by dynamic forces and other influences. The interaction of dam and foundation is compounded by a third force, that of the impounded water acting both on the foundation and in the foundation, compressing the valley bottom and the flanks, producing uplift, seepage and percolation forces in voids and pores which can result in instabilities, erosion and leaching of supporting strata.

Site description and geologal setting of the proposed dam site

The proposed Dam site is to be erected across the Opa Stream that flows approximately east west of Ile-Ife town. It falls within the geographical coordinates of latitudes 07° 30′ 59.1″ N to 07° 31′ 13.0″ N and longitudes: 04° 33′ 03.7″ E to 04° 33′ 11.0″ E (Figures 1, 2 and 3). The study area is an area of undulating topography with elevation ranging from 250 m to 270 m above sea level with isolated outcrops. The drainage of the shallow valley is poor, with conspicuous presence of stagnant water bodies in the flood plain. The largest parts of the flood plain are essentially swampy. On average, the rainfall and temperature of the area respectively are 1 260.23 mm and 26.6 °C, this is in accordance with the tropical annual rainfall of 1 262.38 mm and temperature of range between 26.6 °C and 28.8 °C[16].
The area is underlain by the basement complex terrain of Nigeria. The main lithological units in the dam site environment are pegmatite and schist (Figure 4). The pegmatite and undifferentiated schist rocks are highly weathered and this result into the preponderance of clay horizons upon which the dam will be erected. The basement rocks are concealed in most parts of the site. However, very few isolated outcrop relics were encountered along the stream channels.

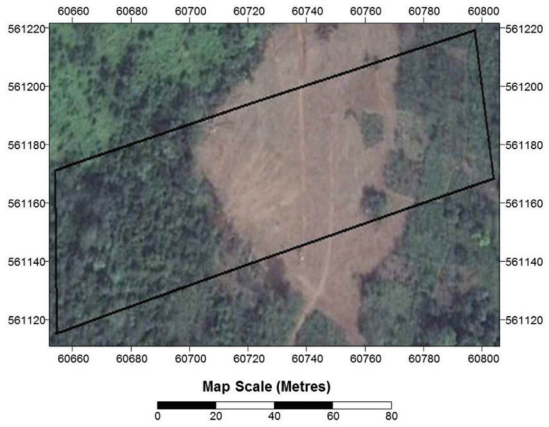

Figure 1: *Location map of the study area showing the boundary of proposed OAUTHC dam site (Google Earth 2014).*

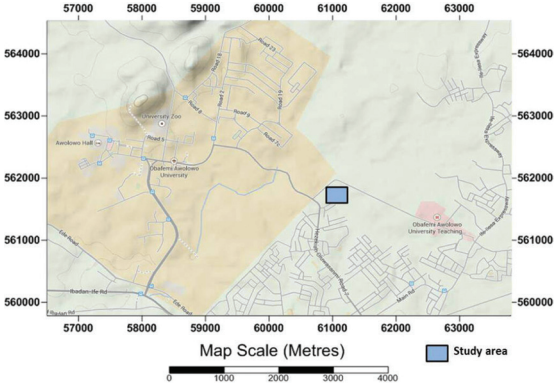

Figure 2: *Location map of OAU and the study area showing the proposed OAUTHC dam site (Google Earth 2014).*

Materials and methods

The geophysical investigation involved the WADI VLF electromagnetic (EM) and the electrical resistivity methods. Horizontal profiling (Wenner) and Vertical Electrical Sounding (VES) techniques were employed.
EM measurements were made at every 10 m interval along the dam axis and 5 m interval along the left and right abutements.
The VES measurements were made at 15 locations along the dam axis, the two abutements and the upstream using the Schlumberger array with electrode spacing, AB/2, varying from 1 m to 75 m. VES were carried out at 50 m interval along the dam axis and the two abutements. The Wenner profiling utilised a fixed electrode spacing of 5 m and an expansion factor (n) varies from 1 to 5.

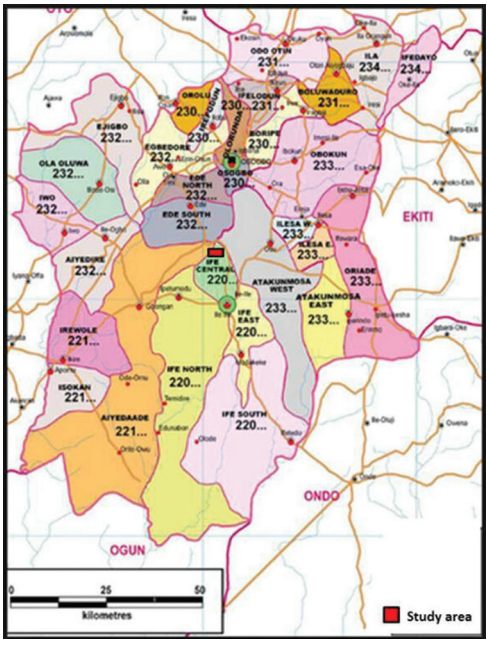

Figure 3: *Administrative map of Osun state showing the local Government and the study area.*

The geotechnical investigation involved soft rock boring and hard rock coring. The Standard Penetrometer Test (SPT) was conducted in four boreholes along the dam axis. The field layout of the geophysical and geotechnical traverses and measurement stations are shown in Figure 5.

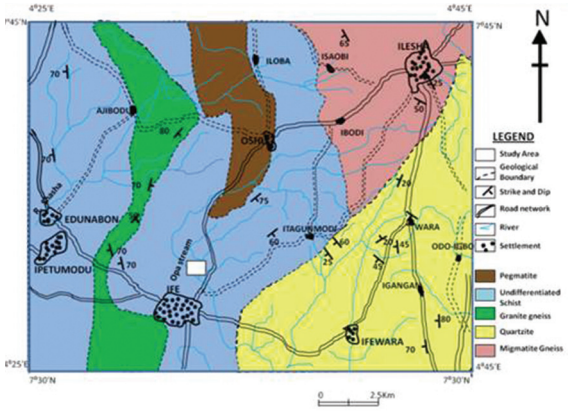

Figure 4: *Geological map of the area around Ile-Ife showing the study Area.*

The Very low frequency Electromagnetic Method (EM) data are displayed as profiles while the Vertical Electrical Sounding (VES) data are presented as depth sounding curves. Geo-electric sections, isopach, bedrock and resistivity contour maps were prepared from the VES data.

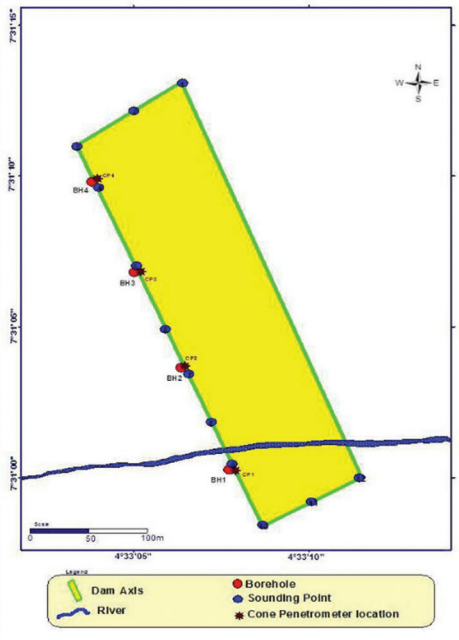

Figure 5: *Spacial distribution of VES points, SPT Test locations and Boreholes in the study area.*

2D-resistivity model for deeper depths of up to 13.5 m were prepared from the Wenner data for the dam axis and the two abutments. Quantitative (1D) interpretation of the VES curve involved partial curve matching and computer iteration techniques. The VES modelling was aided by the availability of borehole lithological logs.

Results and discussion

The EM profiles, Schlumberger and Wenner inverted sections showed the inhomogeneity in the subsurface. Very Low Frequency electromagnetic survey of the dam site revealed the conductive and the resistive nature of the subsurface, the resistive materials predominate the subsurface while the subsurface materials are generally of low average conductivity. There are however, localized regions of anomalous conductivity/resistivity, distributed along the profiles. The Karous-Hjelt contour for the dam axis (Figure 6a) shows a varying resistive sections, pockets of highly resistive unit and highly conductive unit were embedded within the low resistive background, the conductive (Siemen/metres) pockets occur between 320 m to 340 m and 360 m to 400 m up to 40 m deep, similar pockets of high conductive unit occur along a veinlet like structure, dipping approximately 45° N and cutting across the section at offset 220 m at the base and 280 m at the top of the profile. The abutments (Figures 6b and c) are characterized by alternation of conductive and resistive materials from left to right.

The VES curves are mostly the H and A-types, characterized by three geoelectric/lithologic layers consisting of topsoil (sand or sandy clay) weathered layer and fractured/fresh bedrock. The summary of the layer model interpretation and the inferred lithologies are presented in Table 1 while representative VES curves are presented in Figures (7a, b). The electrical resistivity contrasts existing between geoelectric layers in the area enabled the delineation of lithologic units, occurring at varying depths with variable thicknesses. The results of the interpretation were used to construct three sections on the dam axis, the left and the right abutments, taken in the north-south, and east-

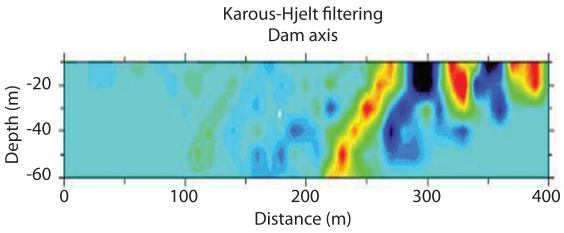

Figure 6a: *Frazer Graph and Karous-Hjelt Contour for the Dam axis.*

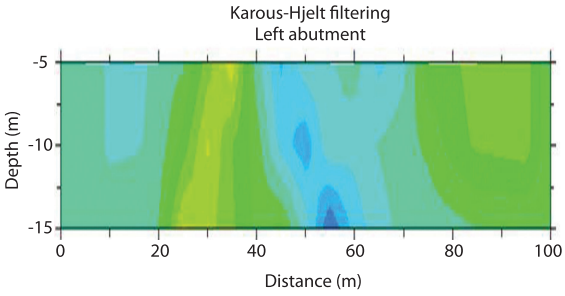

Figure 6b: *Frazer Graph and Karous-Hjelt Contour for the Left Abutment.*

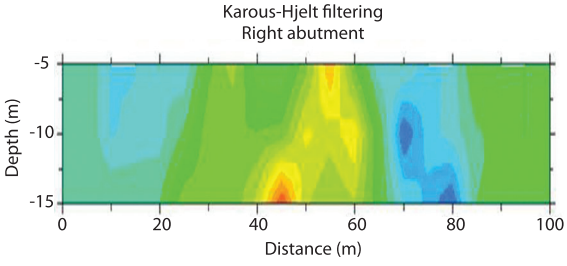

Figure 6c: *Frazer Graph and Karous-Hjelt Contour for the Right Abutment.*

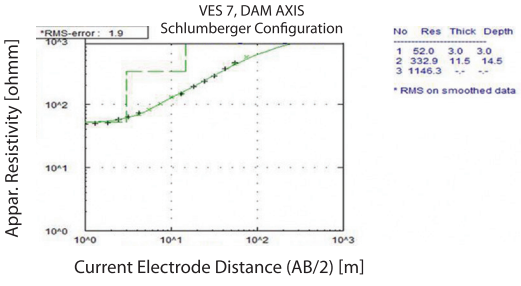

Figure 7a: *Computer Iterated Graph for VES 7.*

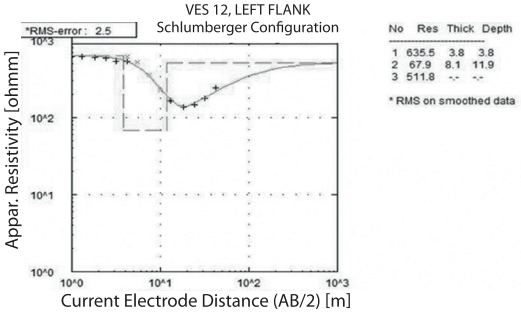

Figure 7b: *Computer Iterated Graph for VES 12.*

west directions (Figures 8a, c). The sections show three geoelectric/lithologic layers.

Geoelectric sections

Dam axis

The resistivity of the dam axis ranges from 18 Ω m to 32 Ω m (Figure 8a) while thickness varies from 0.4 m to 4.8 m in the first layer (topsoil). In the second and third layers, resistivity varies from 11 Ω m to 333 Ω m and 447 Ω m to 1 386 Ω m respectively while the weathered basement thickness ranges between 0.3 m to 12.1 m. The topography of the dam axis is uneven the basement with competent bedrock is closer to the surface at the central part of the dam axis and deepening towards the two abutments.

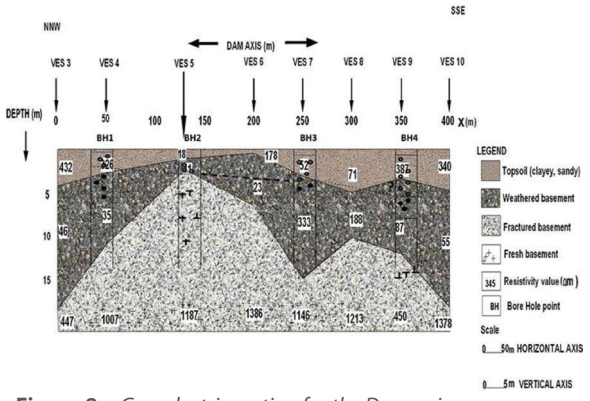

Figure 8a: *Geo-electric section for the Dam axis.*

Left Abutment

The left flank is underlain by three layers representing the topsoil, the weathered basement and the bedrock (Figure 8b). The first two units is the overburden comprising the topsoil and the weathered basement with resistivity and thickness values ranging from 340 Ω m to 635 Ω m / 3.7 m to 4.6 m and 55 Ω m to 81 Ω m / 8.1 m to 16.2 m respectively. The topsoil and weathered basement interface have a near horizontal geometry. The basement resistivity is relatively high, ranging from 512 Ω m to 1 378 Ω m. Its thickness increases progressively towards the centre of the profile from both ends.

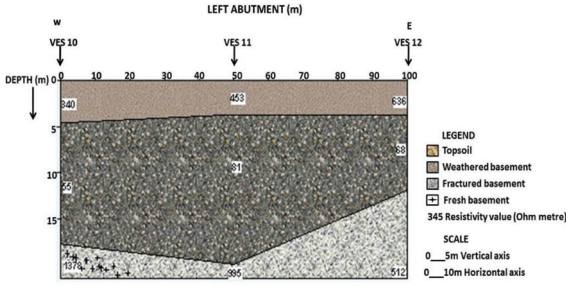

Figure 8b: *Geo-electric section for the Left abutment.*

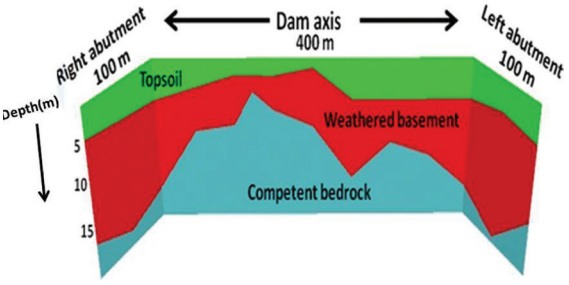

Figure 8d: *Fence diagram of the study area showing the dam axis and the abutments.*

Right Abutment

The right abutment is underlain by three geologic layers comprising the topsoil, the weathered basement and the bedrock (Figure 8c). The layer parameters from the VES interpretation show that the topsoil and the weathered basement have resistivity and thickness values ranging from 432 Ω m to 804 Ω m /3.3 m to 4.1 m and 45 Ω m to 58 Ω m /13 m to 14.9 m respectively. The topsoil and weathered basement interface have a near horizontal geometry. The basement resistivity is relatively low, ranging from 268 Ω m to 673 Ω m, with gently undulating topography.

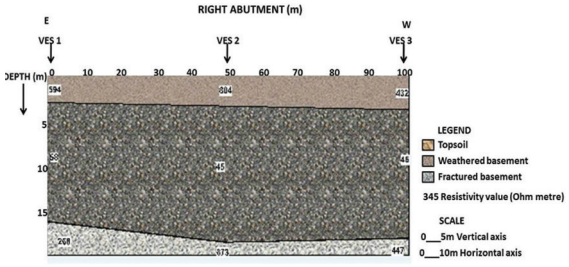

Figure 8c: *Geo-electric section for the Right abutment.*

Fence diagram

This represents two dimensional views of the geo-electric sections. The basement relief as revealed from the fence diagram (Figure 8d) slopes from the dam axis to the abutments. This aids groundwater flow as it was not encountered at boreholes BH1 and BH4 but was seen at borehole BH2 and BH3. The bedrock is closer to the surface along the dam axis with thin overburden. However, at the abutments, the overburden is relatively thick.

Isopach map of the overburden

Figure 9a shows the contoured map of the overburden thicknesses for the proposed dam site. This encompasses all materials above the presumably fractured/fresh bedrock. The overburden is relatively thick around the northern and southern part of the dam axis (abutments), with thickness values ranging from 16 m to 19.9 m while the overburden of the remaining part (middle part of the proposed dam axis) is relatively shallow (2.3 m to 14.5 m). Generally, the overburden of the study area is relatively shallow when compared to the range given by some authors,[17–19] for the southwest basement overburden thickness. They ranged overburden thickness less than 30 m as thin overburden and overburden greater than 30 m as thick overburden.

Bedrock relief map

The bedrock relief map (Figure 9b) is a contour map of the bedrock elevation beneath all the VES stations of the survey area. The significance of this is the reflection of the bedrock topography and its structural disposition. Depressions are characterized by thick overburden while ridges are noted for thin overburden cover. Ridges are characterized at the middle portion of the dam axis due to the closeness of the bedrock to the surface at this portion. Hence, there is poor drainage along the dam axis. The left and the right abutments are characterized by depression.

Resistivity of the bedrock

The resistivity values of the bedrock vary from 268 Ω m to 1 483 Ω m. According to[2, 3, 20], the resistivity values that exceed 1 000 Ω m is fresh

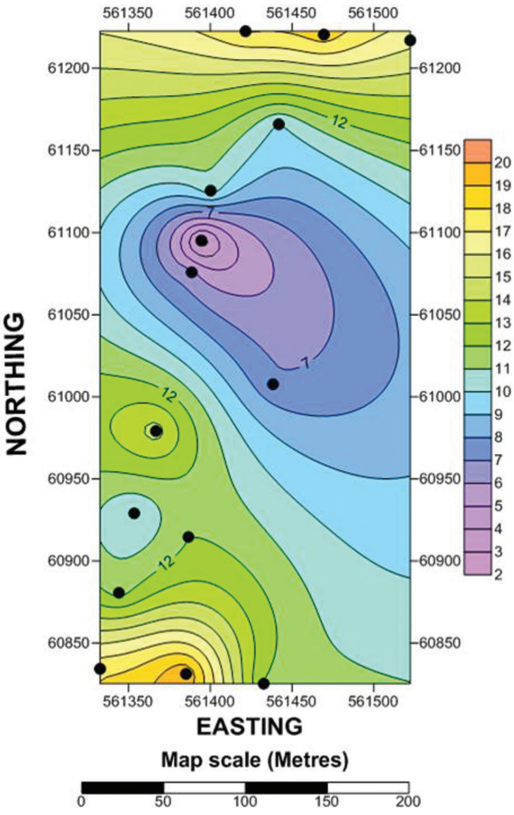

Figure 9a: *Isopach map of the study area.*

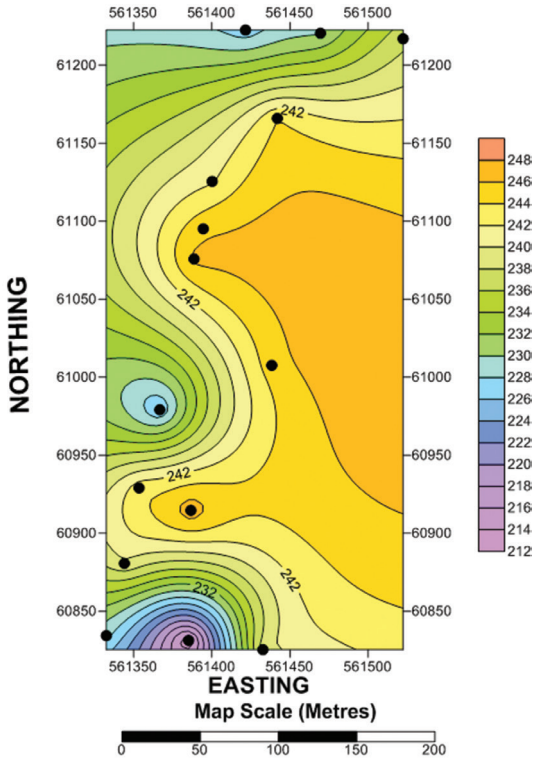

Figure 9b: *Bedrock relief map of the study area.*

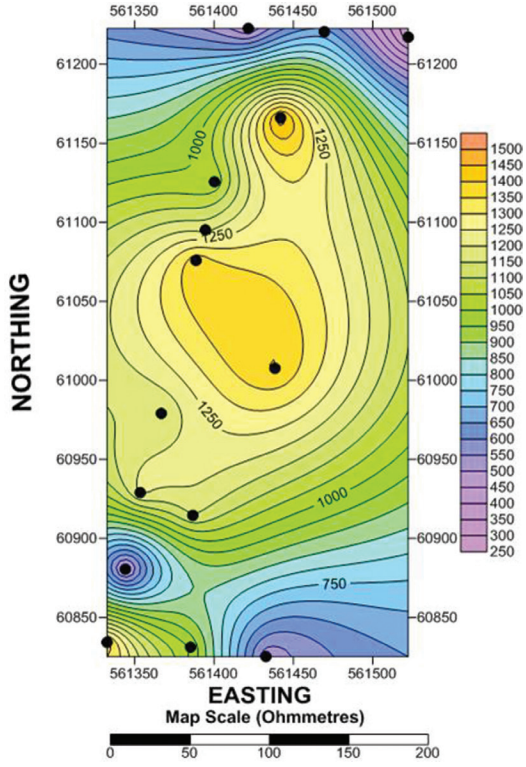

Figure 9c: *Resistivity contour map of the study area.*

bedrock and for a value below 1 000 Ω m, the bedrock is fractured and saturated. From the resistivity contour map (Figure 9c), higher resistivity values (1 007 Ω m to 1 483 Ω m) are typical of the dam axis while the abutments are characterized with low values indicating fractured bedrock. It can be deduced from (Figures 8a, c) that the dam axis with thin overburden thickness corresponds to area with high resistivity values which invariably correspond to area with bedrock ridges. Generally, the fresh bedrock along the dam axis can be said to be poorly saturated (low porosity and permeability) while the overburden is highly saturated (poor drainage).

2D-resistivity models

From the inversion of field data using RES 2DINV, the two-dimensional inverse resistivity models for the subsurface terrain underlying the dam axis, the left and right abutments generally indicate relative uniformity in the values of resistivity along the horizontal direction, especially beneath the two abutments.

2D-Resistivity model for the Dam axis

The complete resistivity inversion model along the dam axis is shown in Figure 10a. Low resistivity zones in the inversion sections are prevalent across the entire topmost layer of the dam axis, however the resistivity increase with depth. The thickness of this very low resistive (high conductive) region decreases from about 7.4 m at the extreme left down to about 2.4 m at 160 m offset. Similar phenomenon was noticed towards the extreme right of the dam axis. The second horizon, interpreted as a weathered water-saturated layer with resistivity ranging from 50 Ω m to 300 Ω m has an average thickness of about 3.5 m. The value of resistivity increases with depth. The regions with high values of resistivity, which is an indication of the basement rock, are closer to the surface at (160, 280 and 330) m offsets. This is indicative of the variation in thickness of the overburden as revealed by the isopach map of overburden and the basement relief map in which the thickness of the overburden is much reduced at 160 m offset. The thickness of the overburden is however, much higher around the left extreme at zero offset (abutment), around the central region at 200 m offset and around the right extreme at 400 m offset (abutment). The resistivity of the third layer is over 3 000 Ω m interpreted as competent basement.

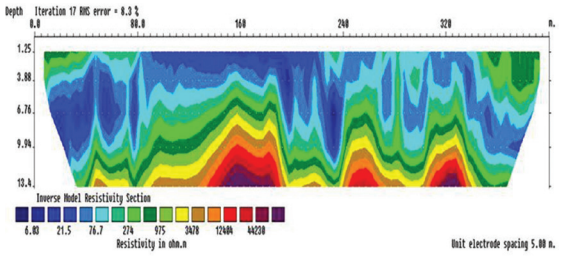

Figure 10a: *Inverse resistivity model for the Dam axis.*

2D-Resistivity model for the Left abutment

The model resistivity values generally decrease with depth (Figure 10b). The uppermost layer that is relatively dry and sandy on the left abutment shows consistently high resistivity values of between 472 Ω m and 780 Ω m, the downward decrease in resistivity result in the occurrence of a thicker layer when compared to the uppermost horizon with very low resistivity values from a depth of about 6.8 m down to the base of the section at a depth of 13.4 m around 57 m to 60 m offset. This horizon corresponds to the water saturated region of the clayey weathered basement material. High resistive (780 Ω m) basement rock was found gradually intruding the second layer at distance 25–35 m and 65–70 m. This was not conspicuously revealed in this section because the overburden is very thick.

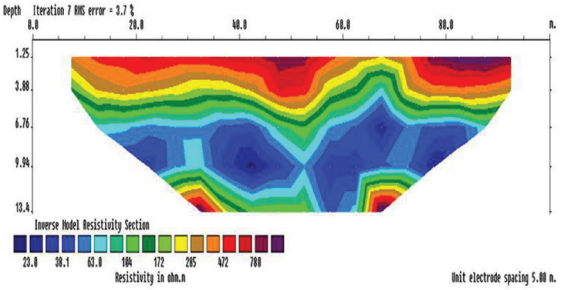

Figure 10b: *Inverse resistivity model for the left abutment.*

2D-Resistivity model for the Right abutment

Resistivity image interpretation shown in Figure 10c indicates that the resistivity values are decreasing gradually downward in the section from surface to bottom of the section and are uniform in nature. A highly (769 Ω m) resistive lithology (dry and sandy) was revealed at the uppermost layer to a depth of 5 m on the right flank of the proposed dam site. The downward decrease in resistivity, result in the occurrence of a layer with very low resistivity values (18 Ω m to 50 Ω m) from a depth of about 6.5 m down to the base of the section within a depth of 13.4 m, at 45 m offset. This horizon corresponds to a region with water saturation, within the clayey weathered basement material.
High resistivity value is evident at the bottom of the section with offset distance 60–75 m beyond 13 m depth.

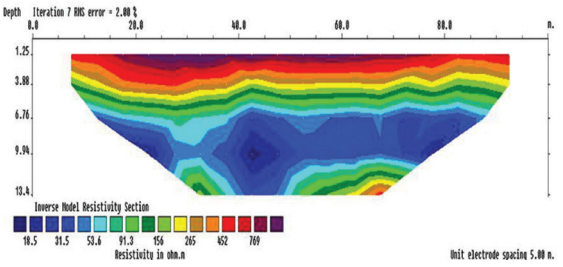

Figure 10c: *Inverse resistivity model for the Right abutment.*

Geotechnical characterization

The stability of any engineering structure is primarily dependent on their supporting foundation which is largely a function of the nature and condition of the underlying soil materials[21]. A correlation of the lithologic section penetrated at position of BH1, BH2, BH3 and BH4 (Figure 11) suggests that the depth to bedrock vary between 3 m to 6 m with an increase in depth at the two extreme boreholes (BH1 and BH4) along the dam axis. Groundwater was not encountered at boreholes BH1 and BH4, but it was encountered at depth of 3.5 m and 2.5 m in boreholes BH2 and BH3 respectively. The Standard Penetrometer Test (SPT) investigation was undertaken between 1.5 m and 6.0 m depth range (Figures 12). The SPT blows range between 12 and 50. At depth of 1.5 m, the SPT number of blows (*N*) for BH1 and BH4 was respectively 35 and 48 and decreases for BH2 and BH3 along the proposed dam axis. At depth of 3 m, the trend of the SPT number of blows are low at BH2 and BH3 indicating the type of clay present is very soft (easy penetration) and the region is marshy but the number of blows increases for BH1 and BH4 towards the edges of the proposed dam axis and showing a well drained portion. This shows proportional rate of penetration with the nature and hardness of rock encountered when correlated with borehole log and geoelectric parameters.

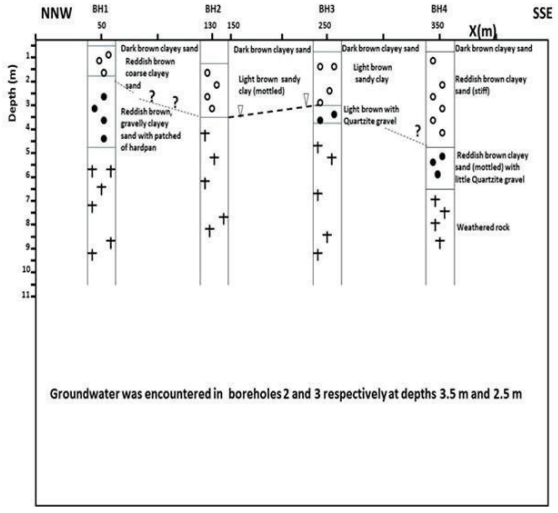

Figure 11: *Boreholes lithologic correlation along the dam axis.*

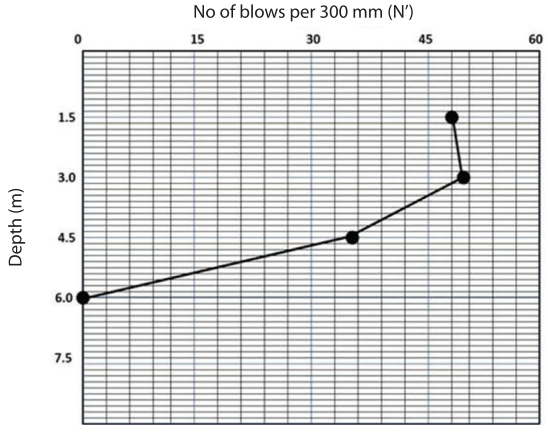

Figure 12: *SPT plot for BH4.*

Conclusions

The results from Very Low Frequency electromagnetic method indicated that the host rock is generally of low conductivity with pockets of highly resistive and highly conductive units embedded within the low background. From the geoelectric sections, the thickness of the overburden is relatively thick at the dam abutments and shallow along the dam axis with the lowest thickness at the central part of the dam axis. It can be deduced from the Isopach, Bedrock relief and Resistivity contour maps that the dam axis with thin overburden thickness correspond to area with high resistivity values which invariably correspond to the area with bedrock ridges, more so, the bedrock (fresh) along the dam axis is poorly saturated (low porosity and permeability) and the overburden is highly saturated (poor drainage). However, at the abutments, the reversed was experienced and the bedrock is fractured. Uniformity in resistivity values along the horizontal direction and variation in resistivity values in the vertical direction was revealed from inverse resistivity 2-dimensional models. The geotechnical results revealed that the stability of the proposed dam axis is lowest at the central part of the axis and increases away to the two extremes.The uneven nature of the basement topography is a potential threat to the stability of engineering structures. As a result, the site was considered unsuitable for concrete dam but suitable for earth dam. If the dam will however be constructed, proactive measures, such as deep excavation and grouting must be taken against the structural and geological defects.

Table 1: *Summary of VES data interpretation*

S/N	Layers	Resistivity (Ωm)	Thickness (m)	Depth (m)	Curve Type	Reflection Coefficient	Probable Lithology
VES 1	I.	594	3.3	3.3	H type $\rho_1 > \rho_2 < \rho_3$	0.642	Topsoil
	II.	58	13.0	16.3			Weathered basement (clayey)
	III.	268	–	–			Fractured basement
VES 2	I.	804	3.7	3.7	H type $\rho_1 > \rho_2 < \rho_3$	0.874	Topsoil
	II.	45	14.9	18.6			Weathered basement (clayey)
	III.	673	–	–			Fresh basement
VES 3	I.	432	4.1	4.1	H type $\rho_1 > \rho_2 < \rho_3$	0.812	Topsoil
	II.	46	14.0	18.1			Weathered basement (clayey)
	III.	447	–	–			Fresh basement
VES 4	I.	326	2.6	2.6	H type $\rho_1 > \rho_2 < \rho_3$	0.933	Topsoil
	II.	35	8.0	10.6			Weathered basement (clayey)
	III.	1 007	–	–			Fresh basement
VES 5	I.	18	1.0	1.0	H type $\rho_1 > \rho_2 < \rho_3$	0.981	Topsoil
	II.	11	1.3	2.3			Weathered basement (clayey)
	III.	1 187	–	–			Fresh basement
VES 6	I.	178	0.4	0.4	H type $\rho_1 > \rho_2 < \rho_3$	0.967	Topsoil
	II.	23	5.9	6.3			Weathered basement (clayey)
	III.	1 385	–	–			Fresh basement
VES 7	I.	52	3.0	3.0	A-type $\rho_1 > \rho_2 < \rho_3$	0.549	Topsoil
	II.	333	11.5	14.5			Weathered basement (sandy clay)
	III.	1 146	–	–			Fresh basement
VES 8	I.	71	4.8	4.8	A-type $\rho_1 > \rho_2 < \rho_3$	0.731	Topsoil
	II.	188	5.1	9.9			Weathered basement (clayey)
	III.	1 213	–	–			Fresh basement
VES 9	I.	387	3.3	3.3	H type $\rho_1 > \rho_2 < \rho_3$	0.677	Topsoil
	II.	87	8.3	11.6			Weathered basement (sandy clay)
	III.	450	–	–			Fractured basement
VES 10	I.	340	4.6	4.6	H type $\rho_1 > \rho_2 < \rho_3$	0.923	Topsoil
	II.	55	13.1	17.7			Weathered basement (clayey)
	III.	1 378	–	–			Fresh basement
VES 11	I.	453	3.7	3.7	H type $\rho_1 > \rho_2 < \rho_3$	0.849	Topsoil
	II.	81	16.2	19.9			Weathered basement (clayey)
	III.	995	–	–			Fresh basement
VES 12	I.	636	3.8	3.8	H type $\rho_1 > \rho_2 < \rho_3$	0.766	Topsoil
	II.	68	8.1	11.9			Weathered basement (clayey)
	III.	512	–	–			Fractured basement

Acknowledgement

Special thanks to Prof. M. O. Olorunfemi and Prof. J. O. Ajayi of the Department of Geology, Obafemi Awolowo University Ile-Ife for critically reviewing the manuscript.

References

[1] Coduto, D. P. (1999): *Geotechnical Engineering*: *Principles and Practice*. Prentice Hal Inc. Upper Saddle River, New Jersey 07458.

[2] Olorunfemi, M. O., Ojo, J. S., Sonuga, F. A., Ajayi, O., Oladapo, M. I. (2000): Geoelectric and electromagnetic investigation of the failed Koza and Nassarawa earth dams, around Katsina, Northern Nigeria. *Journal of Mining and Geology*, 36(1), pp. 51–65.

[3] Olorunfemi, M. O., Ojo, J. S., Sonuga, F. A., Ajayi, O. and Oladapo, M. I. (2000): Geophysical investigation of Karkarku earth dam embankment. *Global Journal of Pure and Applied Sciences,* 6(1), pp. 117–124.

[4] Bell, F. G. (2007): *Engineering Geology*. Butterworth-Heinimann Publishers, Oxford, UK, 524p.

[5] Price, D. G., Frectas, M. H. (2009): *Engineering geology, principles and practise.* Springer-Verlag Berlin Heidelburg, Germany, pp. 103–384.

[6] Ako, B. D. (1976): An integration of geological and geophysical data in dam site investigation, a case study of Opa dam, Ile-Ife, Osun state, Southwestern Nigeria. *Journal of Mining and Geology,* 13(1), pp. 1–6.

[7] Drake, C. L. (1962): Geophysics and Engineering. *Geophysics,* 27(2), pp. 193–197.

[8] Dutta, N. P. (1984): Seismic Refraction Method to study the foundation rock of a dam. *Geophysical Prospecting,* 32, pp. 1103–1110.

[9] Early, K. R., Dyer, K. R. (1964): The use of resistivity survey in a foundation site underlain by Karst Dolomite. *Geotechniques,* 4, 341–348.

[10] Moore, R. W. (1952): Geophysical method adapted to Highway Engineering Problems. *Geophysics,* 17(3), p. 530.

[11] Olorunfemi, M. O., Mesida, E. A. (1987): Engineering Geophysics and its application in Engineering site Investigations (Case study from Ile-Ife area). *The Nigerian Engineers,* 22(2), pp. 57–66.

[12] Ojo, J. S., Ayangbesan, T. A., Olorunfemi, M. O. (1990): Geophysical survey of a dam site. *Journal of Mining and Geology,* 26(2), pp. 201–296.

[13] Aina, A, Olorunfemi, M. O., Ojo, J. S. (1996): An integration of aeromagnetic and electrical resistivity methods in dam site investigation. *Geophysics,* 61(2), pp. 349–356.

[14] Olorunfemi, M. O., Idoringie, A. I., Fagunloye, H. O., Ogun, O. A. (2003): Assessment of anomalous seepage conditions in the Opa dam embankment, Ile-Ife, southwestern Nigeria. *Global Journal of Geological Sciences*, 2, pp. 23–31

[15] Olorunfemi, M. O., Idoringie, A. I., Coker, A. T., Babadiya, G. E. (2004): The application of the electrical resistivity method in foundation failure investigation. *Global Journal of Geological Sciences*, 2, pp. 39–51.

[16] Faniran, A. (1971): *Water supply to rural communities. A case of the Ibarapa water scheme.* Paper presented at the Geographical Association Conference held at the University of Ife, Ile-Ife, Nigeria, March 20–25, 1971.

[17] Olorunfemi, M. O., Okhue, E. I. (1991): Electrical Resistivity investigation of a typical basement complex area. The Obafemi Awolowo University Campus case study. *Journal of Mining and Geology*, 27(2), pp. 63–69

[18] Dan-Hassan, M. A., Olorunfemi, M. O. (1999): Hydrogeophysical investigation of a basement terrain in the north-central part of Kaduna State Nigeria. *Journal of Mining and Geology,* 35(2), pp. 189–205.

[19] Omosuyi, G. O., Ojo, J. S., Enikanselu, P. A. (2003): Geophysical investigation for Groundwater around Obanla-Obakekere in Akure Area within the basement complex of Southwestern Nigeria. *Journal of Mining and Geology,* 39(2), pp. 109–116.

[20] Olayinka, A. I., Mbachi, C. N. (1992): A technique for the interpretation of electrical soundings from crystalline basement areas of Nigeria. *Journal of Mining Geology,* 37, pp. 163–175.

[21] Faleye, E. T., Omosuyi, G. O. (2011): Geophysical and Geotechnical characterization of foundation beds at Kuchiyaku, Kuje area, Abuja, Nigeria. *Journal of emerging trends in Engineering and Applied Sciences*, 2(5), pp. 864–870.

Instructions to Authors
Navodila avtorjem

RMZ – MATERIALS & GEOENVIRONMENT (RMZ – Materiali in geookolje) is a periodical publication with four issues per year (established in 1952 and renamed to RMZ – M&G in 1998). The main topics are Mining and Geotechnology, Metallurgy and Materials, Geology and Geoenvironment.
RMZ – M&G publishes original scientific articles, review papers, preliminary notes and professional papers in English. Only professional papers will exceptionally be published in Slovene. In addition, evaluations of other publications (books, monographs, etc.), in memoriam, presentation of a scientific or a professional event, short communications, professional remarks and reviews published in RMZ – M&G can be written in English or Slovene. These contributions should be short and clear.
Authors are responsible for the originality of the presented data, ideas and conclusions, as well as for the correct citation of the data adopted from other sources. The publication in RMZ – M&G obligates the authors not to publish the article anywhere else in the same form.

RMZ – MATERIALS AND GEOENVIRONMENT (RMZ – Materiali in geookolje), kratica RMZ – M&G je revija (ustanovljena kot zbornik 1952 in preimenovana v revijo RMZ – M&G 1998), ki izhaja vsako leto v štirih zvezkih. V reviji objavljamo prispevke s področja rudarstva, geotehnologije, materialov, metalurgije, geologije in geookolja.
RMZ – M&G objavlja izvirne znanstvene, pregledne in strokovne članke ter predhodne objave samo v angleškem jeziku. Strokovni članki so lahko izjemoma napisani v slovenskem jeziku. Kot dodatek so zaželene recenzije drugih publikacij (knjig, monografij …), nekrologi In memoriam, predstavitve znanstvenih in strokovnih dogodkov, kratke objave in strokovne replike na članke, objavljene v RMZ – M&G v slovenskem ali angleškem jeziku. Prispevki naj bodo kratki in jasni.
Avtorji so odgovorni za izvirnost podatkov, idej in sklepov v predloženem prispevku oziroma za pravilno citiranje privzetih podatkov. Z objavo v RMZ – M&G se tudi obvežejo, da ne bodo nikjer drugje objavili enakega prispevka.

Specification of the Contributions

Optimal number of pages is 7 to 15; longer articles should be discussed with the Editor-in-Chief prior to submission. All contributions should be written using the ISO 80000.

- Original scientific papers represent unpublished results of original research.
- Review papers summarize previously published scientific, research and/or expertise articles on a new scientific level and can contain other cited sources which are not mainly the result of the author(s).
- Preliminary notes represent preliminary research findings, which should be published rapidly (up to 7 pages).
- Professional papers are the result of technological research achievements, application research results and information on achievements in practice and industry.

Vrste prispevkov

Optimalno število strani je 7–15, za daljše članke je potrebno soglasje glavnega urednika. Vsi prispevki naj bodo napisani v skladu z ISO 80000.

- Izvirni znanstveni članki opisujejo še neobjavljene rezultate lastnih raziskav.
- Pregledni članki povzemajo že objavljene znanstvene, raziskovalne ali strokovne dosežke na novem znanstvenem nivoju in lahko vsebujejo tudi druge (citirane) vire, ki niso večinsko rezultat dela avtorjev.
- Predhodna objava povzema izsledke raziskave, ki je v teku in zahteva hitro objavo obsega do sedem (7) strani.
- Strokovni članki vsebujejo rezultate tehnoloških dosežkov, razvojnih projektov in druge informacije iz prakse in industrije.

— Publication notes contain the author's opinion on newly published books, monographs, textbooks, etc. (up to 2 pages). A figure of the cover page is expected, as well as a short citation of basic data.
— In memoriam (up to 2 pages), a photo is expected.
— Discussion of papers (Comments) where only professional disagreements of the articles published in previous issues of RMZ – M&G can be discussed. Normally the source author(s) reply to the remarks in the same issue.
— Event notes in which descriptions of a scientific or a professional event are given (up to 2 pages).

Review Process

All manuscripts will be supervised shall undergo a review process. The reviewers evaluate the manuscripts and can ask the authors to change particular segments, and propose to the Editor-in-Chief the acceptability of the submitted articles. Authors are requested to identify three reviewers and may also exclude specific individuals from reviewing their manuscript. The Editor-in-Chief has the right to choose other reviewers. The name of the reviewer remains anonymous. The technical corrections will also be done and the authors can be asked to correct the missing items. The final decision on the publication of the manuscript is made by the Editor-in-Chief.

Form of the Manuscript

The contribution should be submitted via e-mail as well as on a USB flash drive or CD.
The original file of the Template is available on RMZ – Materials and Geoenvironment Home page address: **www.rmz-mg.com**.
The contribution should be submitted in Microsoft Word. The electronic version should be simple, without complex formatting, hyphenation, and underlining. For highlighting, only bold and italic types should be used.

Composition of the Manuscript

Title

The title of the article should be precise, informative and not longer that 100 characters. The author should also indicate the short version of the title. The title should be written in English as well as in Slovene.

— Recenzije publikacij zajemajo ocene novih knjig, monografij, učbenikov, razstav … (do dve (2) strani; zaželena slika naslovnice in kratka navedba osnovnih podatkov).
— In memoriam obsega do dve (2) strani, zaželena je slika.
— Strokovne pripombe na objavljene članke ne smejo presegati ene (1) strani in opozarjajo izključno na strokovne nedoslednosti objavljenih člankov v prejšnjih številkah RMZ – M&G. Praviloma že v isti številki avtorji prvotnega članka napišejo odgovor na pripombe.
— Poljudni članki, ki povzemajo znanstvene in strokovne dogodke zavzemajo do dve (2) strani.

Recenzentski postopek

Vsi prispevki bodo predloženi v recenzijo. Recenzent oceni primernost prispevka za objavo in lahko predlaga kot pogoj za objavo dopolnilo k prispevku. Recenzenta izbere uredništvo med strokovnjaki, ki so dejavni na sorodnih področjih, kot jih obravnava prispevek. Avtorji morajo predlagati tri recenzente. Pravico imajo predlagati ime recenzenta, za katerega ne želijo, da bi recenziral njihov prispevek. Uredništvo si pridržuje pravico, da izbere druge recenzente. Recenzent ostane anonimen. Prispevki bodo tudi tehnično ocenjeni in avtorji so dolžni popraviti pomanjkljivosti. Končno odločitev za objavo da glavni urednik.

Oblika prispevka

Prispevek lahko posredujte preko e-pošte ter na USB-mediju ali CD-ju.
Predloga za pisanje članka se nahaja na spletni strani: **www.rmz-mg.com**.
Besedilo naj bo podano v urejevalniku besedil Word. Digitalni zapis naj bo povsem enostaven, brez zapletenega oblikovanja, deljenja besed, podčrtavanja. Avtor naj označi le krepko in kurzivno poudarjanje.

Zgradba prispevka

Naslov

Naslov članka naj bo natančen in informativen in naj ne presega 100 znakov. Avtor naj navede tudi skrajšan naslov članka. Naslov članka je podan v angleškem in slovenskem jeziku.

Information on the Authors
Information on the authors should include the first and last name of the authors, the address of the institution and the e-mail address of the leading author.

Abstract
The abstract presenting the purpose of the article and the main results and conclusions should contain no more than 180 words. It should be written in Slovene and English.

Key words
A list of up to 5 key words (3 to 5) that will be useful for indexing or searching. They should be written in Slovene and English.

Introduction

Materials and methods

Results and discussion

Conclusions

Acknowledgements

References
The sources should be cited in the same order as they appear in the article. They should be numbered with numbers in square brackets. Sources should be cited according to the SIST ISO 690:1996 standards.

Monograph:
[1] Trček, B. (2001): *Solute transport monitoring in the unsaturated zone of the karst aquifer by natural tracers*. Ph. D. Thesis. Ljubljana: University of Ljubljana 2001; 125 p.

Journal article:
[2] Higashitani, K., Iseri, H., Okuhara, K., Hatade, S. (1995): Magnetic Effects on Zeta Potential and Diffusivity of Nonmagnetic Particles. *Journal of Colloid and Interface Science*, 172, pp. 383–388.

Electronic source:
CASREACT – Chemical reactions database [online]. Chemical Abstracts Service, 2000, renewed 2/15/2000 [cited 2/25/2000]. Available on: <http://www.cas.org/casreact.html>.

Podatki o avtorjih
Podatki o avtorjih naj vsebujejo imena in priimke avtorjev, naslov pripadajoče inštitucije ter elektronski naslov vodilnega avtorja.

Izvleček
Izvleček namena članka ter ključnih rezultatov z ugotovitvami naj obsega največ 180 besed. Izvleček je podan v angleškem in slovenskem jeziku.

Ključne besede
Seznam največ 5 ključnih besed (3–5) za pomoč pri indeksiranju ali iskanju. Ključne besede so podane v angleškem in slovenskem jeziku.

Uvod

Materiali in metode

Rezultati in razprava

Sklepi

Zahvala

Viri
Uporabljane literaturne vire navajajte po vrstnem redu, kot se pojavljajo v prispevku. Označite jih s številkami v oglatem oklepaju. Literatura naj se navaja v skladu s standardom SIST ISO 690:1996.

Monografija:
[1] Trček, B. (2001): *Solute transport monitoring in the unsaturated zone of the karst aquifer by natural tracers*. doktorska disertacija. Ljubljana: Univerza v Ljubljani 2001; 125 str.

Članek v reviji:
[2] Higashitani, K., Iseri, H., Okuhara, K., Hatade, S. (1995): Magnetic Effects on Zeta Potential and Diffusivity of Nonmagnetic Particles. *Journal of Colloid and Interface Science*, 172, str. 383–388.

Spletna stran:
CASREACT – Chemical reactions database [online]. Chemical Abstracts Service, 2000, obnovljeno 15. 2. 2000 [citirano 25. 2. 2000]. Dostopno na svetovnem spletu: <http://www.cas.org/casreact.html>.

Scientific articles, review papers, preliminary notes and professional papers are published in English. Only professional papers will exceptionally be published in Slovene.

Annexes

Annexes are images, spreadsheets, tables, and mathematical and chemical formulas.
Annexes should be included in the text at the appropriate place, and they should also be submitted as a separate document, i.e. separated from the text in the article.
Annexes should be originals, made in an electronic form (Microsoft Excel, Adobe Illustrator, Inkscape, AutoCad, etc.) and in .eps, .tif or .jpg format with a resolution of at least 300 dpi.
The width of the annex should be at least 152 mm. They should be named the same as in the article (Figure 1, Table 1).
The text in the annexes should be written in typeface Arial Regular (6 pt).
The title of the image (also schemes, charts and graphs) should be indicated in the description of the image.
When formatting spreadsheets and tables in text editors, tabs, and not spaces, should be used to separate columns. Each formula should have its number written in round brackets on its right side.
References of the annexes in the text should be as follows: "Figure 1…" and not "as shown below:". This is due to the fact that for technical reasons the annex cannot always be placed at the exact specific place in the article.

Manuscript Submission

Contributions should be sent to the following e-mail address: rmz-mg@ntf.uni-lj.si.

In case of submission on CD or USB flash drive, contributions can be sent by registered mail to the address of the editorial board:
RMZ – Materials and Geoenvironment, Aškerčeva 12, 1000 Ljubljana, Slovenia.

The contributions can also be handed in at the reception of the Faculty of Natural Sciences and Engineering (ground floor), Aškerčeva 12, 1000 Ljubljana, Slovenia with the heading "for RMZ – M&G".

Znanstveni, pregledni in strokovni članki ter predhodne objave se objavijo v angleškem jeziku. Izjemoma se strokovni članek objavi v slovenskem jeziku.

Priloge

K prilogam prištevamo slikovno gradivo, preglednice in tabele ter matematične in kemijske formule.
Priloge naj bodo vključene v besedilu, kjer se jim odredi okvirno mesto. Hkrati jih je potrebno priložiti tudi kot samostojno datoteko, ločeno od besedila v članku.
Priloge morajo biti izvirne, narejene v računalniški obliki (Microsoft Excel, Adobe Illustrator, Inkscape, AutoCad ...) in shranjene kot .eps, .tif ali .jpg v ločljivosti vsaj 300 dpi. Širina priloge naj bo najmanj 152 mm. Datoteke je potrebno poimenovati, tako kot so poimenovane v besedilu (Slika 1, Preglednica 1).
Za besedilo v prilogi naj bo uporabljena pisava Arial navadna različica (6 pt).
Naslov slikovnega gradiva, sem prištevamo tudi sheme, grafikone in diagrame, naj bo podan v opisu slike.
Pri urejevanju preglednic/tabel, v urejevalniku besedila, se za ločevanje stolpcev uporabijo tabulatorji in ne presledki.
Vsaka formula naj ima zaporedno številko zapisano v okroglem oklepaju na desni strani.
V besedilu se je potrebno sklicevati na prilogo na način: „Slika 1 ...", in ne „... kot je spodaj prikazano:" saj zaradi tehničnih razlogov priloge ni vedno mogoče postaviti na točno določeno mesto v članku.

Oddaja članka

Prispevke lahko pošljete po elektronski pošti na naslov rmz-mg@ntf.uni-lj.si.

V primeru oddaje prispevka na CD- ali USB-mediju le-te pošljite priporočeno na naslov uredništva:
RMZ – Materials and Geoenvironment, Aškerčeva 12, 1000 Ljubljana, Slovenija

ali jih oddajte na:
recepciji Naravoslovnotehniške fakultete (pritličje), Aškerčeva 12, 1000 Ljubljana, Slovenija s pripisom „za RMZ – M&G".

The electronic medium should clearly be marked with the name of the leading author, the beginning of the title and the date of the submission to the Editorial Office of RMZ – M&G.

Information on RMZ – M&G

— Editor-in-Chief
  Assoc. Prof. Dr. Peter Fajfar
  Telephone: +386 1 200 04 51
  E-mail address: peter.fajfar@omm.ntf.uni-lj.si

— Secretary
  Ines Langerholc, Bachelor in Business Administration
  Telephone: +386 1 470 46 08
  E-mail address: ines.langerholc@omm.ntf.uni-lj.si

These instructions are valid from July 2013.

Elektronski mediji morajo biti jasno označeni z imenom vsaj prvega avtorja, začetkom naslova in datumom izročitve uredništvu RMZ – M&G.

Informacije o RMZ – M&G

— urednik
  izr. prof. dr. Peter Fajfar
  Telefon: +386 1 200 04 51
  E-poštni naslov: peter.fajfar@omm.ntf.uni-lj.si

— tajnica
  Ines Langerholc, dipl. poslov. adm.
  Telefon: +386 1 470 46 08
  E-poštni naslov: ines.langerholc@omm.ntf.uni-lj.si

Navodila veljajo od julija 2013.

ISSN 1408-7073